ALKALI METAL NMR STUDIES OF SODIUM, RUBIDIUM AND CESIUM ANIONS AND THE KINETICS OF SODIUM - CRYPTATE EXCHANGE REACTIONS

Dissertation for the Degree of Ph. D.

MICHIGAN STATE UNIVERSITY
JOSEPH MICHAEL CERASO

1975

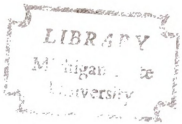

This is to certify that the

thesis entitled

ALKALI METAL NMR STUDIES OF
SODIUM, RUBIDIUM AND CESIUM ANIONS
AND THE KINETICS OF
SODIUM-CRYPTATE EXCHANGE REACTIONS

presented by

Joseph Michael Ceraso

has been accepted towards fulfillment
of the requirements for

Ph. D. degree in Chemistry

James L. Dye

Major professor

Date 9-29-75

O-7639

ABSTRACT

ALKALI METAL NMR STUDIES OF SODIUM, RUBIDIUM AND CESIUM ANIONS AND THE KINETICS OF SODIUM-CRYPTATE EXCHANGE REACTIONS

By

Joseph Michael Ceraso

The solvent influence on the kinetics of the release of sodium ion from its complex with the macrobicyclic hexaoxadiamine $N(CH_2CH_2OCH_2CH_2OCH_2CH_2)_3N$ (2,2,2 cryptand) has been investigated by using the pulsed ^{23}Na Fourier transform NMR technique. Each of the four solvents used, water, ethylenediamine (EDA), pyridine (PYR), and tetrahydrofuran (THF), showed two well-defined resonance absorptions below the corresponding coalescence temperature. In all cases it was possible to separately measure line widths and chemical shifts of the free and complexed sodium ion as a function of temperature in the absence of exchange. Since the spins are non-interacting, the transient solution of the modified Bloch equations which describe the response of a spin system undergoing chemical exchange between two nonequivalent sites is applicable. Exchange times, τ, were calculated by fitting

the modified Bloch equations to the observed ^{23}Na line shape by using a weighted non-linear least-squares technique. For EDA solutions, a mechanism in which the rate limiting step is release of sodium ion from the cryptate complex was found to be in agreement with the observed concentration dependence of exchange times throughout the entire temperature range examined. The activation energy for sodium cryptate exchange was found to vary from 12.9 kilocalories for EDA solution to 16.7 kilocalories for H_2O solution.

When 2,2,2 cryptand and an excess of sodium, rubidium or cesium metal are placed into contact with THF, ethylamine or methylamine, solutions at least as concentrated as 0.1 M total metal were obtained. Major species in solution are the complexed cation and the alkali metal anion M^-. The NMR chemical shift and linewidth have been measured for $^{23}Na^-$ in THF, EA and MA, for $^{87}Rb^-$ in THF and EA and for $^{133}Cs^-$ in THF. The chemical shift of Na^- is, within experimental error, the same as that calculated for the gaseous anion (based upon the measured value for the gaseous atom) and is independent of solvent. Comparison with the solvent-dependent chemical shift of Na^+ provides conclusive evidence that Na^- is a "genuine" anion with two electrons in a 3s orbital which shield the 2p electrons from the influence of solvent. The linewidth increases from THF to EA to MA, suggesting either an increasing exchange rate with the cryptated cation or, more probably, the influence of an increasing concentration

of solvated electrons.

In the case of sodium solutions in all solvents both Na^+C_{222} and Na^- are detected by their NMR peaks. However, probably because of extreme line-broadening, Rb^+C_{222} and Cs^+C_{222} are not observed, but only the relatively narrow line of the corresponding anion. The chemical shifts (diamagnetic shift in ppm from the infinitely dilute aqueous ion) are 185 and 197 for Rb^- in EA and THF, respectively, and 292 for Cs^- in THF compared with 212 and 344, respectively, for the gaseous Rb and Cs atoms.

A synthesis of the first crystalline salt of the sodium anion is described. The salt has the stoichiometry $Na^+C_{222}\cdot Na^-$ (where C_{222} is 2,2,2 cryptand) and is gold in color at low temperatures.

ALKALI METAL NMR STUDIES OF SODIUM, RUBIDIUM AND CESIUM ANIONS AND THE KINETICS OF SODIUM-CRYPTATE EXCHANGE REACTIONS

By

Joseph Michael Ceraso

A DISSERTATION

Submitted to
Michigan State University
in partial fulfillment of the requirements
for the degree of

DOCTOR OF PHILOSOPHY

Department of Chemistry

1975

To my Parents

ACKNOWLEDGMENTS

The author wishes to express his sincere appreciation to Professor James L. Dye for his endless encouragement and guidence throughout this research program.

Special thanks go to Steve Landers and Patrick Smith for their collaborative efforts in the exchange studies. Thanks go to Professor Max T. Rogers for being second reader and to Drs. Yves Cahen, Mei-Tak Lok and F. J. Tehan for assistance in synthesizing 2,2,2 cryptand. Additional thanks go to C. W. Andrews, Dr. M. G. DeBacker, Miss E. Mei, Dr. L. D. Long, Dr. N. Papadakis and Dr. D. A. Wright for their help and suggestions.

Financial assistance from the Atomic Energy Commission and Michigan State University and a summer term of fellowship from the Dow Chemical Company is acknowledged.

TABLE OF CONTENTS

Page

LIST OF TABLES viii

LIST OF FIGURES. xi

I. INTRODUCTION 1

II. HISTORICAL. 7

2.1 Metal Ammonia Solutions. 7

2.1.1. Species in $M-NH_3$ Solutions 8

2.1.1.1. Evidence for Monomer Species in $M-NH_3$ Solutions 8

2.1.1.2. Evidence for Diamagnetic Species in $M-NH_3$ Solutions. 10

2.1.2. Models for Metal Ammonia Solutions . . 12

2.2 Alkali Metals in Amines and Ethers 15

2.2.1. General Properties 15

2.2.2. Major Species Involved in Metal-Amine and Metal-Ether Solutions. 16

2.2.2.1. Solvated Electrons. 16

2.2.2.2. Monomers. 18

2.2.2.3. Spin-paired Species 19

2.2.2.4. Alkali Metal Anions 20

2.3 Overall Equilibrium Scheme 26

III. GENERAL FEATURES OF ALKALI METAL ION NMR 28

3.1 Introduction 28

3.2 Shielding Constants of Alkali Metal Ions . . . 31

Chapter Page

3.2.1. Alkali Metal Ions in Crystals. 32

3.2.2. Alkali Metal Ions in Solution. 38

3.3 Quadrupole Relaxation of Alkali Metal Ions in Solution 42

IV. EXPERIMENTAL. 47

4.1 General Techniques 47

4.1.1. Glassware Cleaning 47

4.1.2. Vacuum Techniques. 47

4.2 Metal Purification 48

4.2.1. Storage of Alkali Metal in Small Quantities 48

4.2.1.1. Sodium Metal. 48

4.2.1.2. Cesium and Rubidium Metals. . . 48

4.3 Solvent Purification 50

4.4 Preparation and Purification of 2,2,2 Cryptand 52

4.4.1. Synthesis of Diethyl Ester of Triglycolic Acid 53

4.4.2. Hydrolysis of the Diester. 54

4.4.3. Purification of 2,2,2 Cryptand 54

4.5 Synthesis of a Crystalline Salt of the Sodium Anion. 55

4.6 Solution Preparation 58

4.6.1. Salt Solutions for NMR Exchange Studies. 58

Chapter Page

4.6.2. Preparation of Metal Solutions 58
4.7 The NMR Spectrometer 61
4.8 Temperature Control and Calibration. 63
4.9 Data Reduction 64
V. SODIUM-23 NMR STUDY OF SODIUM ION - SODIUM CRYPTATE EXCHANGE RATES IN VARIOUS SOLVENTS 66
5.1 Introduction 66
5.2 Determination and Interpretation of the Line Shapes 68
5.2.1. Measurements in the Absence of Exchange 70
5.2.2. Evaluation of Exchange Times 88
5.2.2.1. Exchange Times in EDA Solutions 90
5.2.2.2. Exchange Times in THF, H_2O and PYR Solutions 94
5.3 Results and Discussion 106
5.3.1. Some Sources of Systematic Error . . . 106
5.3.2. Mechanism of Exchange. 121
VI. ALKALI METAL NMR STUDIES OF SODIUM, RUBIDIUM AND CESIUM ANIONS 131
6.1 Introduction 131
6.2 Magnetic Shielding Constants of Alkali Metal Ions 131
6.3 Results. 133

Chapter Page

6.4 Discussion 134

APPENDIX A - MODIFICATION OF RELAX 2 143

APPENDIX B - PROGRAM CONVERT 145

APPENDIX C - SOLUTION TO MODIFIED BLOCH EQUATIONS. . . . 146

BIBLIOGRAPHY 153

LIST OF TABLES

Table		Page
I	Values of the average excitation energy Δ, and the expectation value $\langle r_i^{-3} \rangle_p$ for alkali metals. . .	37
II	Experimental and calculated chemical shifts for rubidium and cesium ions in halide crystals and aqueous solution.	39
III	Chemical shifts of free and cryptated sodium ions in solution	41
IV	Temperature calibration for NMR	65
V	Variation of the relaxation rate and chemical shift of free sodium cation with temperature in ethylenediamine	75
VI	Variation of the relaxation rate and chemical shift of bound sodium cation with temperature in ethylenediamine	76
VII	Variation of relaxation rate and chemical shift of free sodium cation with temperature in water. . . .	77
VIII	Variation of relaxation rate and chemical shift of bound sodium cation with temperature in water . . .	78
IX	Variation of the relaxation rate ($1/T_2$) and chemical shift of free sodium cation with temperature in tetrahydrofuran.	79

Table Page

X Variation of relaxation rate and chemical shift of bound sodium cation with temperature in tetrahydrofuran 80

XI Variation of relaxation rate and chemical shift of free sodium cation with temperature in pyridine. 81

XII Variation of relaxation rate and chemical shift of bound sodium cation with temperature in pyridine. 82

XIII Activation energy, E_r, for solvent reorganization in various solvents 89

XIV Temperature dependence of the exchange time in EDA1 and corresponding relaxation rates in the absence of exchange 101

XV Temperature dependence of the exchange time in EDA2 and corresponding relaxation rates in the absence of exchange 102

XVI Temperature dependence of the exchange time in EDA3 and corresponding relaxation rates in the absence of exchange 103

XVII Temperature dependence of the exchange time in H_2O and corresponding values for relaxation rates in the absence of exchange. 111

Table Page

XVIII Temperature dependence of the exchange time in PYR and corresponding relaxation rates in the absence of exchange 112

XIX Temperature dependence of the exchange time in THF and corresponding relaxation rates in the absence of exchange 113

XX Comparison of exchange times with and without intensity correction for EDA3 120

XXI Exchange rates and thermodynamic parameters of sodium cryptate exchange in various solvents. . . 129

XXII Selected list of shielding constants and linewidths. 136

LIST OF FIGURES

Figure		Page
1	2,2,2 Cryptand and 18-crown-6.	3
2	Spectra at 25°C of e^-_{solv} (1), Cs^- (2), K^- (3) and Na^- (4) in THF in the presence of cryptand or crown.	21
3	The relation between the peak position of Na^- and of K^- in diisopropyl ether (DIPE), diethyl ether (DE), hexamethyl phosphoric triamide (HMPA), tetrahydrofuran (THF), dimethoxyethane (DME), diglyme, ethylamine (EA), 1,2-propanediamine (PDA) and ethylenediamine (EDA) at 25°C.	23
4	The relation between the peak position of K^- and of e^-_{solv} in various solvents at 25°C	24
5	(a) Effect of quadrupole coupling upon nuclear Zeeman energies in first order. (b) Hypothetical spectrum corresponding to energy levels of (a) . .	30
6	Semilog plot of $1/T_2$ for ^{23}Na vs the reciprocal absolute temperature for a solution containing 0.15 M NaBr in EDA	45
7	Apparatus for the preparation of storage tubes for sodium metal	49
8	Apparatus for preparation of small ampoules of rubidium and cesium metal.	51
9	Vessel for preparation of $Na^+C \cdot Na^-$	56

Figure Page

10 Vessel for preparation of NMR samples. 59

11 Block diagram of the multinuclear magnetic resonance spectrometer 62

12 A typical KINFIT analysis of the ^{23}Na lineshape for a solution containing 0.60 M NaBr in EDA. X represents an experimental point, O, a calculated point, =, an experimental and calculated point which are the same within the resolution of the plot . . 74

13 Semilog plots of $1/T_2$ for ^{23}Na vs reciprocal absolute temperature for solutions containing 0.6 M NaBr (●) and 0.3 M $Na^+C_{222} \cdot Br^-$ (O) in EDA. 83

14 Semilog plots of $1/T_2$ for ^{23}Na vs reciprocal absolute temperature for solutions containing 0.2 M NaCl (●) and 0.2 M $Na^+C_{222} \cdot Cl^-$ (O) in H_2O. 84

15 Semilog plots of $1/T_2$ for ^{23}Na vs reciprocal absolute temperature for solutions containing 0.4 M $Na\phi_4B$ (●) and 0.2 M $Na^+C_{222} \cdot \phi_4B^-$ (O) in THF 85

16 Semilog plots of $1/T_2$ for ^{23}Na vs reciprocal absolute temperature for solutions containing 0.2 M $Na\phi_4B$ (●) and 0.2 M $Na^+C_{222} \cdot \phi_4B^-$ (O) in PYR 86

17 Spectra at various temperatures for a solution of 0.15 M C_{222} and 0.6 M NaBr in EDA (1 ppm = 15.87 Hz). 91

Figure Page

18 Spectra at various temperatures for a solution of 0.30 M C_{222} and 0.6 M NaBr in EDA (1 ppm = 15.87 Hz). 92

19 Spectra at various temperatures for a solution of 0.45 M C_{222} and 0.6 M NaBr in EDA (1 ppm = 15.87 Hz). 93

20 Computer fit of spectra obtained with 0.15 M C_{222} and 0.6 M NaBr in EDA. (a) 42.6°C; (b) 25.5°C. 95

21 Computer fit of spectra obtained with 0.15 M C_{222} and 0.6 M NaBr in EDA. (a) 64.9°C; (b) 53.9°C. 96

22 Computer fit of spectra obtained with 0.30 M C_{222} and 0.6 M NaBr in EDA. (a) 45.0°C; (b) 30.4°C. 97

23 Computer fit of spectra obtained with 0.30 M C_{222} and 0.6 M NaBr in EDA. (a) 76.4°C; (b) 50.2°C. 98

24 Computer fit of spectra obtained with 0.45 M C_{222} and 0.6 M NaBr in EDA. (a) 30.6°C; (b) 19.3°C. 99

25 Computer fit of spectra obtained with 0.45 M C_{222} and 0.6 M NaBr in EDA. (a) 41.9°C; (b) 36.1°C. 100

Figure Page

26 Computer fit of spectra obtained with 0.2 M C_{222} and 0.4 M NaI in H_2O. (a) 23.6°C; (b) 3.3°C 104

27 Computer fit of spectra obtained with 0.2 M C_{222} and 0.4 M NaI in H_2O. (a) 39.3°C; (b) 26.9°C. 105

28 Computer fit of spectra obtained with 0.2 M C_{222} and 0.4 M $Na\phi_4B$ in PYR. (a) 93.2°C; (b) 66.7°C. 107

29 Computer fit of spectra obtained with 0.2 M C_{222} and 0.4 M $Na\phi_4B$ in PYR. (a) 135.4°C; (b) 116.4°C 108

30 Computer fit of spectra obtained with 0.2 M C_{222} and 0.4 M $Na\phi_4B$ in THF. (a) 49.4°C; (b) 44.1°C. 109

31 Computer fit of spectra obtained with 0.2 M C_{222} and 0.4 M $Na\phi_4B$ in THF. (a) 56.8°C; (b) 62.8°C. 110

32 Computer analysis of the ^{23}Na lineshape for a solution containing 0.15 M C_{222} and 0.6 M NaBr in EDA at 25.5°C. (a) No first-order phase correction; (b) first-order phase corrected 115

Figure Page

33 Arrhenius plot of k (rate of release of Na^+ from C_{222}) for EDA1 solution. (□) No first-order phase correction; (●) first-order phase corrected. 117

34 Plot of attenuated intensity I/I_o *vs* frequency for a 5000 Hz 4-Pole Butterworth active filter 118

35 Plot of the ratios τ_{obs}/τ_{calc} *vs* temperature (^oC) for EDA1, EDA2 and EDA3 solutions. 124

36 Arrhenius plot of k (rate of release of Na^+ from C_{222}) for EDA2 solution. 125

37 Arrhenius plot of k (rate of release of Na^+ from C_{222}) for EDA3 solution. 126

38 Arrhenius plots of k (rate of release of Na^+ from C_{222}) for H_2O, THF and PYR solutions 127

39 Three possible models for a species of stoichiometry M^- (other than an alkali anion). All of these models permit solvent interaction with the outer p electrons of the cation. Ammonia is used to represent any amine or ether solvent. 132

40 ^{23}Na NMR spectrum of a solution of $Na^+C_{222} \cdot Na^-$ in EA (≃0.2 M) at 1.4°C. Reference is saturated aqueous NaCl; positive shifts are diamagnetic. . . 135

41 ^{23}Na NMR spectra of $Na^+C_{222} \cdot Na^-$ solutions (≃0.1 M) in three solvents. All chemical shifts are referenced to aqueous Na^+ at infinite dilution. 139

I. INTRODUCTION

Sodium and potassium were first observed to be soluble in liquid ammonia by Weyl in 1863.[1] Since that time, the study of physical and chemical properties of metal ammonia ($M\text{-}NH_3$) solutions has been given considerable attention. Properties of these solutions range from electrolytic at infinite dilution to metallic at high concentrations. A number of models have been postulated[2-10] to describe the species that exist in solution at low and moderate concentrations (< 0.1 M). Most everyone agrees that the properties in very dilute solutions (< 10^{-3}M) can be predicted by a two-species model. These two species are the solvated cation and the solvated electron ($e^-_{solv.}$). The situation becomes much more complex at concentrations above 0.005 M, since cation-electron and electron-electron interactions become increasingly important. Some properties such as conductance[11,12] and magnetic susceptibility[13-15] are concentration dependent and imply that new species are formed, while other properties such as the optical spectrum and extinction coefficient,[16-18] ESR absorption line shape,[19-21] and partial molar volume of the solute[9,22,24] change so little with concentration that formation of distinctly different new species seems to be ruled out. To this date no one model appears to describe satisfactorily the behavior of properties of $M\text{-}NH_3$ solutions.[24] Dye[25] has pointed out that a "weak-interaction" model qualitatively agrees with the experimental results, but that the quantitative agreement is poor.

In contrast to metal ammonia solutions which show only a single, metal independent ESR and optical absorption band (both attributed to the solvated electron), the ESR and optical properties of metal-amine and metal-ether solutions are much richer in information about distinguishable species. Some of the most obvious differences between metal-amine or metal-ether and $M-NH_3$ solutions are the drastic reduction in solubility of the former, the identification by ESR[25-28] of a monomeric species with stoichiometry M and the appearance of metal-dependent absorption bands[29,30] attributed to a diamagnetic species with stoichiometry M^-. This availability of specific spectroscopic information makes the study of these solutions particularly attractive. In spite of these advantages, past studies had been severely hampered because of poor solubility of the metals (in many cases the metal does not even dissolve). In 1969 a major breakthrough came from the work of Dye, Nicely, and DeBacker.[31] They demonstrated that dicyclohexyl 18-crown-6 (a member of a class of monocyclic polyether complexing agents first synethsized by Pedersen,[32] Figure 1) considerably enhances alkali metal solubility in ethers. Further investigations[30,33] disclosed that the complexing agent 2,2,2 cryptand (C_{222}, a member of a class of macroheterobicyclic complexing agents first synthesized by Lehn et al.,[34] Figure 1) enhances metal solubilities in amines and ethers even more effectively than dicyclohexyl 18-crown-6. The use of these synthetic complexing agents extends the solvent range in addition to increasing the concentration of

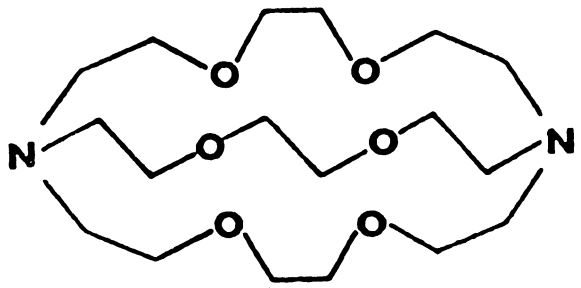

1

2,2,2 Cryptand

(C_{222})

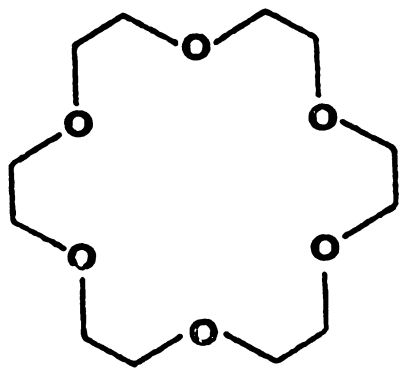

2

18-Crown-6

(18-C-6)

Figure 1. 2,2,2 Cryptand and 18-crown-6.

dissolved metals in solvents which dissolve metal unassisted.

The research efforts described in this thesis are focused on the nature of the species responsible for the metal-dependent visible absorption band in metal-amine and metal-ether solutions. The evidence to date indicates that this species is diamagnetic and has the stoichiometry M^-. On the basis of optical evidence alone one cannot distinguish among several species with stoichiometry M^-. These are: (1) an ion-triple between a cation and two spin-paired electrons, $e^- \cdot M^+ \cdot e^-$, (2) an ion-pair between a cation and a di-electron, $M^+ \cdot e_2^{2-}$, (3) a cation with a pair of electrons in an expanded orbital which includes the first solvation sheath molecules, and (4) a genuine alkali anion. A method which can distinguish among the various models is alkali metal NMR. A genuine anion M^- with two electrons in an outer s orbital should have considerably different NMR properties than the corresponding cation M^+. Chapter VI includes a summary of a multinuclear alkali metal NMR study of metal-ether and metal-amine solutions which contain Na^-, Rb^- and Cs^-. The results strongly favor the alkali anion model. A detailed description of the first synthesis of a crystalline salt of the sodium anion is included in the experimental section (Chapter IV) . This crystalline salt of the sodium anion and the alkali metal NMR results are the strongest evidence that genuine alkali metal anions do exist.[35-38]

The key factor which makes alkali metal NMR studies of metal solutions feasible is the enhancement of metal solubility

which is provided by cryptands and crowns. Prior to 1970 the maximum concentrations of sodium in amines and ethers were less than 0.01M. These concentrations were too low for practical NMR studies. With the aid of C_{222}, solutions as concentrated as 0.4M in sodium metal can be prepared.

A second goal of this research is focused on the application of pulsed ^{23}Na Fourier transform NMR lineshape analysis to permit quantitative examination of exchange rates of sodium cations in the presence of C_{222}. Initially it was felt important to examine the effect of sodium cation exchange upon the observed lineshape of a sample which contained a dissolved sodium salt and half the stoichiometric amount of C_{222}. The overall chemical equilibrium is given by reaction 1.

$$Na^+C_{222} + {}^*Na^+ \overset{k}{\underset{k}{\rightleftarrows}} {}^*Na^+C_{222} + Na^+ \qquad 1.1$$

Sodium cations undergo an exchange between bound and solvated sites which can affect the NMR lineshape. The influence of exchange was first investigated in order to determine whether ^{23}Na NMR studies of metal-amine and metal-ether solutions would be feasible. Exchange rates[39] have been reported from PMR studies on D_2O solutions which contain Na^+C_{222} cryptate. It was clear from the results of this study sodium cation exchange may be slow enough to be observed directly by using ^{23}Na NMR. A preliminary investigation by Ceraso and Dye[40] did indeed show that exchange rates are slow in ethylenediamine (EDA) at 25°C. This is the first example of sodium

cation exchange which is slow enough to exhibit clearly defined separate signals for two environments. Since the study of such cation exchange phenomena was relatively new, we decided to examine the influence of the solvent on the exchange rates. Chapter V describes an in-depth study of the kinetics of complexation reactions of Na^+-C_{222} complexes in several solvents. This chapter also includes a discussion of some of the causes of systematic errors which are common to pulse Fourier transform NMR techniques.

Since some of the ^{23}Na NMR lineshape analysis was done in collaboration with Patrick B. Smith, his M. S. thesis should also be consulted for further details.

II HISTORICAL

2.1 Metal Ammonia Solutions

Alkali and alkaline earth metals dissolve in liquid ammonia to form blue-colored, paramagnetic solutions. A wide range of concentrations exists due to the high solubility of metals in ammonia. In the very dilute concentration range the solutions behave as binary electrolytes with solvated cations and solvated electrons as the ionic species. Complex association of these species occurs in the intermediate concentration region (10^{-3} - 10^{-1} M). These interactions influence the physical and chemical properties and complicate our understanding of the solutions. Above 1 M, a non-metal to metal transition occurs. Solution properties become metallic and the conductivity of saturated solutions approaches that of the free metal.

In the description of the properties and existing models of M-NH_3 solutions, attention will be mainly given to solutions with dilute and intermediate concentrations of metal. It is not the author's intention to give a complete history of the properties of these solutions. A comprehensive history is contained in the Proceedings of Colloque Weyl I,[41] II,[42], III,[43] and IV.[44] The author merely intends to focus on selected and current topics of interest.

2.1.1. Species in $M-NH_3$ Solutions

A variety of models have been postulated[2-10] to describe the species at low and intermediate concentrations. Species with stoichiometry M^+, e^-, M, M^-, e_2^{2-} and M_2 have been postulated to exist within these models. To add to the complexity of these models, the nature of species with the same stoichiometry may vary according to the model. The solvated electron as a species is well established and will not be directly considered in this discussion.

2.1.1.1. Evidence for Monomer Species in $M-NH_3$ Solutions - Certain properties of metal solutions indicate the presence of cation-electron interactions. The strongest evidence comes from the electrical conductance of $M-NH_3$ solutions. Conductance[11,12] and transference measurements[45] yield the concentration dependence of the cation conductance. The cationic equivalent conductance decreases with increasing concentration of metals, similar to ordinary electrolytes in ammonia. The total equivalent conductance also decreases with increasing concentration of metal and shows a pronounced minimum at 0.04 M concentration of metal. A single equilibrium constant, K_1, suffices to describe the concentration dependence of the conductance below about 0.005 M. Furthermore, the magnitude of K_1 is similar to that observed for normal 1 to 1 electrolytes which form ion-pairs in ammonia.

Cation NMR spectra[46-48] also show the effects of

cation-electron interactions. Concentration dependent paramagnetic (Knight) shifts are observed. The Knight shift of a nucleus is caused by the hyperfine interaction between unpaired electrons and the nucleus. This interaction also contributes to the spin-lattice relaxation time of the metal nucleus. The correlation times are very short (10^{-11} sec.)[48] indicating a short lived cation-electron interaction.

A single extremely narrow ESR line (assigned to the solvated electron, $e^-_{solv.}$) is observed in dilute solutions.[19-21] The band is structureless and has a g-value of 2.0012. No hyperfine interaction with the metal is observed. Metal solutions also exhibit a broad optical absorption band (assigned to $e^-_{solv.}$), which peaks at 0.85 e.v. and is independent of solute. The band shape and molar extinction coefficient are independent of concentration and the position of the peak maximum is only slightly concentration dependent.[16-18] Cation-electron interactions strongly influence the conductance and NMR properties whereas they have almost no effect upon ESR and optical properties.

Recent pulse radiolysis studies of liquid deuterated ammonia solutions which contain dissolved sodium and potassium amides show at least two optical absorption bands.[49,50] The initial transient (λ_{max} = 1500 nm) is extremely short-lived (<150 μsec.) and is assigned to the solvated electron at infinite dilution. The residual absorption (λ_{max} = 1640 nm.) is shifted to the red and is interpreted as representing two or more overlapping bands corresponding to $e^-_{solv.}$

and a metal-electron species. However, from pulse radiolysis experiments performed on mixed ammonia-amine solutions, one would expect that ion-pairing effects would shift the peak maximum of $e^-_{solv.}$ towards the blue.[50]

2.1.1.2. Evidence for Diamagnetic Species in M-NH_3 Solutions - Magnetic data offer the most convincing evidence that at least one diamagnetic species is formed in M-NH_3 solutions. Static magnetic susceptibility studies performed by Freed and Sugarman[14] and radio-frequency ESR studies performed by Hutchison and Pastor[15] both show a dramatic decrease in molar paramagnetic susceptibility with increasing metal concentration. At 0.1 M metal concentration, the electrons are over 90% spin-paired. The molar paramagnetic susceptibility is strongly temperature dependent with the diamagnetic states preferred at lower temperatures. Susceptibility data for potassium indicate a temperature dependent spin-pairing enthalpy, whereas data for sodium do not.[15] Studies by DeMortier et al.[51] indicate that electrons in sodium-NH_3 solutions are much less spin-paired than those in K-NH_3 solutions. However, studies of Lok[52] and Tehan[53] indicate that spin-pairing is the same for both K-NH_3 and Na-NH_3 solutions. More experimental work is needed to determine whether or not the cation plays an important role in the spin-pairing reaction.

An extremely narrow ESR line is observed in M-NH_3

solutions up to concentrations where the electrons are 90% spin-paired. The narrowness of this line requires that reactions of the type

$$2\ D \rightarrow S$$

in which D can be any doublet state (such as e^- or M) and S any singlet state (such as e_2^{2-}, M^- or M_2), have lifetimes longer than a microsecond. Since magnetic interactions resulting from collision complexes or long-range interactions would not be expected to exist for more than a few nanoseconds, it seems appropriate to refer to the presence of a diamagnetic species.

Enthalpy measurements for $Na\text{-}NH_3$ solutions performed by Gunn[22] parallel the change in magnetic susceptibility of $K\text{-}NH_3$ solutions with both concentration and temperature. The enthalpy data can be described satisfactorily by the following reactions:

$$M^+ + e^- \underset{}{\overset{K_1}{\rightleftharpoons}} M$$

$$M + e^- \overset{K_2}{\rightleftharpoons} M^-$$

where K_2 comes from potassium magnetic susceptibility data and K_1 is determined from sodium-ammonia conductance data.[24] The slight red shift in the optical absorption band with increasing concentration of metal is the only other property

which correlates with the concentration dependence of the magnetic susceptibility.[16-18] Several diamagnetic species with different stoichiometries have been postulated to exist in these solutions. The nature of this diamagnetic species will be considered in a later section.

2.1.2. Models for Metal Ammonia Solutions

A variety of models have been postulated[2-10] to describe the species that exist in M-NH_3 solutions. The strength of any of these models depends on how well they can predict all of the known properties of these solutions. Dye[24] has classified the models under one or a combination of three general categories: (1) metal-based species; (2) double occupancy of cavities; (3) electrostatic aggregates.

Models classified under metal-based species include those which form species such as M, M^- and M_2.[2,4,6,7,10] The formation of these species results from strong interactions between cation and electrons (stronger than simple electrostatic interactions between charged ions). Double occupancy models[3,54,55] consider a pair of electrons, e_2^{2-}, in the same polarization center (or cavity). A number of calculations[56-62] have been done to determine whether or not two solvated electrons at separate sites would be more or less stable than two spin-paired electrons trapped at the same site, but the results tend to oscillate between the stability of one over the other. In any event, consideration of the ion-pairing interaction for a normal 1-2 electrolyte in ammonia

shows that the fraction of free e_2^{2-} relative to the ion-pair, $M^+ \cdot e_2^{2-}$ (stoichiometry M^-) will be negligibly small even at concentrations where spin-unpairing is complete. Both metal-based models and double-occupancy models have a common weakness. They both predict the formation of new species even though there is no observable change in the optical spectrum and molar volume of the solute.

The final category considers the formation of ionic aggregates between M^+ and $e^-_{solv.}$ without destroying the basic characteristics of the species.[8,9] Species with stoichiometry M, M^- and M_2 are viewed as ionic clusters formed from the fundamental species M^+ and $e^-_{solv.}$. The principle advantage of the ion cluster model is that the optical spectrum and molar volume of the solute are preserved. However, electrostatic considerations alone, do not permit concentrations of triple ions and ion quadrapoles in high enough concentration to explain the magnetic susceptibility or enthalpy data.

While not all models claim the same stoichiometry, M^+, e^-, M, M^- and M_2 include simpler models as special cases. Before arguing the merits of one structure over another with species of the same stoichiometry, let us note that Dye[24] has tested the stoichiometry represented by these species to determine whether it agrees with the experimental data.

The choice of equations used to describe the equilibria among all the species for any model is somewhat arbitrary. The following set is complete and independent:

(1) $M^+ + e^- \overset{K_1}{\rightleftharpoons} M$

(2) $M + e^- \overset{K_2}{\rightleftharpoons} M^-$

(3) $M^- + M^+ \overset{K_3}{\rightleftharpoons} M_2$

Values for K_1 were calculated from Na conductance data and values for K_2 were calculated from potassium magnetic susceptibility data. Because both are ion-pairing reactions, K_3 was assumed to be equal to K_1. With these values of K_1, K_2 and K_3, activity coefficients and transference numbers were calculated and compared with measured values. The results indicate that reaction 1 alone satisfactorily describes these electrochemical properties. Inclusion of reactions 2 and 3 gave large deviations from measured behavior.[24]

In conclusion, none of the present models for concentration dependence of the properties of M-NH_3 solutions are able to describe completely the experimental results. Dye has suggested that a "weak-interaction" model involving normal electrostatic interactions between two species M^+ and e^- is attractive.[24] The concentration independence of partial molar volume of M and the optical spectrum of $e^-_{solv.}$ will be preserved with this type of model. In addition, the electrochemical properties will also be described by normal electrostatic interactions which include ion-pairing interactions. As for spin-pairing, a long range electron-electron interaction is assumed and this should have little or no effect upon the electrochemical properties

or the optical spectrum. To explain the long lifetime of the diamagnetic species, the following type of exchange process can be invoked:

$$e^- + M^- \rightarrow M^- + e^-$$

In this case one electron in the singlet state is replaced by another. This need not lead to ESR line-broadening. Although qualitatively correct, this model lacks quantitative treatment.

2.2 Alkali Metals in Amines and Ethers

2.2.1. General Properties

Alkali metals dissolve in amines and ethers to a much lesser extent than in ammonia (in many cases the metals do not dissolve). In spite of the low solubility of metals in amines and ethers, studies of these solutions are rich in information about distinguishable species.

The optical spectrum consists of two bands, one in the visible and the other is near the infrared (IR). The position and width of the IR band is solvent dependent and nearly metal independent. In contrast, the visible band is only slightly influenced by solvent and is strongly metal dependent. The species responsible for the metal independent IR band has been identified as the solvated electron. The identification is based upon a comparison

of IR bands in metal solutions with those produced by pulse radiolysis in pure solvents.[63-68] The species responsible for the metal dependent visible absorption band was not clearly identified until after 1968. Prior to this date, there was much discrepancy about the nature of the species responsible for the visible band. Experimental results in one laboratory could not be reproduced in another. The chaos ended after Hurley, Tuttle and Golden[69] demonstrated that potassium ions in solution could exchange with sodium in borosilicate glass. It quickly became clear that for a given metal, at most two optical bands need be considered and that the visible band could be associated with a species of stoichiometry M^-. The ESR spectrum shows a narrow singlet (assigned to the solvated electron) with an additional hyperfine pattern superimposed upon it.[25,26] The hyperfine structure comes from a strong interaction of the electron spin with the nuclear spin of the metal. This observation gave the first unambiguous identification for a species with stoichiometry M (referred to as a monomer or ion pair).

2.2.2. Major Species Involved in Metal-Amine and Metal-Ether Solutions

2.2.2.1. Solvated Electrons - The strongest evidence that solvated electrons exist in metal-amine and metal-ether solutions comes from the comparison of the IR band with the spectrum produced by pulse radiolysis of the pure

solvent. The band shape and peak position for both ammonia and ethylenediamine are independent of the method used. With the discovery that "crown"[31] and "cryptand"[30,33] can be used to dissolve metals in a number of solvents and that an excess of cryptand yielded the IR band, it was possible to compare the IR band in metal solutions with those produced by pulse radiolysis and flash photolysis. Extensive comparison of this was made by Lok et al.[30] and the agreement between the two methods was good. However, the agreement is not exact and it has been noted[70] that the metal solution bands are, in general, broader and at slightly higher energies than those found by pulse radiolysis. The variation in width and peak position is probably due to the higher concentrations of metal solutions and may be attributed to formation of a second diamagnetic species (other than M^-) or to an ion-pairing effect. The single narrow ESR line with the same g-value as that of $M-NH_3$ solutions also supports the existence of $e^-_{solv.}$ in these solutions. Additional evidence comes from the conductance of cesium-ethylenediamine (EDA) solutions.[71-73] When Walden's rule is used to account for viscosity differences between ammonia and ethylenediamine, the limiting conductance of Cs-EDA and $Cs-NH_3$ solutions is nearly the same. Cs-EDA solutions do not show any visible absorption band and, hence, the conducting anions must be the same species which are responsible for the IR band.

2.2.2.2. Monomers - The first evidence of the existence of a monomeric species, M, was obtained by Vos and Dye[25] from ESR studies of rubidium and cesium methylamine solutions and independently by Bar-Eli and Tuttle[74] from ESR studies of potassium in ethylamine solutions. A marked increase in hyperfine splitting with a decrease in solvent polarity and an increase in temperature is observed.[75] The intensity of the hyperfine signal is low and indicates that the monomer species is only a minor constituent of the metal-solution (no optical spectrum is observed for the monomer species in metal solution under equilibrium conditions).

Other evidence for the existence of monomers comes from flash photolysis and pulse radiolysis of metal solutions (in these cases an optical spectrum for the monomer is detected, but only under transient conditions). A number of flash-photolysis studies have been performed on metal-ether and metal-amine solutions.[74-81] Most of the solutions studied contain M^+ and M^- as major species. When a solution is flashed with light at a wavelength corresponding to λ_{max} M^- (band maximum of M^-) photo bleaching of this band occurs with subsequent formation of a broad IR band. This IR band transforms rapidly to an intermediate absorption in the visible and then the intermediate band decays slowly back to the original M^- band. Even though earlier studies had been done by others, Kloosterboer et al.[81] were the first to demonstrate that the intermediate absorption band has the

stoichiometry M. These results are consistent with the following reaction sequence

$$M^- \xrightarrow{h\nu} M^+ + 2e^- \xrightarrow{M^+} 2M^+ \cdot e^- \rightarrow M^- + M^+.$$

Pulse radiolysis studies also indicate the existence of monomers (again under transient conditions). Bockrath and Dorfman[65] reported the spectrum of the sodium-electron ion pair (Na) in THF. Pulse radiolysis studies[82] of ethylamine-THF mixtures show only a single monomer band and the peak position lies at wavelengths intermediate to that observed in the pure components. A correlation is observed between the shift in λ_{max} of the monomer and the magnitude of the hyperfine splitting constant in these solutions.[82] As the percent atomic character increases (increased hyperfine splitting constant, corresponding to a larger contact density at the nucleus) the optical spectrum of the monomer shifts increasingly toward the blue.

2.2.2.3. Spin-paired Species - The existence of a spin-paired species, other than M^-, in these solutions has not been shown. Studies of solutions of K in ethylamine-ammonia mixtures with spin concentrations of the order of 10^{-6} M indicate a total concentration for the IR absorbing species to be about 10^{-4} M.[70] If these results are reliable, the IR absorption must include contributions from both paramagnetic

and diamagnetic species other than K^-, since the band maximum of K^- would appear in the visible. If other diamagnetic species besides M^- exist in these solutions, then it may be possible to correlate the magnetic properties of this new species with the spin-paired species that exists in $M-NH_3$ solutions.

2.2.2.4. Alkali Metal Anions - Chemists may view the existence of alkali metal anions with skepticism (this was especially true at the beginning of this research, since no known salts of alkali metal anions existed), but the evidence for the existence of these species has mushroomed in the past six years. The assignment of the stoichiometry M^- to the species responsible for the metal dependent visible band is based on numerous experimental facts.

That alkali anions exist in the gas phase was shown by Russian scientists in the 1960's.[83] Metal solutions which yield a large visible band and no IR band have very weak or no ESR signals. The optical spectra of these solutions, unlike $M-NH_3$ solutions, exhibit metal-dependent absorption bands. Figure 2 shows the spectra of $e^-_{solv.}$, Cs^-, K^- and Na^- in tetrahydrofuran at 25°C in the presence of either crown or cryptand. It seems unlikely that normal electrostatic interactions between cation and electrons can cause such a large shift and metal dependence of the solvated electron absorption band. By comparing the temperature and solvent

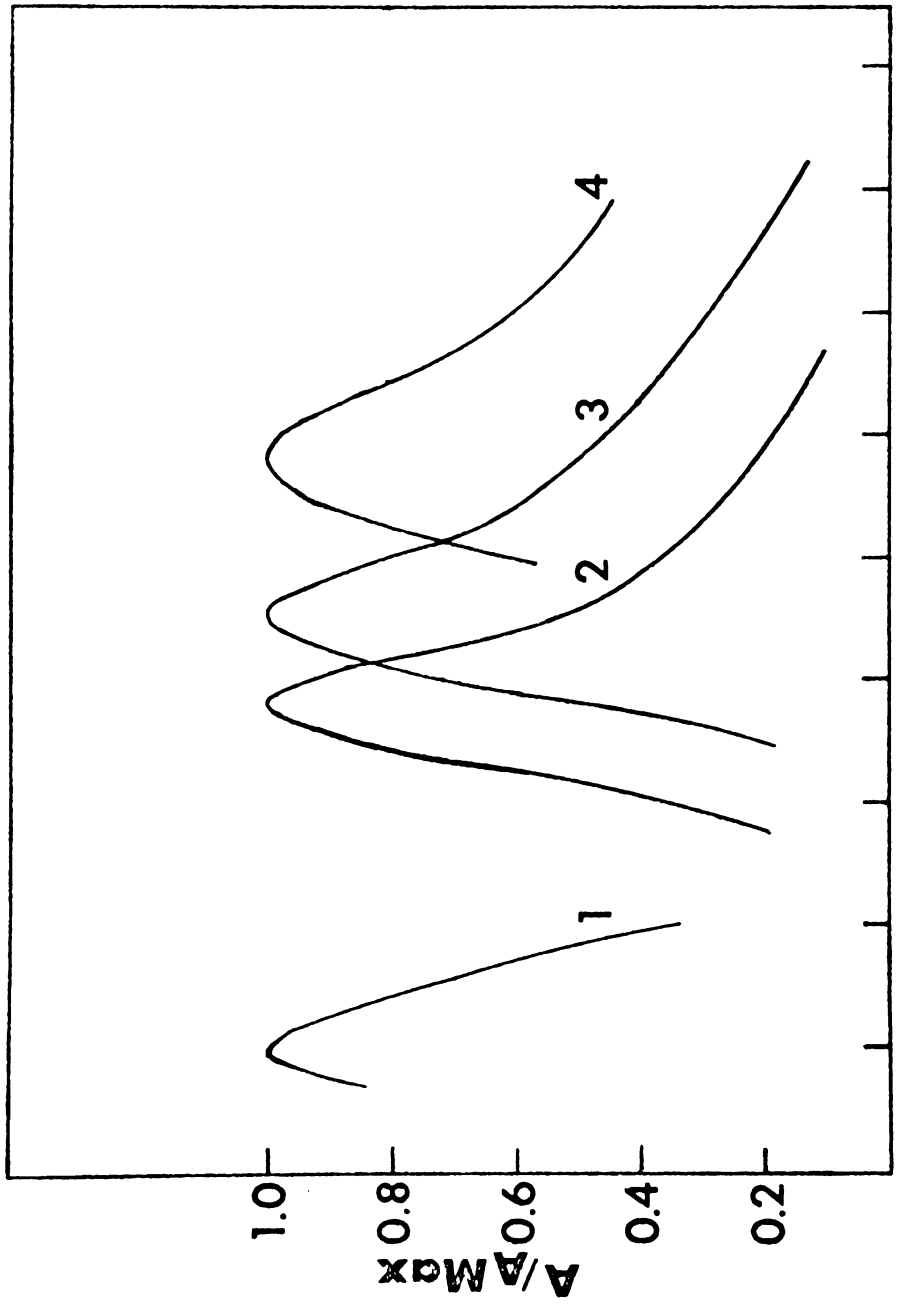

Figure 2. Spectra at 25°C of e^-_{solv} (1), Cs^- (2), K^- (3) and Na^- (4) in THF in the presence of cryptand or crown.

dependence of the optical bands in metal-amine solutions with the charge-transfer-to-solvent bands of I^-,[84-86] Matalon, Golden and Ottolenghi[29] assigned the metal-dependent band to the alkali anion. Some of the characteristics of CTTS transitions are:

1. Pronounced dependence of λ_{max} upon solvent.
2. Shift of λ_{max} to lower energies with a decrease in temperature.
3. Correlation between the shift of λ_{max} with solvent and the temperature coefficient of λ_{max}.
4. Correlation between the position of λ_{max} and the size of the anion, with a shift to lower energies for larger ions.

All of these characteristics have been observed for M^- bands. Lok, Tehan and Dye[30] have made an in-depth study and have shown excellent correlations between the peak positions of Na^- and K^- as shown in Figure 3. CTTS theory, therefore, strongly suggests that the species responsible for the visible band is an alkali anion, but it does not prove this. For example, solvated electrons also have many of the same CTTS characteristics as the M^- species. This is shown in Figure 4 by the excellent correlation of the solvated electron peak position with the K^- peak position in various solvents. Thus, it might be expected that a species like $e^- \cdot Na^+ \cdot e^-$ (triple-ion) should give rise to spectra with CTTS characteristics. Additional evidence

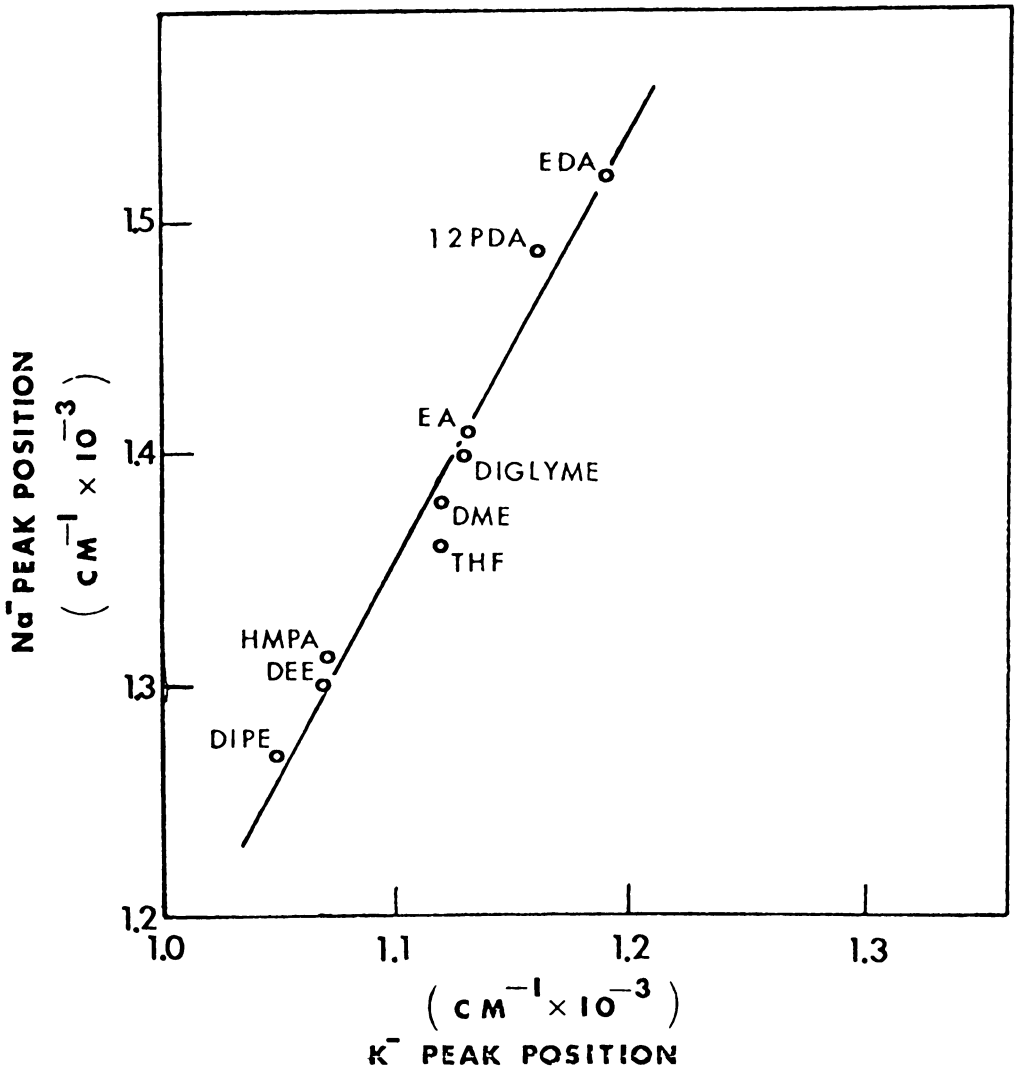

Figure 3. The relation between the peak position of Na^- and of K^- in diisopropyl ether (DIPE), diethyl ether (DE), hexamethyl phosphoric triamide (HMPA), tetrahydrofuran (THF), dimethoxyethane (DME), diglyme, ethylamine (EA), 1,2-propanediamine (PDA) and ethylenediamine (EDA) at 25°C.

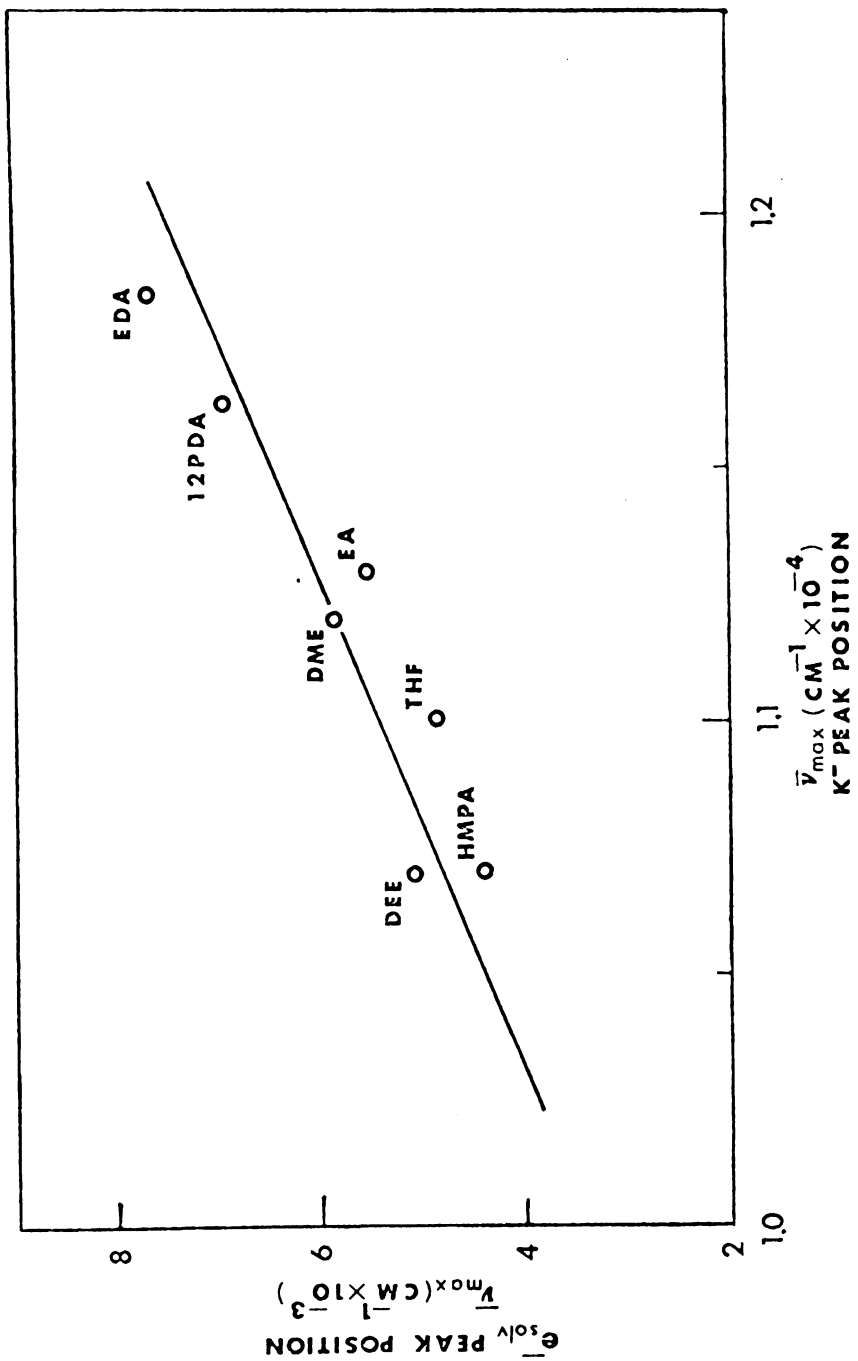

Figure 4. The relation between the peak position of K^- and of e^-_{solv} in various solvents at 25°C.

for the stoichiometry of the metal dependent species comes from flash photolysis[78-81] and pulse radiolysis[63,87] studies. In pulse radiolysis studies, a solution containing only a sodium salt was pulsed and the growth of a visible band was observed. The decay of the initially produced solvated electron band was found to be second-order in $e^-_{solv.}$ and is consistent with the following stoichiometry

$$2e^-_{solv.} + Na^+ \rightarrow Na^-.$$

The same general results were obtained from flash photolysis studies. The limiting conductances[71,73] of metal solutions which show a visible band are much lower than those found when large concentrations of solvated electrons are present. The equivalent conductance when only the metal-dependent band is present is similar to that of normal salts in amines. Strong evidence for the assignment of stoichiometry M^- was obtained by measuring the oscillator strength of the visible transition. Dye and DeBacker[88,89] found an oscillator strength of 1.9±0.2 for Na^- in EDA solution. This requires that at least two equivalent electrons be involved in the transition and may be easily satisfied by a species with stoichiometry M^-. Finally, the Faraday effect[90] indicates a magnetic moment of about 1 Bohr magneton for the excited state responsible for the visible absorption band. This is consistent with the highly symmetric structure of M^-.

The most convincing evidence that genuine alkali anions do exist comes from the isolation of the first crystalline salt of the sodium anion.[36,37] The synthesis of this compound will be described in the experimental section (Chapter IV).

Prior to the work described in this thesis it was clear that species with stoichiometry M^- exist in metal solutions. There was not available enough evidence to distinguish between genuine alkali anions and several alternative structures such as the ion-triple, $e^- \cdot M^+ \cdot e^-$, or an ion-pair between a cation and a dielectron $M^+ \cdot e_2^{2-}$. Chapter VI will offer strong evidence that genuine alkali metal anions are present rather than other species with stoichiometry M^-.

2.3 Overall Equilibrium Scheme

A general overall equilibrium scheme for species in solution may be represented as follows[33]

$$
\begin{array}{l}
2M(s) \rightleftarrows M^- + M^+ \\
\qquad\quad \uparrow\downarrow \\
\qquad\quad M + e^-_{solv.} \\
\qquad\quad \uparrow\downarrow \\
\qquad\quad M^+ + e^-_{solv.}
\end{array}
$$

Strongly solvating solvents such as ammonia tend to shift the equilibrium all the way to solvated cations and solvated electrons. Solvents such as hexamethyl phosphoric triamide and methylamine tend to yield mixtures of M^-, M

and $e^-_{solv.}$. Less polar amines and ethers give mainly the M^- species with $e^-_{solv.}$ and M as minor constituents. Addition of an excess of a complexing agent such as C_{222} cryptand can cause the equilibrium to shift all the way to the right (similar to ammonia) in suitable solvents and for some of the metals.

III. GENERAL FEATURES OF ALKALI METAL ION NMR

3.1 Introduction

All alkali metals possess at least one isotope with a nuclear magnetic moment and therefore can be examined with the NMR technique. Many studies of the resonances of these nuclei have been performed on aqueous and non-aqueous salt solutions as well as on crystals. In solution the ions exist as separate entities with negligible covalent bonding between opposite charged species. At high concentrations, association among ions can occur, but these associations are short lived and exchange between different sites is rapid. Rapid exchange among sites results in only one resonance signal with an average frequency determined by the magnetic shielding σ and life-time τ of the nucleus in each of the many sites. Because of the fast exchange, no fine structure is observed and the only measureable paramaters are the chemical shift and line width of the resonance.

Although the intensity of alkali metal resonances relative to that of protons is low, the range of magnetic shielding constants (except lithium) is considerably larger and increases with atomic number. The chemical shifts result primarily from changes in the paramagnetic contribution σ_p, to the total magnetic shielding σ (except for lithium, where diamagnetic, σ_D, and paramagnetic shielding

both contribute).

All of the alkali metal nuclei possess a nuclear quadrupole moment, since their spins are greater than 1/2. The dominant relaxation mechanism in solution is quadrupolar, except that a dipole-dipole relaxation mechanism may partially contribute to some of the observed relaxation rates of lithium and cesium ions in solution. In cases where quadrupole relaxation dominates, an investigation of linewidths can yield information about the magnitude of the electric field gradient at the nucleus. Since electric field gradients are produced by ion-solvent and ion-ion interactions in solution, information which pertains to ion rotational and translational motion is obtained. It is experimentally possible to determine the product $(eQq)^2\tau_c$ (eQq is the quadrupole coupling constant and τ_c is the correlation time), but the separation of τ_c from $(eQq)^2$ cannot be made unless τ_c or $(eQq)^2$ are measured by other methods. Generally, independent measurements of τ_c or (eQq) are unavailable for alkali ions in solution.

To first order, the quadrupole moment along with an electric field gradient at the nucleus can perturb the Zeeman energy levels. Figure 5 shows the effect of quadrupole coupling on the energy levels of a nucleus with spin $I = 3/2$. The selection rule for the transition is given by $\Delta M = \pm 1$ and the degeneracy of the Zeeman transitions is lifted with this coupling. Experimentally, three transitions are observed for sodium in single crystals of

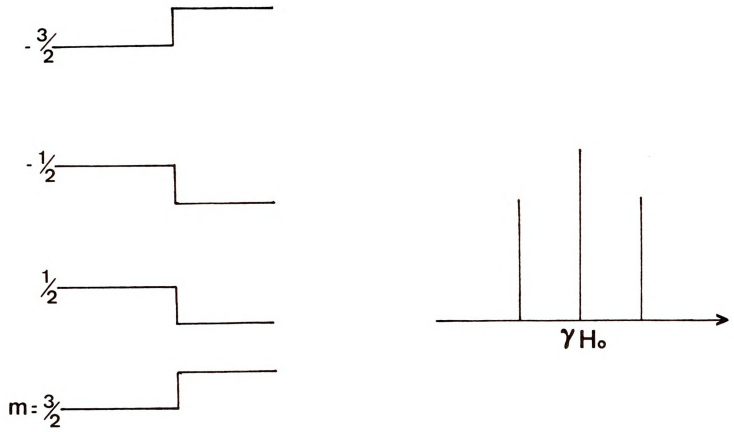

Figure 5. (a) Effect of quadrupole coupling upon nuclear Zeeman energies in first order. (b) Hypothetical spectrum corresponding to energy levels of (a).

$NaNO_3$[91] (hexagonal crystal structure). The NMR spectra of crystals such as the alkali halides do not exhibit quadrupole splitting since the crystals have cubic symmetry and no field gradient exists. In solution, the effect of quadrupole splitting is not observed since for normal liquids, the time scale of solvent fluctuations (which produce field gradients) is 4 to 5 orders of magnitude shorter than the time scale corresponding to the quadrupole coupling.

In this chapter we will describe some of the general features of alkali metal ion NMR. The description is by no means complete. It is only meant to give the necessary background for the NMR studies described in Chapters V and VI.

3.2 Shielding Constants of Alkali Metal Ions

The shielding constant, σ, is defined by $\omega_o = \gamma(1-\sigma)H_o$, where γ is the gyromagnetic ratio of the nucleus and H_o is the external magnetic field. When the gaseous atom is taken as the reference state, then $\sigma = 0$ and γ refers to that for the gaseous atom. A negative value for σ is interpreted as a paramagnetic (low field) shift relative to the reference state and correspondingly a positive value for σ is interpreted as a diamagnetic (high field) shift relative to the reference state. Note that this sign is opposite that frequently used to express chemical shifts but its use provides an internally consistent sign convention.

3.2.1. Alkali Metal Ions in Crystals

The shielding constant of alkali metal ions in crystals is paramagnetically shifted (shifted to lower field) from that of the free gaseous ion. In crystalline salts the chemical shift also depends upon the counter anion.[92] The factors governing these shifts are qualitatively understood, but are not well accounted for quantitatively. During the late 1950's and up to the mid 1960's a number of attempts had been made to calculate paramagnetic shielding constants for alkali metal ions in solid alkali halides. The starting point for all these calculations was Ramsey's expression[93] for the total shielding of a nucleus, given by

$$\sigma = \left(\frac{e^2}{2mc^2}\right)\left[\left(\Psi_o\middle|\sum_k \frac{r_k\hat{\ell}-\hat{r}_k\hat{r}_k}{r_k^3}\middle|\Psi_o\right)\right.$$

$$+ \sum_m (E_o - E_m)^{-1}\{(\Psi_o \mid \sum_k \hat{\ell}_k \mid \Psi_m)$$

$$(\Psi_m \mid \sum_k \frac{\hat{\ell}_k}{r_k^3} \mid \Psi_o) + (\Psi_o \mid \sum_k \frac{\hat{\ell}_k}{r_k^3} \mid \Psi_m)$$

$$\left.(\Psi_m \mid \sum_k \hat{\ell}_k \mid \Psi_o)\}\right], \qquad 3.1$$

where Ψ_o and Ψ_m represent the many-electron ground- and excited-state wave functions, E_o and E_m are the ground- and excited-state energies, $\hat{\ell}_k$ is the angular momentum

operator of the k^{th} electron and r_k is the radial distance of the k^{th} electron from the origin at the nucleus.

The first term in Equation 1 is the diamagnetic contribution to the total shielding. For a gaseous alkali metal ion, the diamagnetic shielding, σ_D, is proportional to the magnetic field produced at the nucleus by induced currents which arise from the Larmor precession of electrons in the external magnetic field. The second term is the paramagnetic contribution to the total shielding and is zero for an isolated gaseous alkali metal atom or ion. A paramagnetic shift is produced by introducing orbital angular momentum into the wavefunction. For alkali metal cations in alkali halide crystals and in solution, the paramagnetic contribution to total shielding is not zero. In the crystal, the wave functions are distorted from those of the hypothetical ideal crystal (considered as combinations of distinct positive and negative ions, each constituent ion having a spherically symmetric closed shell electronic configuration identical to that expected for the isolated ion, with the complete assembly being held together by electrostatic forces) and hence orbital angular momentum is introduced and produces a paramagnetic shift. As can be seen from Equation 3.1, both σ_D and σ_p are tensor quantities in the general case. For all the systems discussed, cubic symmetry is assumed and the scalar part will be used. In order to evaluate σ_p, a knowledge of Ψ_m is needed. Since in almost all cases, Ψ_m is not known,

Ramsey[93] introduced the average-energy approximation. With the assumption of cubic symmetry and the average energy approximation, the total shielding is now given by

$$\sigma = \frac{e^2}{3mc^2}\left(\Psi_o \mid \sum_k \frac{\ell}{r_k} \mid \Psi_o\right) + \frac{e^2}{\Delta m^2 c^2}\left(\Psi_o \mid \sum_{kk'} \frac{\hat{\ell}_{kk'}}{r_k^3} \mid \Psi_o\right), \qquad 3.2$$

where Δ is the average excitation energy.

Two models have been proposed for the origin of magnetic shielding based on the perturbation-theory approach of Ramsey. The first is the charge-transfer-covalency model due to Yosida and Moriya,[94] and the second the overlapping-ion model by Kondo and Yamashita (KY).[95] Ikenberry and Das[96] have pointed out that calculations of quadrupole coupling constants in diatomic-alkali-halide molecules clearly indicate that there is little, if any, covalent bonding of the charge-transfer type in these crystals. Thus, in the most recent calculations, only the KY model has been considered. The KY model assumes that short range repulsive forces between adjacent ions cause a change in the σ_p value of M^+ upon going from the gas phase ($\sigma_p = 0$) to the nonideal crystalline state. From the KY model only overlap between outermost s and p orbitals for both positive and negative ions is considered. Since inner-core orbitals are tightly bound and do not extend appreciably into the region between

the ions, they remain spherical and are not considered. Also calculations show that the change in σ_D for M^+ gas → M^+ crystal is two to three orders of magnitude less than σ_p.[96] Thus, for crystal σ ($M^+_{crystal}$ vs M^+_{gas}) ≈ σ_p (assuming a reference state $\sigma = \sigma_p \approx 0$ for the gaseous metal ion). Under these conditions with the application of Equation 3.2, Ikenberry and Das[96] have calculated chemical shifts for Rb^+ ions in halide crystals. Their final expression for σ_p ($M^+_{crystal}$ vs M^+_{gas}) is given as follows[97]

$$\sigma_p = \frac{16\alpha^2}{\Delta} \langle r_i^{-3} \rangle_p [|S_{ij}^{\sigma s}|^2 + |S_{ij}^{\sigma\sigma}|^2 + |S_{ij}^{\pi\pi}|^2 - 2|S_{ij}^{\sigma\sigma} - S_{ij}^{\pi\pi}|], \qquad 3.3$$

where α is the fine structure constant, $\langle r_i^{-3} \rangle_p$ is the expectation value for an outer p-electron of the central ion i, S_{ij} are the two-center overlap integrals between outer p orbitals of the central ion i and the outermost s and p orbitals of other ions j, s represents an s orbital, and σ and π are p orbitals parallel with the line of nuclear centers and perpendicular to the line of nuclear centers respectively.

In summary, the features that are important for magnetic shielding as given by Equation 3.3 are:

1. The expectation value $\langle r_i^{-3} \rangle_p$ for the outer p orbital of the central ion.

2. The average excitation energy Δ, usually taken to be the energy of the np → np + 1 electronic transition of the central ion.
3. Overlap between neighboring ions, which depends upon the internuclear separation.

The average excitation energy determines the amount of excited state p character introduced into the wavefunction. This causes a deformation from spherical symmetry and produces the paramagnetic shift. Some values of $\langle r_i^{-3} \rangle_p$ and Δ along with their ratios are shown in Table I. Experimentally, the chemical shift range increases as atomic number increases and this increase is in agreement with the increasing values of $\frac{1}{\Delta} \langle r_i^{-3} \rangle_p$.

At the time Ikenberry and Das, and Hafmeister and Flygare performed calculations for magnetic shielding of ions in crystals, there were no experimental values available for $\sigma(M^+_{crystal}$ vs $M^+_{gas})$. It has been only within the last few years that these values could be obtained. Experimental values were determined from a combination of precision NMR,[99-101] atomic beam,[102] and optical pumping[103,104] experiments. From these measurements it is now possible to obtain values for $\sigma(M^+_{H_2O}$ vs $M_{gas})$ and since many determinations of $\sigma(M^+_{crystal}$ vs $M^+_{H_2O})$ have been reported, an experimental value for $\sigma(M^+_{crystal}$ vs $M_{gas})$ can be obtained. However, calculated values of $\sigma(M^+_{crystal})$ from theory are referenced to the gaseous ion. The difference between

Table I. Values of the average excitation energy Δ, and the expectation value $\langle r_i^{-3} \rangle_p$ for alkali metals.[a]

Ion	$\langle r_i^{-3} \rangle_p$ a.u.	Δ Rydbergs	$\frac{1}{\Delta} \langle r_i^{-3} \rangle_p$
Na^+	16	2.72	5.9
K^+	12.94	1.62	7.98
Rb^+	20.22	1.47	13.8
Cs^+	23.42	1.25	18.7

a) All values taken from Reference 98.

$\sigma(M^+_{crystal}$ vs $M_{gas})$ and $\sigma(M^+_{crystal}$ vs $M^+_{gas})$ is σ_D $(M^+_{gas}$ vs $M_{gas})$ which is the diamagnetic contribution caused by the addition of an electron to a gaseous ion. The term σ_D $(M^+_{gas}$ vs $M_{gas})$ can be reliably calculated from accurate atomic wavefunctions by applying the first term in Equation 3.2. Values for these diamagnetic shielding constants for Li, Na and K are less than 5 ppm and tend to get smaller as atomic number increases.[105] Thus, for Rb and Cs, the assumption $\sigma(M^+_{crystal}$ vs $M^+_{gas}) \approx \sigma(M^+_{crystal}$ vs $M_{gas})$ is reasonable. Comparison of the chemical shift values calculated by Hafmeister and Flygare,[106] and Ikenberry and Das[96,97] with the measured values of $\sigma(M^+_{crystal}$ vs $M_{gas})$ are given in Table II. The agreement is qualitative only. However, it should be pointed out that theoretical values for the change in shielding with pressure for alkali halide crystals[96,97,106] and for xenon gas[107] are in much better agreement with the experimentally observed chemical shift changes. From these calculations it appears that the KY model offers a reasonable explanation of magnetic shielding.

3.2.2. Alkali Metal Ions in Solution

Solvated cations also undergo large paramagnetic shifts from the gaseous ions as shown in Table II for rubidium and cesium. Changes in the diamagnetic shielding as a function of solvent are expected to be small compared to changes in σ_p.[109,110] Thus, as for the crystals, changes

Table II. Experimental and calculated chemical shifts for rubidium and cesium ions in halide crystals and aqueous solution.

Ion	Lattice	$\sigma_{exp}(M^+_{crys}$ vs. $M_{gas})^a$ δ(ppm)	$\sigma_{calc}(M^+_{crys}$ vs. $M^+_{gas})$ δ(ppm)	Solvent	Conc. (M)	$\sigma_{exp}(M^+_{solv}$ vs. $M_{gas})$
Rb^+	RbBr	-359	-214[b]	H_2O	∞ dil	-211.6[d]
Rb^+	RbF	-290	-140[c]			
Rb^+	RbCl	-319	-130[c]			
Rb^+	RbBr	-359	-130[c]			
Rb^+	RbI	-379	-120[c]			
Cs^+	CsF	-464	-260[c]	H_2O	∞ dil	-344.3[d]
Cs^+	CsCl	-537	-270[c]			
Cs^+	CsBr	-582	-260[c]			
Cs^+	CsI	-626	-250[c]			

a) Experimental values were obtained by summing $\sigma_{exp}(M^+_{crys}$ vs $M^+_{sat\ aq})$, $\sigma_{exp}(M^+_{sat\ aq}$ vs $M^+_{\infty\text{-dil aq}})$, and $\sigma_{exp}(M^+_{\infty dil\ aq}$ vs $M_{gas})$ from References 92, 108 and 102.

b) Reference 96.

c) Reference 106.

d) Reference 102.

in magnetic shielding are reflected predominantly through changes in σ_p.

An interesting correlation between the Gutmann donor number (D.N.) and the relative chemical shift of sodium ions in different solvents has been reported.[111,112] The Gutmann donor number of a solvent is a measure of its Lewis basicity.[113] As the D.N. increases, the solvent donor ability increases and an increasing paramagnetic shift of the sodium cation is observed. A linear correlation between Gutmann's donor number and the relative magnetic shielding of sodium ion in different solvents is observed.

For sodium, the solvent effect on the magnetic shielding occurs primarily in the first solvation or coordination layer of the sodium cation. If a sodium is trapped within the cavity of a complexing agent such as C_{222} (the first coordination layer of solvent is completely replaced by C_{222}), the chemical shift of the cation is nearly solvent independent. On the other hand, the free sodium ion chemical shifts change appreciably in these solvents as shown by Table III. The same behavior is observed for lithium ion complexed by a smaller cryptand ligand.[114]

Calculation of shielding constants for alkali metal ions in solution is a much more difficult task than for ions in crystals. As a consequence, only one semiquantitative calculation based upon the KY model has been performed for Rb^+ in aqueous solution. The theoretical value for $\sigma(Rb^+_{H_2O}$ vs $Rb^+_{gas}) = -65$ ppm is in poor agreement with the

Table III. Chemical shifts of free and cryptated sodium ions in solution.

Concentration (M)	Solvent	$\sigma(Na^+_{solv}$ vs Na^+_{∞}-dil-$H_2O)$ (ppm)
0.2 NaI	H_2O	-0.1
0.6 NaBr	EDA	-13.7
0.4 $Na\phi_4B$	THF[a]	+7.4
0.2 $Na\phi_4B$	PYR[b]	-0.9
0.2 $Na^+C_{222}I^-$	H_2O	+8.5
0.3 $Na^+C_{222}Br^-$	EDA	+10.6
0.2 $Na^+C_{222}\phi_4B^-$	THF	+11.9
0.2 $Na^+C_{222}\phi_4B^-$	PYR	+12.4

a) THF = tetrahydrofuran.

b) PYR = Pyridine.

experimentally determined value $\sigma(Rb^+_{H_2O}$ vs $Rb_{gas}) = -212$ ppm.[97] However, the model used for the calculation is one in which a Rb^+ is surrounded by six water molecules with the oxygen end oriented towards Rb^+ and the O-H bonds pointing away. The wavefunctions for H_2O were based upon a model of localized electron-pair bonds. In view of the uncertainty of the model and the crudeness of the wavefunctions, the poor agreement between theoretical and observed values is understandable. It seems that Equation 3.3 at least qualitatively predicts the effects of a paramagnetic shift for ions in solution.

3.3 Quadrupole Relaxation of Alkali Metal Ions in Solution

The magnetic relaxation of nuclei with spin greater than 1/2 is almost always caused by the interaction of their electric quadrupole moment with the electrical field gradient at the nuclear site. Thermal motion of ions and solvent molecules can produce fluctuating electric field gradients at the nuclear site. The time evolution of these fluctuations contain Fourier frequency components which are at the Larmor frequency of the alkali metal ion and hence can induce a transition through coupling with the quadrupole moment. The quadrupole relaxation rate for a nucleus in the motionally narrowed limit ($\omega\tau_c << 1$) is given by[115]

$$\frac{1}{T_1} = \frac{3}{40}\,\frac{2I+3}{I^2(2I-1)}\,\left(1+\frac{\eta^2}{3}\right)\,\left(\frac{eQ}{h}\,\frac{\partial^2 V}{\partial Z'^2}\right)\tau_c, \qquad 3.4$$

where I is the spin of the nucleus, η is the asymmetry parameter (η = 0 for a symmetric field gradient), Q is the quadrupole moment of the nucleus, $\partial^2V/\partial Z'^2$ is the Z component of the electric field gradient at the nucleus, and τ_C is the correlation time which characterizes the fluctuations of the field gradient. For solutions, ($\omega\tau_C << 1$), $T_1 = T_2$, and the resonance lineshape is Lorentzian.

The field gradient at the nucleus can be expressed as $\partial^2V^o/\partial Z^2$ $(1 + \gamma_\infty)$ where γ_∞ is the Steinheimer antishielding factor.[117] The term $\partial V^o/\partial Z^2$ represents the field gradient at the nucleus produced by an external charge. The external charge also causes deformation of the spherical symmetry of the inner closed shell electrons and this leads to the correction term $(1 + \gamma_\infty)$. Values of $(1 + \gamma_\infty)$ are calculated from theory and range from 0.74 for Li^+ to 111 for Cs^+.[117] Thus the effect of $(1 + \gamma_\infty)$ can be enormous.

Information obtained from the linewidth contains the product $(eQ/h\ \partial^2V/\partial Z'^2)^2\tau_C$. Only for cases where τ_C can be determined from other measurements can the field gradient, $\partial^2V/\partial Z'^2$, be determined. This has been done recently by Kintzinger and Lehn[118] for sodium nuclei encapsulated in the C_{222} cryptand. The ^{13}C relaxation times $T_1(^{13}C)$ of the CH_2 carbons of the sodium cryptate complex were measured. The dipole-dipole relaxation equation

$$\frac{1}{T_1}(^{13}C) = n^2h^2\gamma_H^2\gamma_C^2r_{CH}^{-6}\tau_C' \qquad 3.5$$

can be used to obtain τ_c' values from the ^{13}C relaxation rates. Then, by making the assumption that, in fairly rigid complexes τ_c' also represents reorientational motions which modulate the ^{23}Na quadrupolar interaction, they calculated the quadrupole coupling constant.

For a simple process one would expect that $\tau_c = A'e^{-E_r/RT}$ where E_r is an activation energy for solvent reorganization.[98] If the value of the quadrupole coupling constant is assumed not to change with temperature, then the relaxation rate will vary exponentially as a function of temperature. This behavior is observed for sodium bromide in ethylenediamine solution as shown in Figure 6.

For many monodentate liquids the infinitely dilute sodium linewidth varies from 4 to 30 Hz at 25°C. When the cation is placed in an environment which does not have cubic symmetry, such as within the cavity of a crown ether (see Figure 1), the linewidth increases by large amounts. This increase is caused by asymmetry of the electric field at the sodium nucleus because of the planar structure of crown ethers. If a bicyclic ligand such as C_{222} cryptand is used, the Na^+C_{222} linewidth is not broadened nearly as much as in the crown case. This indicates that the electric field produced by C_{222} is much more symmetric than that produced by crown complexes.

The difficulty in predicting relaxation rates from Equation 3.4 is in the evaluation of the field gradient. Electrostatic models have been proposed[119-123] in which

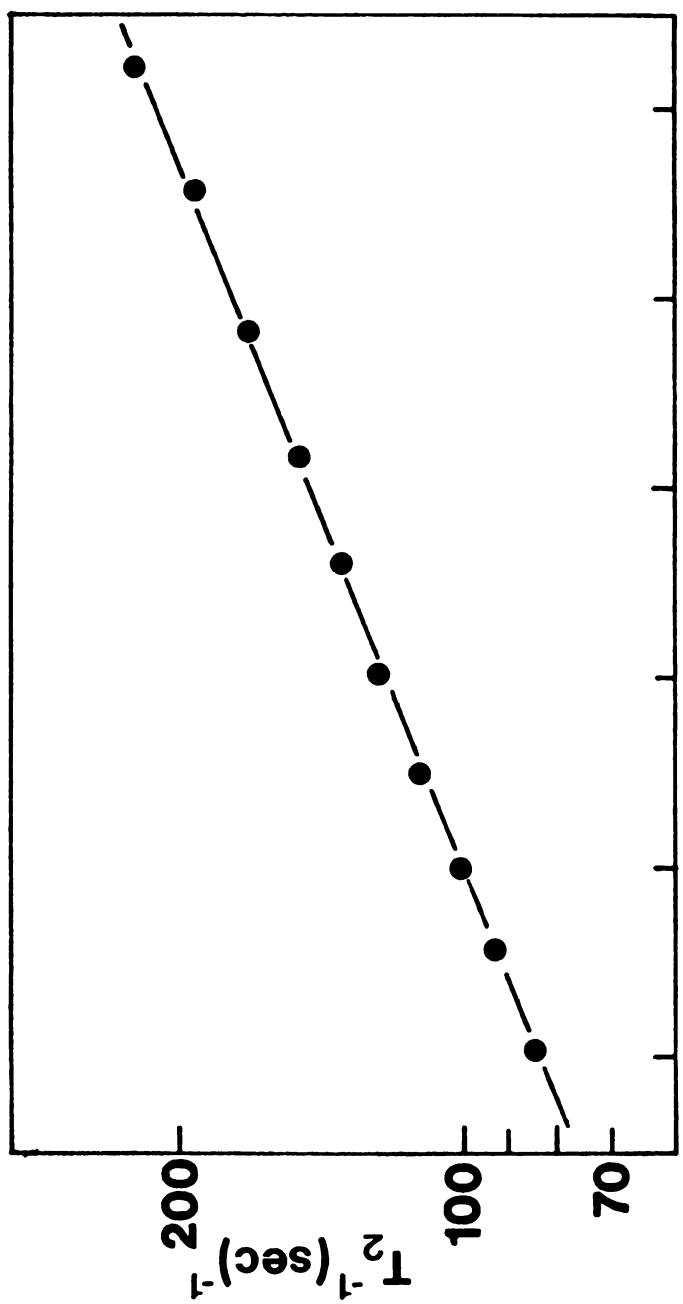

Figure 6. Semilog plot of $1/T_2$ for ^{23}Na vs the reciprocal absolute temperature for a solution containing 0.15 M NaBr in EDA.

the field gradients are produced by electric dipoles or point changes. Deverell[110] has proposed a model in which repulsive forces between molecules and ions are related to a distortion from spherical symmetry of the ionic electron cloud which results in the production of a field gradient. With this model Deverell was able to derive a correct order of magnitude for the relaxation rate of the nucleus. The most recent calculations have been done by Hertz,[124] who assumes an electrostatic model. Hertz includes water-water correlations and ion-ion correlations in his calculations. Calculated values from his electrostatic model agree surprisingly well with the experimentally observed relaxation rates for a number of quadrupole relaxed nuclei. However, it is difficult to determine how much of this agreement is caused by the presence of parameters in the model which must be estimated and cannot be independently measured.

IV. EXPERIMENTAL

4.1 General Techniques

4.1.1. Glassware Cleaning

All glassware was cleaned by a two step procedure (except glassware used with normal salt solutions). First, the glassware was pre-rinsed for several minutes with a solution of HF cleaner (33% HNO_3, 5% HF, 2% acid soluble detergent, 60% water by volume) followed by a thorough rinsing with distilled water. The glass vessels were then filled with boiling aqua regia which remained in the vessel at least six hours. They were then thoroughly rinsed with distilled water (five times) followed with a second rinsing with conductance quality water (five times). The vessels were allowed to dry over night in an oven (110°).

4.1.2. Vacuum Techniques

Standard high vacuum techniques were employed in this work. Pressures of 10^{-6}mm Hg were obtained in Pyrex vacuum lines by using a dual stage mechanical pump and a two-stage oil diffusion pump. Greaseless Teflon valves (Fischer-Porter, Delmar, and Kontes types) were employed for high vacuum work to avoid contamination of metal-amine and metal-ether samples with grease.

4.2 Metal Purification

Alkali metals were purchased as follows:

Na: J. T. Baker Co. (99.99%).

Rb: Fairmount Chemical Co.

Cs: A gift from Dow Chemical Company.

All metals were distilled several times before use.

4.2.1. Storage of Alkali Metal in Small Quantities

4.2.1.1. Sodium Metal - Sodium was cut with a knife into small pieces. The pieces were placed into the bottom of a quartz tube (40mm O.D.) as shown in Figure 7. Twenty to thirty smaller diameter Pyrex tubes were sealed at one end and placed into the quartz tube on top of the sodium with their open ends down. The system was evacuated to a pressure of 10^{-5}mm Hg and then the sodium was gradually heated until it formed a liquid pool at the bottom. Next, helium gas was introduced at a pressure of 1/2 to 1 atm. to force liquid sodium into the small Pyrex tubes. After cooling, the small diameter tubes were then exposed to the atmosphere and small quantities of relatively pure sodium metal could be isolated by simply cutting a specified length of Pyrex tubing.

4.2.1.2. Cesium and Rubidium Metals

Cesium and rubidium burn very easily in air. Large ampoules (greater than 20 gms) of these metals can be

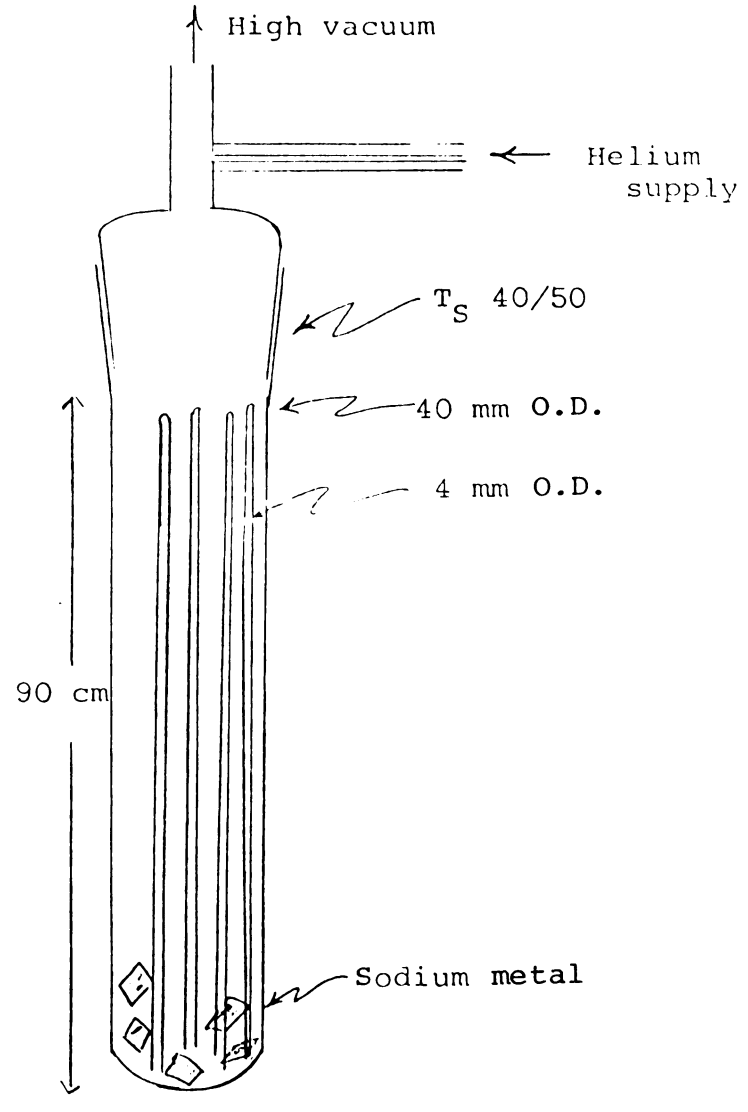

Figure 7. Apparatus for the preparation of storage tubes for sodium metal.

subdivided into ampoules containing 10 to 20 gms metal by the method described by Dewald.[125] To obtain even smaller samples the apparatus shown in Figure 8 was used. An ampoule containing the metal was scored with a glass-cutter and placed into an open-ended Pyrex tube #1 at position A. The Pyrex tube was then connected to a second tube #2, by using a piece of flexible heat shrink tubing (Pope Scientific Company), which made a vacuum tight seal. The system was evacuated to a pressure of at least 10^{-5}mm Hg and the glass ampoule was moved to position B where it was broken. The fragmented ampoule was next moved to position C and two vacuum seal-offs were made at D and E. The metal could then be melted into the long Pyrex tube and a small quantity could easily be obtained by sealing off a portion of this tube.

4.3 Solvent Purification

Ethylendiamine (EDA) was purified by the method described by DeBacker.[88] Tetrahydrofuran was dried over calcium hydride for at least 48 hours. After initial drying, THF was distilled into a vessel containing benzophenone and an excess of sodium-potassium alloy. A blue-purple color resulted, due to formation of the ketyl, and served as an indicator of dryness. If the blue color faded, the THF was redistilled onto a fresh mixture of benzophenone and Na-K alloy. These blue solutions were stable for months.

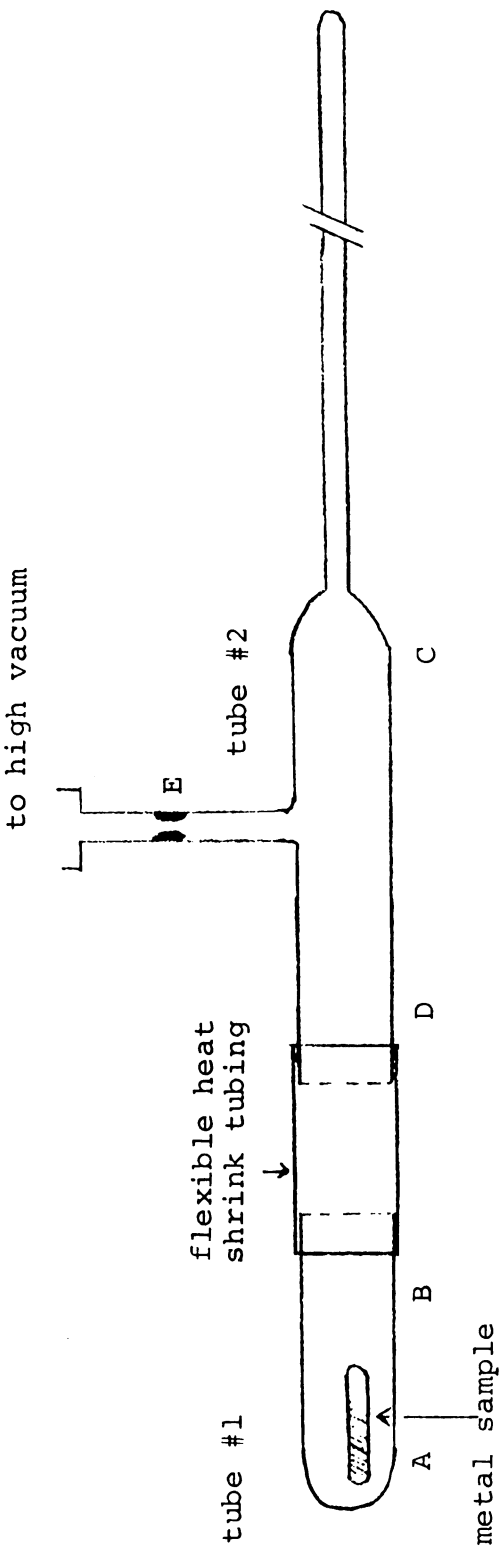

Figure 8. Apparatus for preparation of small ampoules of rubidium and cesium metal.

Methylamine and ethylamine were dried over calcium hydride and then vacuum-distilled into a vessel containing Na-K alloy. If a blue solution did not form, the solvent was repeatedly vacuum distilled into vessels containing fresh Na-K alloy until a stable blue solution did form. Once a stable blue solution formed (usually no observation of color change after one to two days is a good criterion for stability) the solvents were distilled into Pyrex storage bottles. Pyridine was refluxed over granulated barium oxide and then fractionally distilled in a nitrogen atmosphere.

4.4 Preparation and Purification of 2,2,2 Cryptand

During the progress of this research, 2,2,2 cryptand was not commercially available and had to be synthesized by following a brief outline in the literature.[34] The synthesis was carried out in collaboration with M. T. Lok and F. J. Tehan. Several major improvements in the procedure were developed by us in the process of synthesizing the material. The details are reported in the Ph.D. thesis of M. T. Lok[52] and will not be described here. However, an improvement of the purity of one of the precursors is described.

Triglycolic acid ($HOCOCH_2OCH_2CH_2OCH_2OCOH$) is a precursor in the synthesis of the 2,2,2 cryptand molecule. The diacid is produced by oxidation of the corresponding

glycol with 60% nitric acid and a vanadium catalyst (NH_4VO_3). Many by-products are formed in the oxidation and it is difficult to separate the acid from these by-products. The following procedure, partly based on a synthesis reported by Micovic,[126] enables us to obtain triglycolic acid with reasonable purity.

4.4.1. Synthesis of Diethyl Ester of Triglycolic Acid

Add 256 gms of crude diacid to a one neck, 2 liter flask equipped with a magnetic stirring bar, a downward condenser and a collection pot containing 253 gms of K_2CO_3. Add 570 ml of 100% ethyl alcohol, 285 ml of reagent grade toluene and 1.3 ml of reagent grade H_2SO_4 to the flask. The flask is heated and an azeotropic mixture of ethanol, toluene and water distill at 75°C. The heating is continued until 300 to 400 ml of distillate are collected and then it is suspended. The distillate is shaken well with K_2CO_3, next filtered through a fritted glass disk, and is poured back into the reaction flask. The mixture is heated again until 95% of the volatile distillate is removed. The solution is allowed to cool slightly and then it is vacuum distilled (without fractionation).

Next the liquid is redistilled with an efficient fractionation column. The pure diethyl ester boils at 142° under a pressure of 4 mm Hg. The PMR spectrum of the neat liquid consists of a triplet ($-CH_3$) at 1.3 ppm, a singlet ($-OC\underline{H}_2C\underline{H}_2O$) at 3.8 ppm, a singlet ($-\overset{O}{\overset{\|}{C}}-C\underline{H}_2-O$) at 4.2 ppm

and a quartet ($-O-C\underline{H}_2-C\underline{H}_3$) at 4.25 ppm.

4.4.2. Hydrolysis of the Diester

Add 130 ml of diethyl ester, 130 ml of distilled water and 1.3 gms Dowex 50-WX-2 ion exchange resins to a 3-neck 500 ml flask. The solution is heated to a temperature of approximately 90-95°. The diester is not 100% miscible in water and two phases appear at the start of the reaction. After an hour of heating the solution becomes one phase and liquid starts to boil off between 70-95°C. The distillate is a mixture of water and ethanol. When all the ethanol is used, the boiling point of the distillate goes up to 100° and the hydrolysis is completed. Next, the residual solution is filtered to remove the ion exchange resin and then the remaining water is stripped off with a roto-evaporator. The viscous liquid is placed under vacuum until it solidifies. The PMR of the diacid in D_2O shows two sharp singlets with an area ratio of 1:1 and the melting point range is 65-75°C.

4.4.3. Purification of 2,2,2 Cryptand

2,2,2 Cryptand is purified by recrystallization in hexane followed by a vacuum sublimation. If the crude 222 cryptand contained precursor impurities such as the monocyclic diamine,

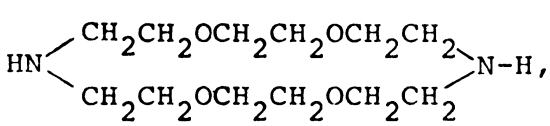

recrystallization was found to be effective for separating a major portion of this impurity. However, some residual

diamine (approximately 5%) could always be detected by PMR studies. The 2,2,2 cryptand in this work gave a PMR spectrum that did not show impurities and had a melting point range of 70.2-71.1°C.

4.5. Synthesis of a Crystalline Salt of the Sodium Anion

The first authentic salt containing a sodium anion was prepared by the following procedure:

A Pyrex vessel of the design shown in Figure 9 was used to prepare polycrystalline samples of $NaC^+ \cdot Na^-$ in which C is 2,2,2 cryptand (see Figure 1). A convenient amount (50 mg to 1 g) of C was placed in compartment B and sodium metal was placed into the side-arm shown which was then sealed off. The vessel was evacuated to $\sim 10^{-6}$ torr and the sodium was distilled into compartment A. Ethylamine was distilled into B by cooling B with a dry-ice isopropanol bath. The quantity of ethylamine (EA) used was adjusted so as to form a 0.1 M solution of C. After removal from the vacuum line, the solution of C in ethylamine was transferred through the glass frit into compartment A. Upon contact with the sodium mirror a dark blue solution formed immediately. The contact with sodium was maintained with shaking for several minutes between 0° and -60°C. The solution was then warmed to 0° to 10°C and allowed to filter through the frit by cooling B. Upon cooling, shiny gold-colored crystals of $Na^+C \cdot Na^-$ formed.

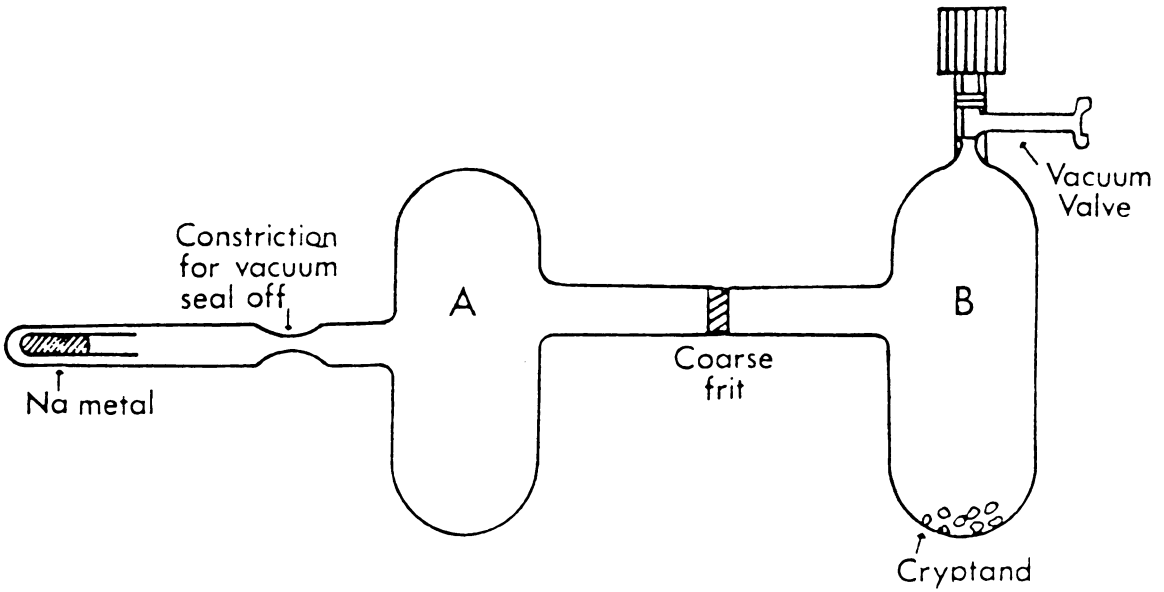

Figure 9. Vessel for preparation of $Na^{+}C \cdot Na^{-}$.

The excess liquid was again poured into A to insure that all of the sodium which could be dissolved was in solution. Since sodium is insoluble in ethylamine in the absence of C, the solubilization stopped when the reaction

$$2Na\ (s) + C \rightarrow NaC^{+} + Na^{-}$$

had used up all of the free complexing agent, C.

After the final crystallization process, the supernatant solution was poured into A, the vessel was again connected to a vacuum line and all of the ethylamine was removed by distillation. Purified diethyl ether (purified in a similar way to THF) was distilled into B. The crystals were only very slightly soluble in diethyl ether, which therefore serves as a convenient washing solvent. The very light blue solution formed in diethyl ether was poured into A and then redistilled back into B. This was repeated several times until all traces of white or blue material had been removed from the crystals. The diethyl ether was poured into A and then distilled out of the vessel. Pure crystals of $Na^{+}C \cdot Na^{-}$ remained in the vessel. The elemental analysis, some properties, and the crystal structure have been reported elsewhere.[36-38,52,53]

4.6 Solution Preparation

4.6.1. Salt Solutions for NMR Exchange Studies

Reagent grade NaBr, NaI and $Na\phi_4B$ were dried and used without further purification. Samples were prepared in a dry box or glove bag under an inert atmosphere of dry nitrogen or argon. 10 mm O.D. thin-wall high resolution NMR tubes purchased from Wilmad Glass Company were modified by placing a standard ground glass joint at the open end. This provided an air-tight seal.

4.6.2. Preparation of Metal Solutions

Figure 10 shows the Pyrex apparatus used in most of the alkali anion NMR studies. Preparation of sodium solutions was done by two methods. In the first method, the 2,2,2 cryptand was dropped into the vessel and rested on the glass frit. An excess of sodium metal was sealed into the glass side arm and the entire vessel was evacuated. Sodium was distilled through the side arm and into bulb A to form a shiny mirror. Ethylamine was distilled into B and a method similar to that discussed in 4.5 was used to form a blue solution, which precipitated gold crystals at dry ice temperatures. The crystals could be rinsed off with diethyl ether as discussed previously and then any of the solvents could be distilled into the vessel to form a blue solution which contained $Na^+C \cdot Na^-$ ($\sim$0.1 to 0.2 M). The solution was then poured into the bottom of the NMR

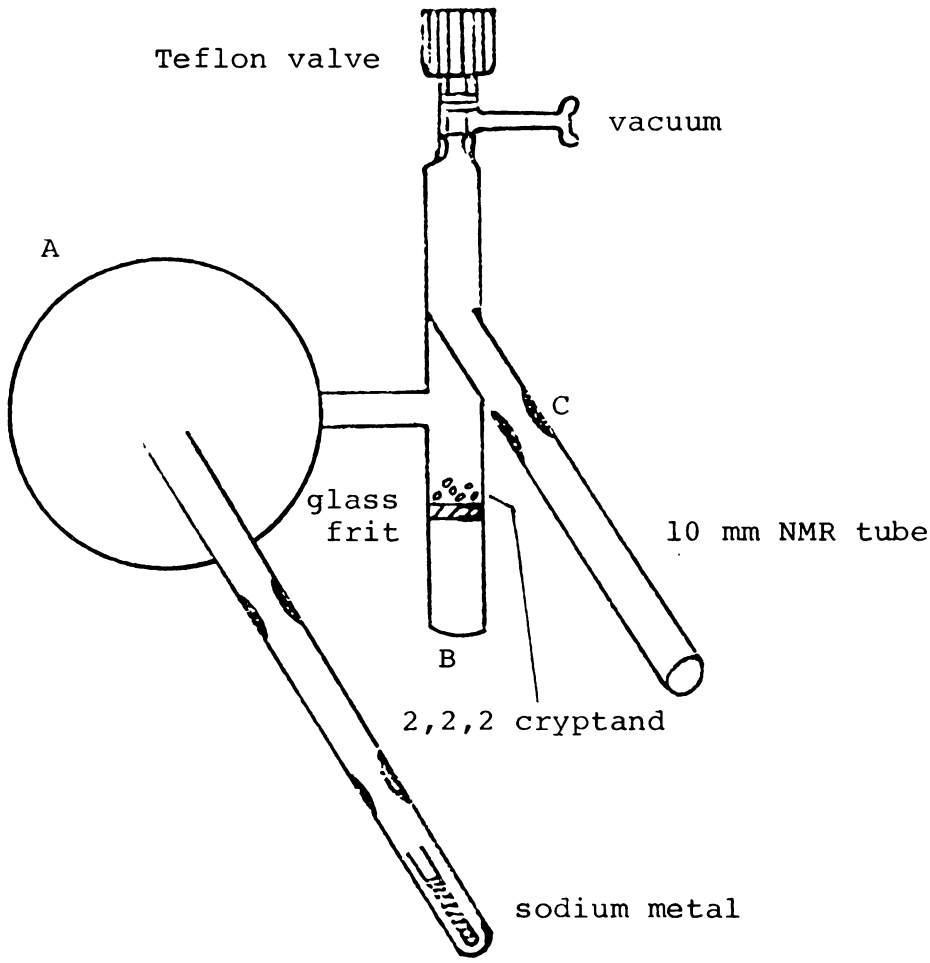

Figure 10. Vessel for preparation of NMR samples.

tube and frozen with liquid nitrogen. The vessel with its frozen solution was pumped to a pressure of $\sim 10^{-5}$ mm of Hg and the NMR tube was sealed off at constriction C.

In the second method, the solutions were prepared directly by distilling the solvent to be used into the vessel containing sodium and 222 cryptand. The 2,2,2 cryptand was dissolved and a blue solution was formed with the previously discussed method. However, in this case no crystals were isolated, the blue solution was poured into the NMR tube and sealed off under vacuum as before. Cesium and rubidium anion solutions were prepared by the second method. Although no gold crystals of $RbC_{222}^{+} \cdot Rb^{-}$ and $CsC_{222}^{+} \cdot Cs^{-}$ were observed to precipitate in solution, shiny bronze films were observed on the glass walls of rubidium samples and copper colored films were observed on the glass walls of cesium samples. Concentrations of all the solutions were adjusted to approximately 0.1 M in 2,2,2 cryptand. The equilibrium

$$C_{222} + \text{excess } M \overset{\text{solvent}}{\rightleftarrows} (C_{222}M^{+}) + (M^{-})$$

lies very far to the right for all metals and all solvents used.

Sodium solutions were stable at temperatures of +5°C for several days. Rubidium and cesium solutions were stable at dry ice temperatures for a week, but at ice temperatures decomposition occurred within an hour. Thus, the working temperatures of rubidium and cesium solutions were maintained

below -30°C where no significant amount of decomposition occurred on the time scale of NMR experiments (3 ∿ 6 hrs.).

4.7 The NMR Spectrometer

A pulsed multinuclear NMR spectrometer was used for most of the studies. The design is similar to one reported by Traficante.[127] A block diagram of the spectrometer is shown in Figure 11. The spectrometer consisted of three main parts. The first is a tuned transmitter/receiver section which operates at 56.44 MHz. The second part consisted of a network of double balanced mixers coupled to a frequency synthesizer. The third part is a wideband transmitter/receiver network coupled to a single coil tunable probe. A magnet from a Varian DA-60 spectrometer was used and maintained at 14.09 Tesla. With the mixing network, the broad band amplifiers and tunable probe it was possible to observe NMR signals in the range of 5 to 30 MHz. Changing frequencies simply required adjustment of the probe, the tunable power amplifier and the frequency synthesizer (which could be done in less than 15 minutes).

A key feature of the spectrometer is the external lock. In collaboration with David Wright a small single coil probe (lock probe) was constructed and tuned to the proton frequency. The probe was filled with doped water (linewidth approximately 4 Hz) and made to insert into the main NMR probe. The lock probe was connected to the normal

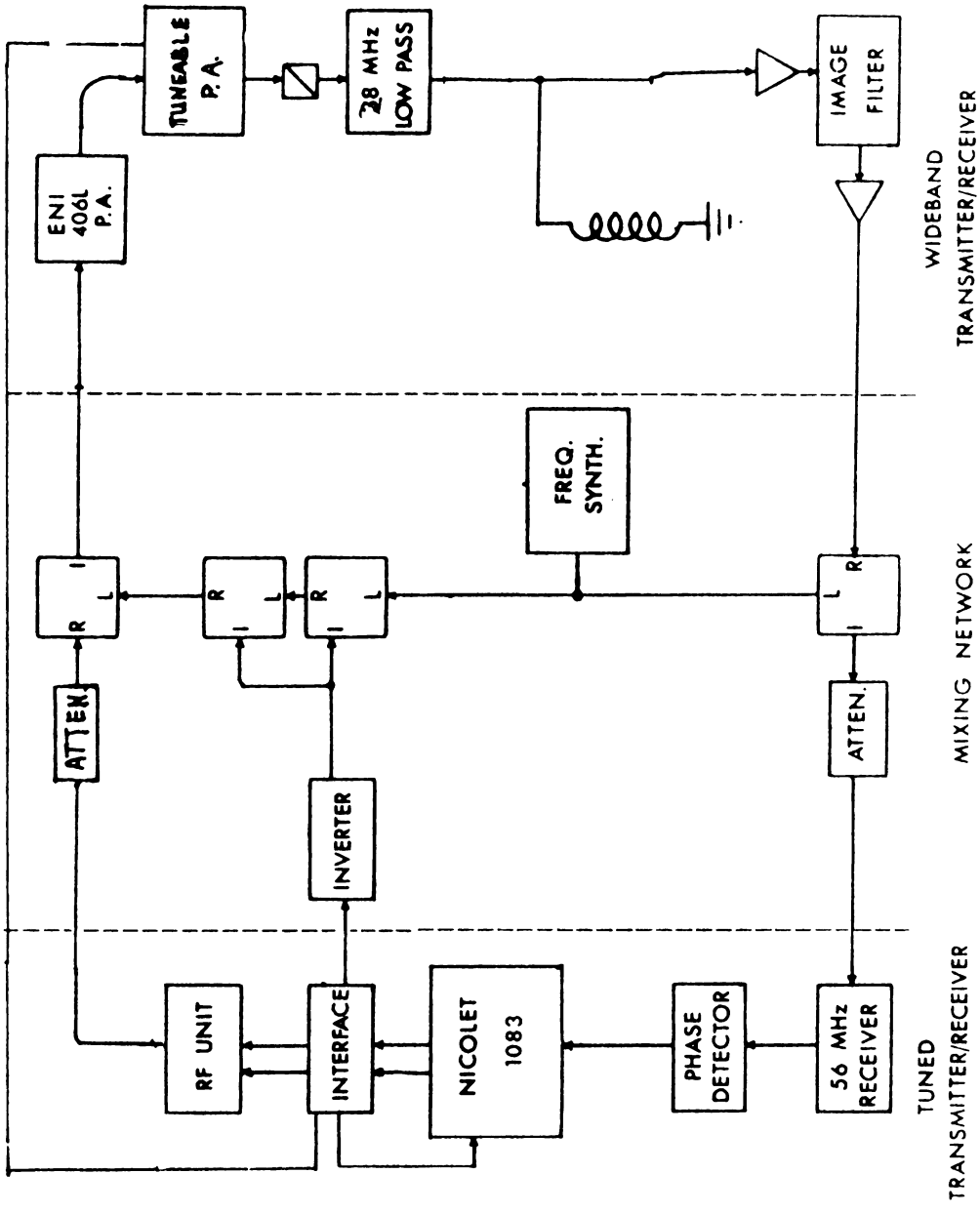

Figure 11. Block diagram of the multinuclear magnetic resonance spectrometer.

proton lock circuitry of an unused Varian DA-60 spectrometer. In this manner it was possible to lock the magnetic field on a proton signal and perform magnetic resonance experiments in the frequency range of 5 to 30 MHz. The maximum drift in an eight hour period was less than 6 Hz. The details of the external lock probe construction are given in David Wright's Ph.D. thesis.[128]

The spectrometer itself is controlled by a Nicolet 1080 computer system equipped with a Diablo magnetic disk. The hard-wired interface and software are described elsewhere.[128]

4.8 Temperature Control and Calibration

Temperature regulation was accomplished by using a standard Varian heater-sensor and V-4343 variable temperature controller. Temperatures were measured with a calibrated Doric digital thermocouple. A thermocouple was placed in a fixed position inside the probe, at a height which is just below the bottom of a sample tube. To make sure that the temperature at the thermocouple and the temperature at the sample tube were the same, a calibration procedure was used. A mercury thermometer and a thermocouple were placed inside the bottom of an NMR tube with 1 ml of solvent. The thermometer bulb and thermocouple were positioned at the center of the receiver coil of the NMR probe. The temperature was varied from 0° to 100°C and the thermometer reading along with the readings from

the thermocouples inside and outside the sample tube were recorded. The results are given in Table IV. From these results, it was not felt necessary to perform any temperature correction and all thermocouple readings were used as read.

4.9 Data Reduction

Free induction decays were stored on magnetic disk. The data were Fourier-transformed without applying smoothing or exponential weighting. The transformed data were zero-order phase corrected and punched onto paper tape with a modified version of RELAX 2 (a program written by David Wright).[128] The modification to RELAX 2 is given in Appendix A. The data from paper tape were punched on keypunch cards in octal format. The octal formatted data were converted to decimal format by program CONVERT (Appendix B). The decimal formatted data were analyzed by a generalized weighted non-linear least-squares program (KINFIT).[129]

Table IV. Temperature calibration for NMR.

Thermometer (°C)	Inside Thermocouple (°C)	Outside Thermocouple (°C)
+4.1	+2.9	+2.9
8.5	7.6	7.9
13.2	12.3	12.3
18.8	18.2	18.3
26.0	26.0	25.9
24.1	23.7	23.7
31.9	32.0	32.1
37.9	37.7	37.7
47.2	47.0	46.9
51.9	51.7	51.5
57.0	56.9	56.6
61.7	61.6	61.4
66.4	66.3	66.2
73.4	73.4	73.2
78.4	78.6	78.3
86.5	86.7	86.3
93.9	94.3	93.9
98.9	99.4	99.1

V. SODIUM-23 NMR STUDY OF SODIUM ION - SODIUM CRYPTATE EXCHANGE RATES IN VARIOUS SOLVENTS

5.1 Introduction

Macrocyclic polyethers (crown ethers), first synthesized by Pederson,[32] and macroheterobicyclic diamines (cryptands) first synthesized by Lehn et al.[34] form very stable complexes with alkali metal and alkaline earth metal cations. X-ray structure determination of cryptate complexes formed from 2,2,2 cryptand (C_{222}, see Figure 1) and alkali metal salts show that the alkali cation is contained within the central cavity of the ligand.[130,131] Association constants for complex formation between many of the synthetic complexing agents of both the crown and cryptand classes and a variety of metal salts are known for aqueous solutions.[132-134] Except for association constants in methanol, very few others have been determined in nonaqueous solvents.[132-134] Even fewer rate data exist for the exchange of metal ions between solvated and bound sites. Exchange rates at the coalescence temperature have been reported from PMR studies on D_2O solutions which contain C_{222} and half the stoichiometric amount of alkali metal salt.[39] From these results it was clear that sodium cation exchange might be slow enough to be observed directly by using ^{23}Na NMR techniques. Ceraso and Dye[40] investigated the kinetics of complexation reactions of Na^+C_{222} cryptates in EDA solutions by using ^{23}Na NMR

techniques. Their work is the first example of sodium cation exchange which is slow enough to exhibit clearly defined separate signals for two environments. Cahen et al.[135] studied the Li^+-cryptate exchange kinetics in water and in several nonaqueous solvents by using ^7Li NMR. Cryptands smaller than C_{222} were used. No other quantitative information exists for alkali cation exchange rates in the presence of C_{222}. Schori et al.[136-138] studied the kinetics of complexation of crown ethers with sodium and potassium cations in several solvents by using ^{23}Na and ^{39}K NMR lineshape analysis. Since for the crown case the chemical shift between the free and bound site is negligible compared to the ^{23}Na and ^{39}K linewidth of the bound site, their experiments only exhibited one apparent resonance. Under their conditions, it was possible to reduce the complete lineshape expression for two site chemical exchange to a single Lorentzian line shape function. This is a special case of the treatment used here.

In this chapter an NMR lineshape analysis of the temperature dependence of sodium ion exchange in the presence of C_{222} in H_2O, EDA, THF and PYR solutions is given. Lineshapes are calculated from the exact expression for a general two site exchange of uncoupled spins and are fitted to the experimentally observed lineshape with the aid of the generalized weighted non-linear least-squares program KINFIT.[129]

We have chosen to use the ^{23}Na pulsed Fourier transform NMR technique because the advantages over continuous wave

NMR techniques are threefold:

1. No modulation distortion from sidebands occurs (particularly a problem with sodium, due to its range of relaxation times);
2. No saturation broadening occurs; and
3. Signal averaging is accomplished in a much shorter time period.

Despite the low sensitivity of ^{23}Na NMR compared to that of PMR, its use has two advantages over PMR:

1. The chemical shift range of sodium nuclei is much greater than that of protons; and
2. Deuterated solvents are not required.

5.2 Determination and Interpretation of the Line Shapes

The bloch equations which describe the motion of the X and Y components of magnetization in the rotating frame, when modified to include chemical exchange, are given by[139,140]

$$\frac{dG_A}{dt} + \alpha_A G_A = -i\gamma H_1 M_{OA} + \tau_B^{-1} G_B - \tau_A^{-1} G_A \qquad 5.1$$

$$\frac{dG_B}{dt} + \alpha_B G_B = -i\gamma H_1 M_{OB} + \tau_A^{-1} G_A - \tau_B^{-1} G_B, \qquad 5.2$$

where

$$G_A = u_A + iv_A,\ G_B = u_B + iv_B,\ \alpha_A = T_{2A}^{-1} - i(\omega_A - \omega),$$

$\alpha_B = T_{2B}^{-1} - i(\omega_B - \omega)$, ω is the variable frequency, H_1 is the radio frequency field, M_{OA} and M_{OB} are the equilibrium z components of magnetization for sites A and B, and τ_A and τ_B are the mean lifetimes in sites A and B respectively. Other symbols have their usual meaning. The solution to these equations for slow passage conditions ($\frac{dG_A}{dt} = \frac{dG_B}{dt} = 0$) and for transient conditions ($H_1 = 0$) have been shown to form a Fourier transform pair.[141,142] The solution for slow passage conditions is given in Appendix C. The shape function is given by

$$G(\omega) = \gamma H_1 M_O \{I\cos\theta - R\sin\theta\} \qquad 5.3$$

$$I = \frac{SU+TV}{S^2+T^2}; \qquad R = \frac{UT-SV}{S^2+T^2} \qquad 5.4$$

$$S = \frac{P_A}{T_{2A}} + \frac{P_B}{T_{2B}} + \frac{\tau}{T_{2A}T_{2B}} - \tau(\omega_A-\omega)(\omega_B-\omega) \qquad 5.5$$

$$U = 1 + \tau\left(\frac{P_B}{T_{2A}} + \frac{P_A}{T_{2B}}\right) \qquad 5.6$$

$$T = P_A\omega_A + P_B\omega_B - \omega + \tau\left[\frac{\omega_A-\omega}{T_{2B}} + \frac{\omega_B-\omega}{T_{2A}}\right] \qquad 5.7$$

$$V = \tau[P_B\omega_A + P_A\omega_B - \omega] \qquad 5.8$$

$$\tau = \frac{\tau_A\,\tau_B}{\tau_A+\tau_B} \qquad 5.9$$

$$P_A = \frac{\tau_A}{\tau_A+\tau_B}, \qquad P_B = \frac{\tau_B}{\tau_A+\tau_B} \qquad 5.10$$

where I represents the absorption mode lineshape and R represents the dispersion mode lineshape. ω_A,ω_B and T_{2A}, T_{2B} are the Larmor frequencies and transverse relaxation times of sites A and B in the absence of exchange. P_A and P_B are the relative populations in sites A and B. Equation 5.3 predicts the lineshape throughout the entire range of exchange from the extreme slow limit to the extreme fast limit (slow exchange occurs for $\tau >> \frac{1}{(\omega_A-\omega_B)}$, fast exchange occurs for $\tau << \frac{1}{(\omega_A-\omega_B)}$). The exchange time τ together with the relative populations P_A and P_B contain all of the kinetics information.

5.2.1. Measurements in the Absence of Exchange

In order to evaluate exchange times through application of Equation 5.3, we must obtain information about the Larmor frequencies and transverse relaxation times for sites A and B in the absence of exchange (A denotes a solvated sodium cation and B denotes a cryptated sodium cation). In addition, the populations P_A and P_B, for exchanging systems must also be known. In many studies of systems which undergo two site chemical exchange, ^1H and ^{13}C NMR lineshape analysis is used to obtain τ values. In some of these studies the assumption that $1/T_{2A} = 1/T_{2B} = 0$ is made. This assumption is not justified for sodium since its relaxation rates are usually much larger (broader lines) than those of ^1H or ^{13}C and these relaxations contribute significantly to the observed NMR lineshapes.

Since the equilibrium constant (K_a) for complex formation between Na^+ and C_{222} is large ($K_a > 10^3$) in all solvents and at all temperatures, P_A and P_B are directly determined from the mole ratios of C_{222} and sodium salt added to solution.

To obtain ω_A,ω_B, T_{2A} and T_{2B}, two solutions in each solvent were prepared. The first contained a sodium salt with no C_{222} and the second contained a sodium salt and equimolar C_{222}. Because K_a is large, the second solution contains only bound sodium cations and these ions cannot undergo chemical exchange since the concentration of unbound sites is too low. The ^{23}Na NMR of each of these solutions was studied as a function of temperature. All experimental lineshapes were found to be Lorentzian.

The values of ω and T_2 were determined by fitting a Lorentzian line to the observed signal. Complete characterization of the intensity of a Lorentzian signal by the Fourier transform NMR technique requires determination of six parameters. These are the amplitude, K, the Larmor frequency, ω, the linewidth parameter, T_2, the height of the baseline, C, the zero-order phase correction, θ_o, and the first-order phase correction, θ'. The zero-order phase correction is constant and independent of frequency. It determines the contribution of dispersion and absorption mode signals to the observed lineshape. Electronic filtering and the finite length of a 90° pulse that initiates a free induction decay, as well as delays in the start of data acquisition can all

lead to a first-order phase correction. The first-order phase correction varies linearly with frequency (and hence channel number, j) according to $\theta' = \theta_1 \cdot \frac{j}{N}$ in which N is the total number of channels in the spectrum and θ_1 is the total change in phase over the entire spectrum.

In terms of these parameters, the intensity is given as a function of frequency by

$$G(\omega) = \frac{K \cdot T_2}{1+T_2^2(\omega_o-\omega)^2} \{\cos(\theta_o+\theta') - T_2(\omega_o-\omega)\sin(\theta_o+\theta') + C \quad 5.11$$

Commonly the phase parameters and the baseline height are instrumentally adjusted by visual inspection of the signal to obtain a symmetric absorption-mode signal with a zero baseline. The value of θ_1 is constant for given instrument settings and may be accurately determined by measuring the signal from a reference sample at several magnetic field settings which span the entire frequency range to be used. Once θ_1 is evaluated in this way it need not be changed from sample to sample and is not an adjustable parameter. By contrast θ_o is influenced, not only by instrument settings, but also by sample position, temperature, etc., and therefore it must be adjusted for each sample.

Since in any event, the parameters must be adjusted (either numerically or instrumentally), we have chosen to evaluate all parameters except θ_1 by fitting the Lorentzian Equation (5.11) to the observed spectrum by a non-linear

least-squares procedure. A typical example of a fit for 0.6 M NaBr in EDA solution at 26.3°C is shown in Figure 12. The variation in linewidths and chemical shifts with temperature for free and unbound sodium in each of the four solvents is listed in Tables V-XII. The measurements of T_2 and ω for free Na^+ in H_2O and PYR were made visually. The data for each solvent are plotted in Figures 13-16, (semi-log plot of $1/T_2$ *vs* $10^3/T$). Simple exponential behavior of the variation of the relaxation rate with temperature is observed for THF, EDA and H_2O solutions but not for PYR solutions. As shown in Figure 16, the relaxation rate levels off between 90 and 140°C. This deviation from exponential behavior might be caused by changes in ion-pairing with temperature. In all cases the activation energy (see Chapter III) is smaller for free sodium cations than for bound sodium cations in the same solvent. All chemical shifts are referenced to the infinitely dilute aqueous sodium cation (a positive shift corresponds to a high field shift).

The Larmor frequencies show only a slight dependence upon temperature. The value of ω at any temperature between those examined was determined by graphical interpolation. A sample of saturated aqueous sodium chloride at 25°C was used as an external reference for both chemical shift and linewidth calibrations. (The chemical shift of saturated aqueous sodium chloride relative to infinitely dilute aqueous sodium ion is -0.7 ppm). Linewidth contributions from magnetic field inhomogeneties ranged from 2 to 6 Hz and

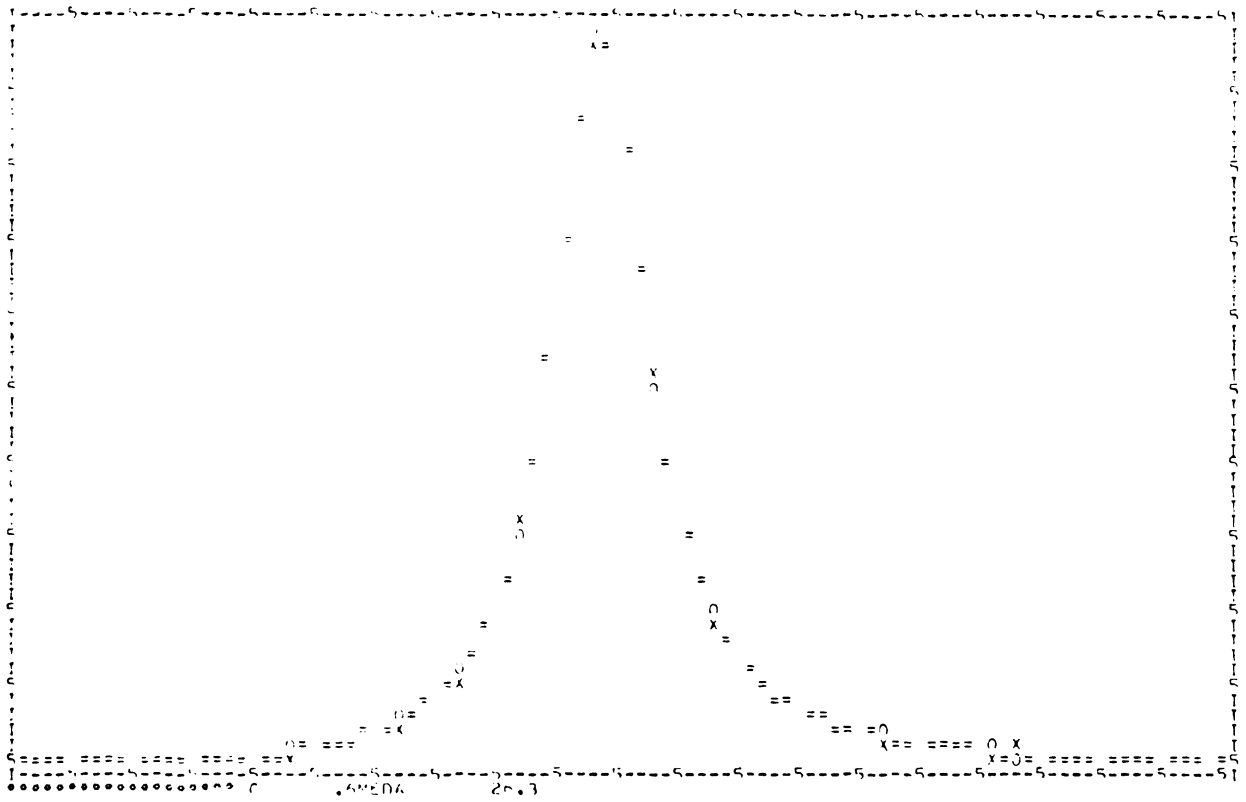

Figure 12. A typical KINFIT analysis of the ^{23}Na lineshape for a solution containing 0.60 M NaBr in EDA. X represents an experimental point, O, a calculated point, =, an experimental and calculated point which are the same within the resolution of the plot.

Table V. Variation of the relaxation rate and chemical shift of free sodium cation with temperature in ethylenediamine.[a]

T(°C)	$10^3/T(°K)$	$1/T_{2B}(sec)$[b]	δ(ppm)[c]
20.6	3.404	255.3	-13.86
26.3	3.340	220.3	-13.75
32.1	3.276	192.8	-13.67
38.0	3.214	173.3	-13.65
43.5	3.158	154.7	-13.61
49.1	3.103	139.7	-13.59
54.9	3.048	124.0	-13.56
60.0	3.002	113.8	-13.53
64.5	2.962	104.8	-13.47
70.1	2.913	94.79	-13.42

a) 0.6 M NaBr in EDA solution.

b) Natural relaxation rate.

c) Referenced to infinite dilute aqueous Na^+.

Table VI. Variation of the relaxation rate and chemical shift of bound sodium cation with temperature in ethylenediamine.[a]

T(°C)	$10^3/T(°K)$	$1/T_{2B}(sec)$[b]	δ(ppm)[c]
20.2	3.409	273.6	10.41
26.6	3.336	231.5	10.65
32.3	3.274	202.8	10.90
35.1	3.244	182.6	10.83
41.4	3.179	158.0	10.92
48.3	3.111	138.3	11.21
52.4	3.072	127.0	11.10
59.0	3.011	110.4	11.17
67.7	2.934	95.79	11.24

a) 0.3 M $Na^+C \cdot Br^-$ in EDA solution.

b) Natural relaxation rate.

c) Referenced to infinite dilute aqueous Na^+.

Table VII. Variation of relaxation rate and chemical shift of free sodium cation with temperature in water.[a]

T(°C)	$10^3/T(°K)$	$1/T_{2B}(sec)$[b]	δ(ppm)[c]
7.8	3.556	37.5	0.3
13.9	3.484	27.3	0.3
21.2	3.397	24.9	0.3
33.3	3.263	18.6	---
36.2	3.233	17.1	0.6

a) 0.2 M NaI in H_2O solution.

b) Natural relaxation rate.

c) Referenced to infinite dilute aqueous Na^+.

Table VIII. Variation of relaxation rate and chemical shift of bound sodium cation with temperature in water.[a]

T(°C)	$10^3/T(°K)$	$1/T_{2B}(sec)$[b]	δ(ppm)[c]
2.8	3.624	520.7	7.45
8.3	3.553	438.1	7.68
13.4	3.490	355.3	7.84
19.2	3.421	311.3	8.12
21.0	3.400	282.3	8.45
25.0	3.354	245.5	8.54
29.7	3.302	233.1	8.53
35.3	3.242	184.3	8.83
40.6	3.187	164.5	9.07
45.9	3.134	149.3	9.28
50.7	3.088	134.3	9.46
54.6	3.051	122.4	9.54
60.8	2.995	110.5	9.72
66.1	2.948	100.5	9.86

a) 0.2 M $Na^+C \cdot I^-$ in H_2O Solution.

b) Natural relaxation rate.

c) Referenced to infinite dilute aqueous Na^+.

Table IX. Variation of the relaxation rate ($1/T_2$) and chemical shift of free sodium cation with temperature in tetrahydrofuran.[a]

T(°C)	$10^3/T(°K)$	$1/T_{2B}(sec)$[b]	δ(ppm)[c]
25.7	3.346	96.92	+7.43
30.7	3.291	94.29	+7.53
35.4	3.241	91.97	+7.58
42.8	3.165	88.60	+7.72
47.9	3.114	87.43	+7.82
53.1	3.065	85.79	+7.93

a) 0.4 M $Na\phi_4B$ in THF solution.

b) Natural relaxation rate.

c) Referenced to infinite dilute aqueous Na^+.

Table X. Variation of relaxation rate and chemical shift of bound sodium cation with temperature in tetrahydrofuran.[a]

T(°C)	$10^3/T(°K)$	$1/T_{2B}(sec)$[b]	δ(ppm)[c]
19.7	3.415	169.5	11.89
25.1	3.353	154.3	12.03
30.3	3.295	139.0	12.17
35.4	3.241	129.5	12.26
42.1	3.172	119.7	12.52
46.6	3.127	111.1	12.48
53.2	3.064	101.4	12.62
59.5	3.006	94.72	12.57
64.2	2.964	89.25	12.67
68.4	2.928	86.46	12.74
70.9	2.907	84.57	12.81

a) 0.2 M $Na^+C \cdot \phi_4B^-$ in THF solution.

b) Natural relaxation rate.

c) Referenced to infinite dilute aqueous Na^+.

Table XI. Variation of relaxation rate and chemical shift of free sodium cation with temperature in pyridine.[a]

T(°C)	$10^3/T(°K)$	$1/T_{2B}$(sec)[b]	δ(ppm)[c]
22.6	3.383	86.8	-1.2
45.0	3.145	70.4	-0.6
57.6	3.025	62.1	-0.3
69.0	2.924	57.2	-0.2
80.3	2.830	53.9	0.0
88.3	2.768	55.5	0.1
100.8	2.675	53.9	0.3
112.4	2.595	53.6	0.4
125.4	2.510	53.9	1.0
133.8	2.458	58.8	1.1
140.3	2.420	57.2	1.3
144.8	2.393	58.8	1.3

a) 0.2 M $Na\phi_4B$ in PYR solution.

b) Natural relaxation rate.

c) Referenced to infinite dilute aqueous Na^+.

Table XII. Variation of relaxation rate and chemical shift of bound sodium cation with temperature in pyridine.[a]

T(°C)	$10^3/T(°K)$	$1/T_{2B}(sec)$[b]	δ(ppm)[c]
25.5	3.348	150.9	12.38
32.9	3.267	134.8	12.54
38.6	3.208	124.9	12.56
43.7	3.156	116.5	12.65
55.1	3.047	97.43	12.76
61.4	2.989	90.14	12.82
68.8	2.924	83.87	12.93
74.9	2.873	78.12	12.98
82.6	2.811	72.75	13.05
88.6	2.764	67.45	13.10
102.2	2.664	63.73	13.22
109.2	2.615	59.06	12.79
114.0	2.583	61.01	13.28
121.2	2.537	60.24	13.18
128.6	2.489	60.50	13.19
133.8	2.457	57.71	13.18
140.2	2.419	59.33	13.07

a) 0.2 M $Na^+C \cdot \phi_4B^-$ in PYR solution.

b) Natural relaxation rate.

c) Referenced to infinite dilute aqueous Na^+.

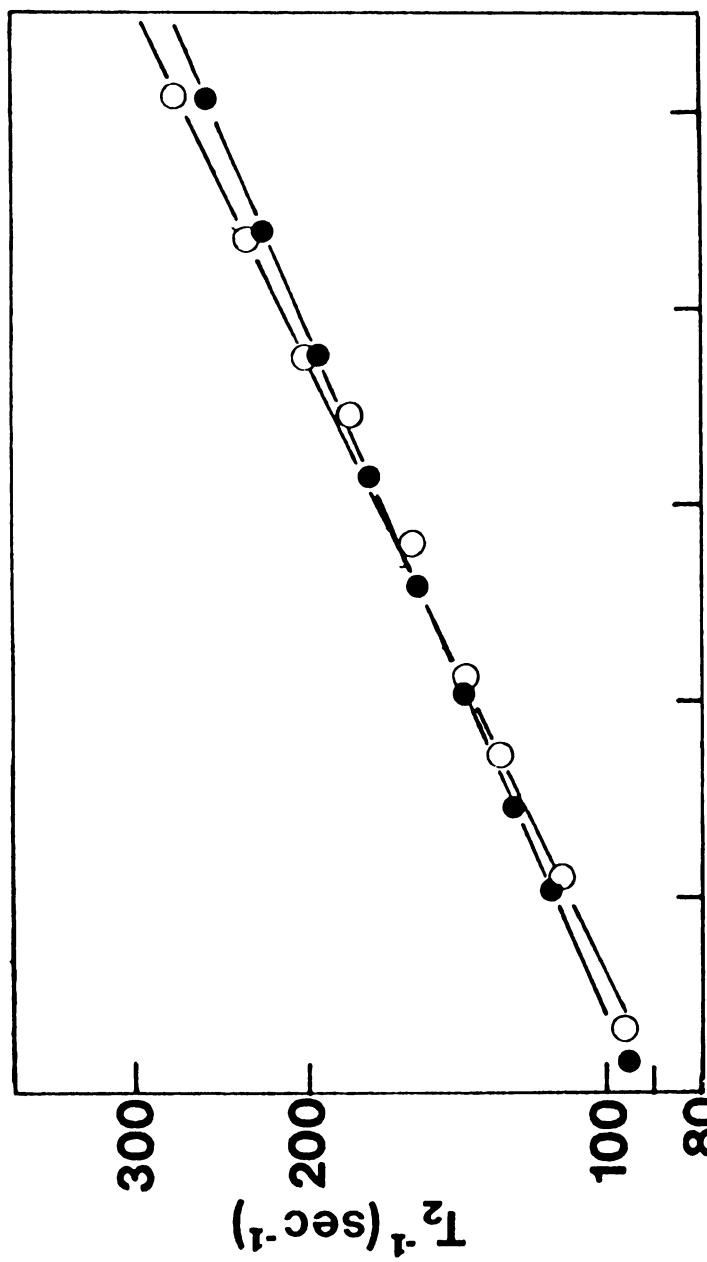

Figure 13. Semilog plots of $1/T_2$ for ^{23}Na vs reciprocal absolute temperature for solutions containing 0.6 M NaBr (●) and 0.3 M $Na^+C_{222} \cdot Br^-$ (○) in EDA.

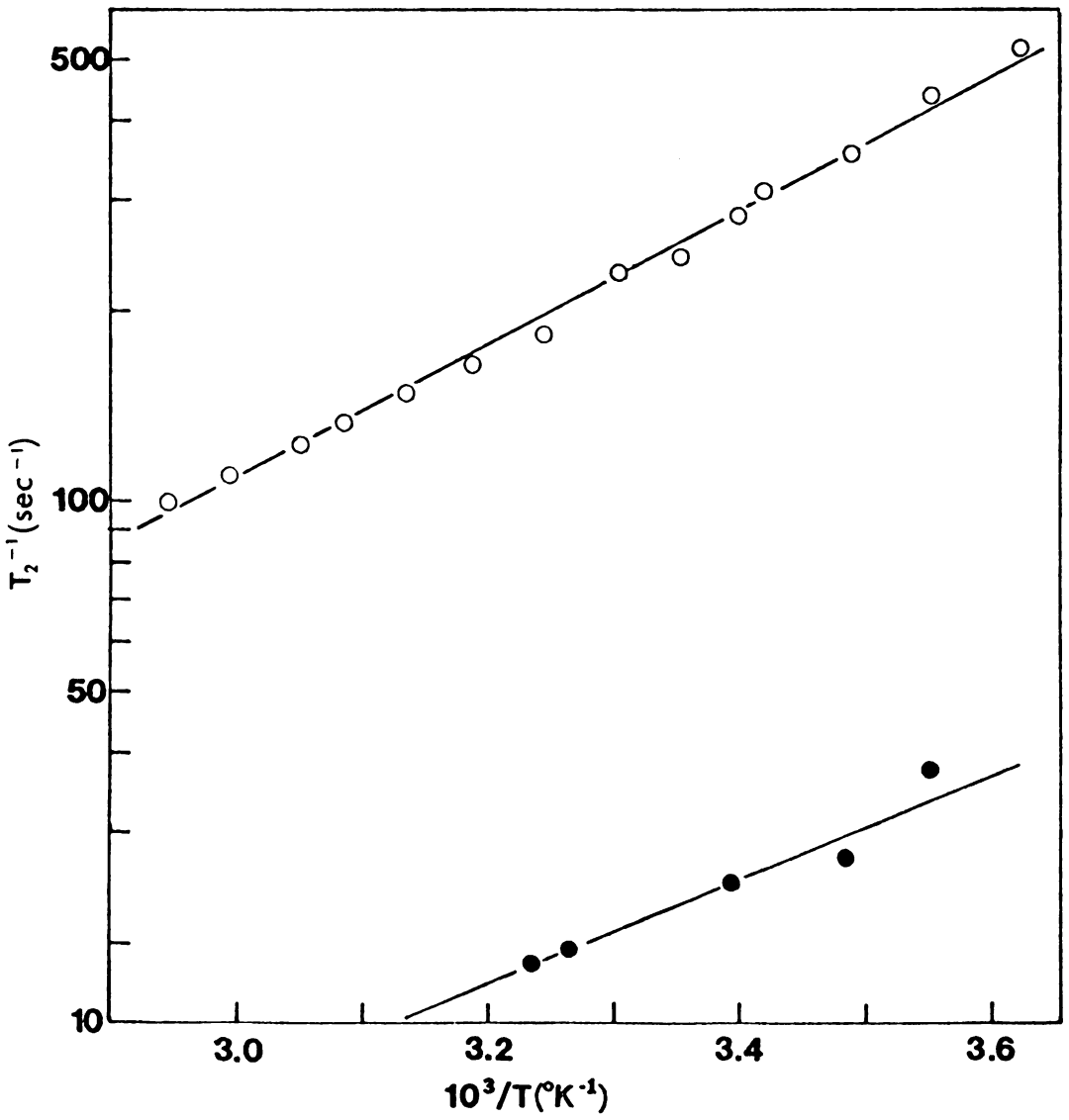

Figure 14. Semilog plots of $1/T_2$ for ^{23}Na vs reciprocal absolute temperature for solutions containing 0.2 M NaCl (●) and 0.2 M $Na^+C_{222} \cdot Cl^-$ (○) in H_2O.

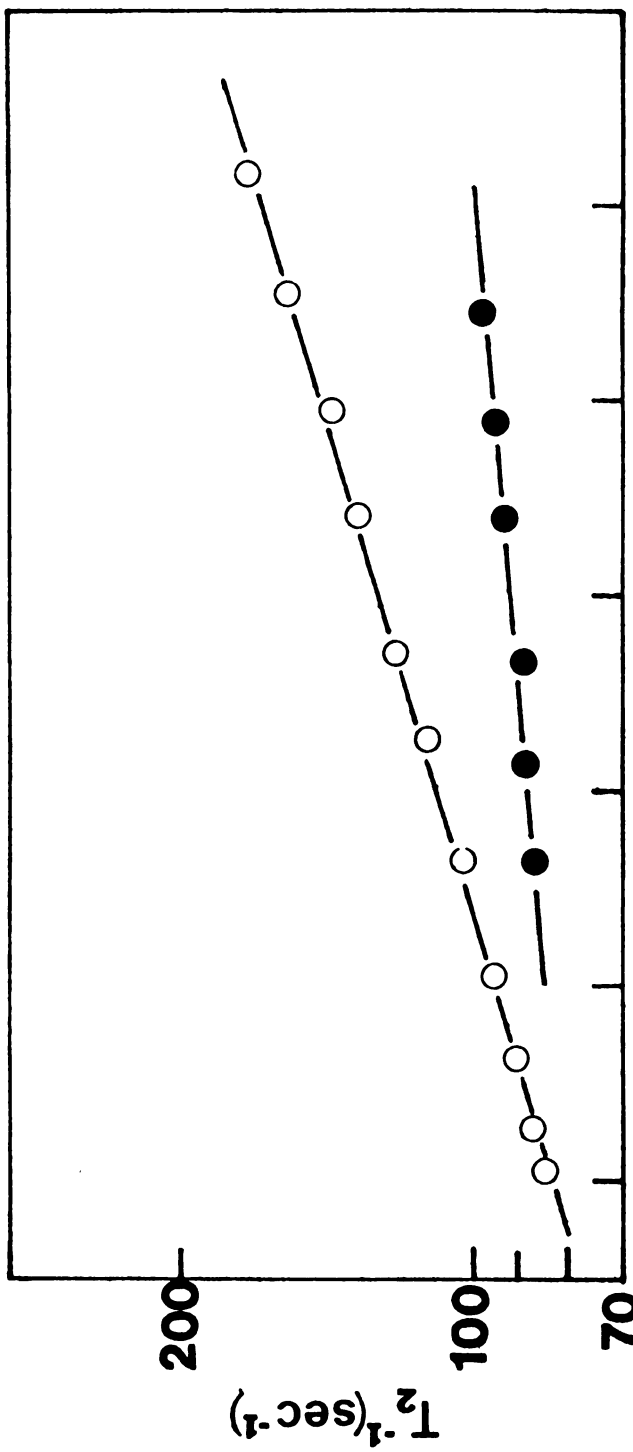

Figure 15. Semilog plots of $1/T_2$ for ^{23}Na vs reciprocal absolute temperature for solutions containing 0.4 M $\overline{Na}\phi_4B$ (●) and 0.2 M $Na^+C_{222} \cdot \phi_4B^-$ (○) in THF.

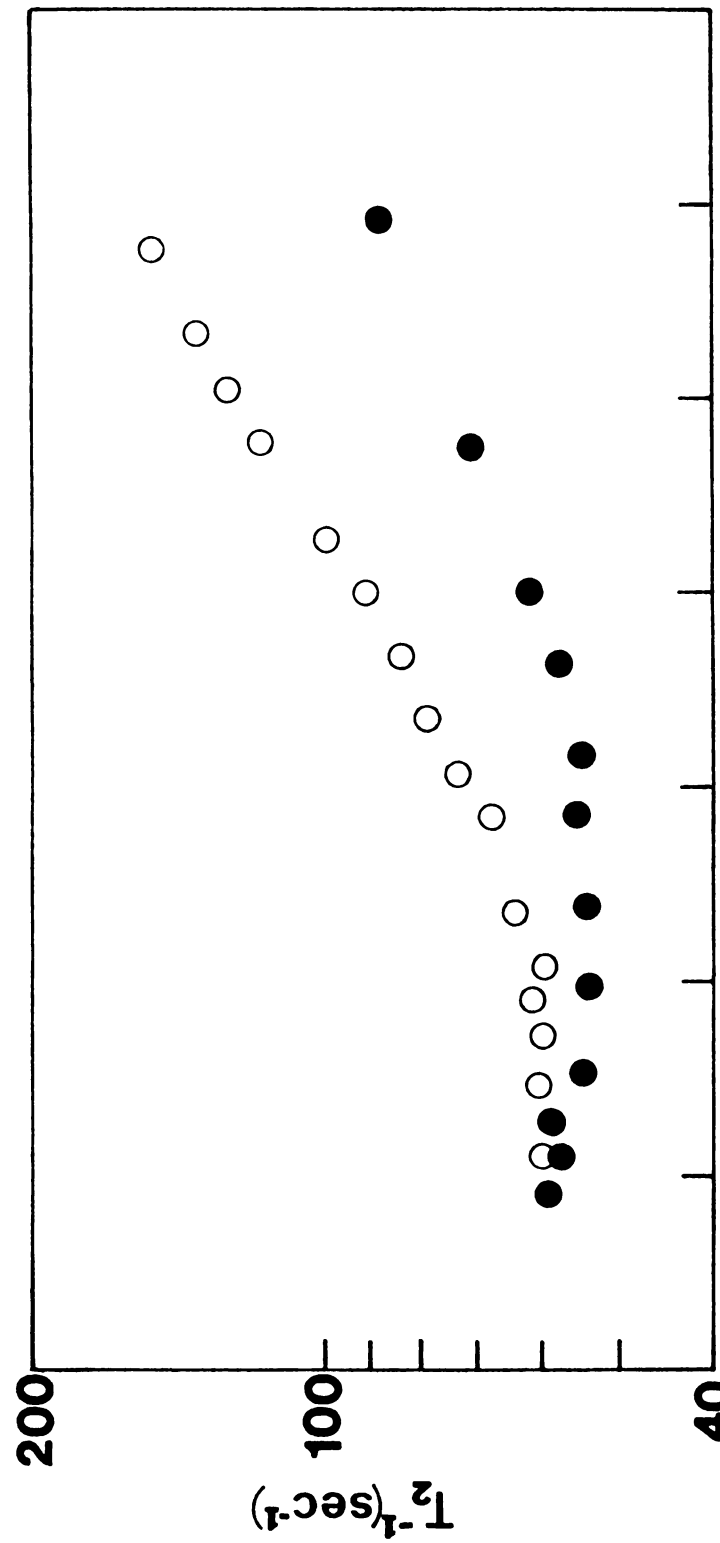

Figure 16. Semilog plots of $1/T_2$ for ^{23}Na vs reciprocal absolute temperature for solutions containing 0.2 M $\overline{Na}\phi_4B$ (●) and 0.2 M $Na^+C_{222} \cdot \phi_4B^-$ (○) in PYR.

were, for all cases except aqueous solutions, a small fraction of the measured width. Inhomogeneous line broadening varied from one set of experiments to the next. This contribution to the linewidth was determined for each set of experiments by using an aqueous reference sample with a known relaxation time (saturated aqueous NaCl; natural linewidth is 8.0 Hz at 25°C), according to

$$(1/T_2)_{inhomo.} = (1/T_2)_{obs.} - (1/T_2)_{nat.}$$

This value was then added to the previously determined value of $(1/T_2)_{nat.}$ for each of the sites so that the values of $1/T_{2A}$ and $1/T_{2B}$ used in the following line shape equations include both the natural contribution to the linewidth and the inhomogeneous contribution. This method assumes that the shape function of the field inhomogeneity also has a Lorentz form, which is often not true. However, for all cases but free sodium cation in H_2O, the inhomogeneous contributions to the observed linewidth are small and are approximated well by a Lorentz shape function (see Figure 12). Even the narrow lines observed for free Na^+ in H_2O were Lorentzian.

Values for $(1/T_2)$ at any temperature were evaluated by fitting the following exponential equation to the observed data (corrected for inhomogeneity).

$$(1/T_{2A \text{ or } B})_{nat.} = (1/T_{2_{298.15}})_{nat.} e^{E_r/R\,(1/T-1/298.15)}$$

This was done for all solutions except free sodium in H_2O and free and bound sodium in PYR. In these cases graphical extrapolation and interpolation was used. The values for E_r are listed in Table XIII.

5.2.2. Evaluation of Exchange Times

To evaluate the exchange time τ, Equations 5.3, 5.5, 5.7 and 5.8 were modified as follows

$$G(\omega) = K\{I\cos(\theta_o+\theta') - R\sin(\theta_o+\theta')\} + C \qquad 5.3'$$

$$S = \frac{P_A}{T_{2A}} + \frac{P_B}{T_{2B}} + \frac{\tau}{T_{2A}T_{2B}} - \tau(\omega_A+\Delta-\omega)(\omega_B+\Delta-\omega) \qquad 5.5'$$

$$T = P_A\omega_A + P_B\omega_B + \Delta - \omega + \tau\left[\frac{\omega_A+\Delta-\omega}{T_{2B}} \frac{\omega_B+\Delta-\omega}{T_{2A}}\right] \qquad 5.7'$$

$$V = [P_B\omega_A + P_A\omega_B + \Delta - \omega]. \qquad 5.8'$$

Application of Equation 5.3' requires evaluation of six parameters. These are amplitude, K, baseline height, C, zero-order phase correction, θ_o, first-order phase correction, θ', frequency shift, Δ, and the exchange time, τ. Again the first-order phase correction was not adjusted numerically, but was measured visually for a given set of instrumental settings as described previously. Thus, in most cases, we chose to adjust five parameters to obtain the best fit of Equation 5.3' to the observed data. The frequency shift parameter was introduced because of experimental

Table XIII Activation energy, E_r, for solvent reorganization in various solvents.

Ion	Concentration (M)	Solvent	E_r (Kcal)
Na^+	0.6M NaBr	EDA	3.6
Na^+C_{222}	0.3M $Na^+C_{222}\cdot Br^-$	EDA	4.4
Na^+	0.4M $Na\phi_4B$	THF	0.86
Na^+C_{222}	0.2M $Na^+C_{222}\cdot\phi_4B^-$	THF	2.7
Na^+	0.2M $Na^+C_{222}\cdot I^-$	H_2O	4.8

difficulties with referencing absolute frequencies from one set of data to the next. The relative chemical shifts at the two sites were not adjusted. The errors in precise referencing of one set of data to another were caused by the method of external referencing. If an internal reference in each sample and an internal lock had been employed, there would be no need for the correction term Δ. The frequency shift parameter allows the absolute frequency in Equation 5.3' to shift, without changing the shape of the function. In most cases Δ was less than 0.5 ppm.

For each spectrum analyzed, 90 to 99 data points were found to be more than sufficient to determine τ. The program used (KINFIT) gave complete statistical information about the fit to the data, including standard deviation estimates for each of the parameters and the multiple correlation coefficient, which gives a measure of the coupling of each parameter to all of the others. Coupling between τ and the other four parameters was lowest at intermediate rates of exchange ($\tau \approx 1/(\omega_A-\omega_B)$). This is expected, since τ has its greatest influence upon the lineshape in the intermediate region of exchange.

5.2.2.1. Exchange Times in EDA Solutions - Three solutions (EDA 1, 2, and 3) each containing 0.6 M NaBr but with variable amounts of C_{222} (0.15, 0.30 and 0.45 M respectively) were examined. Selected spectra for EDA 1, 2 and 3 are shown in Figures 17-19. Spectra from solutions EDA 1 and EDA 3

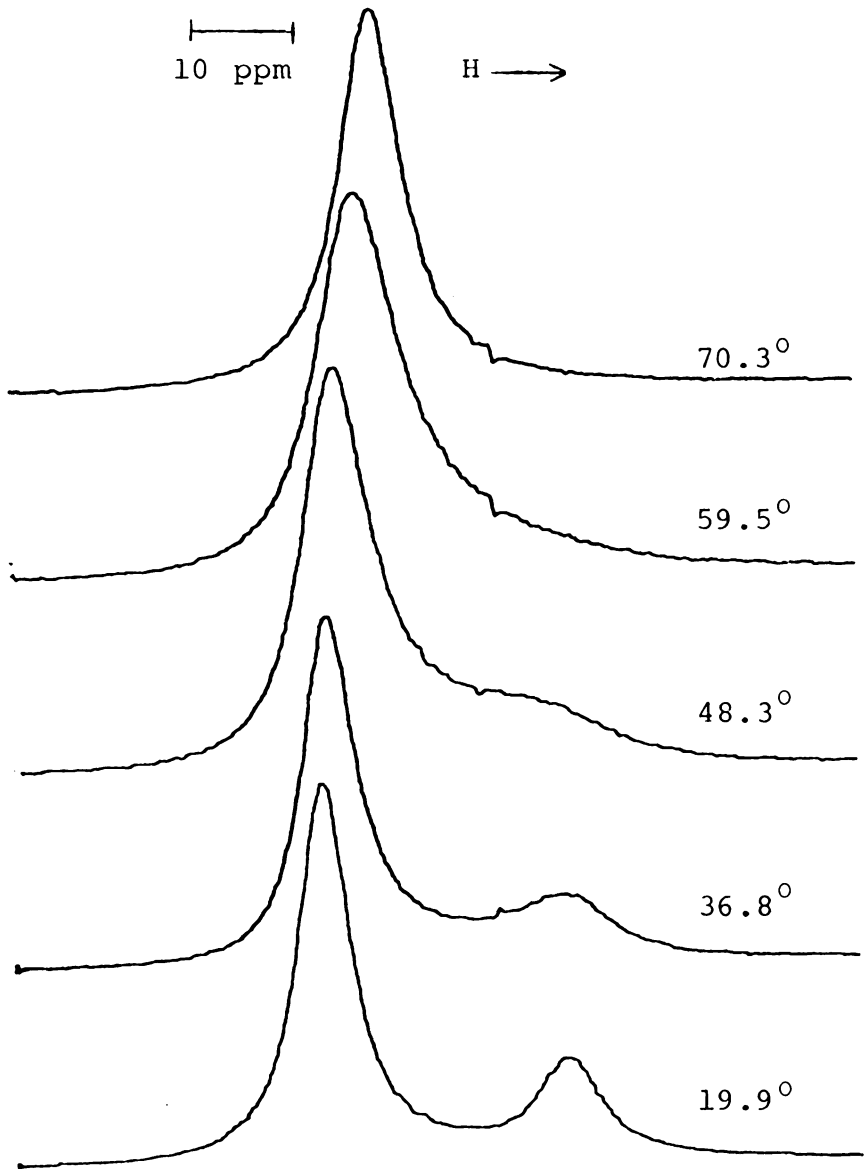

Figure 17. Spectra at various temperatures for a solution of 0.15 M C_{222} and 0.6 M NaBr in EDA (1 ppm = 15.87 Hz).

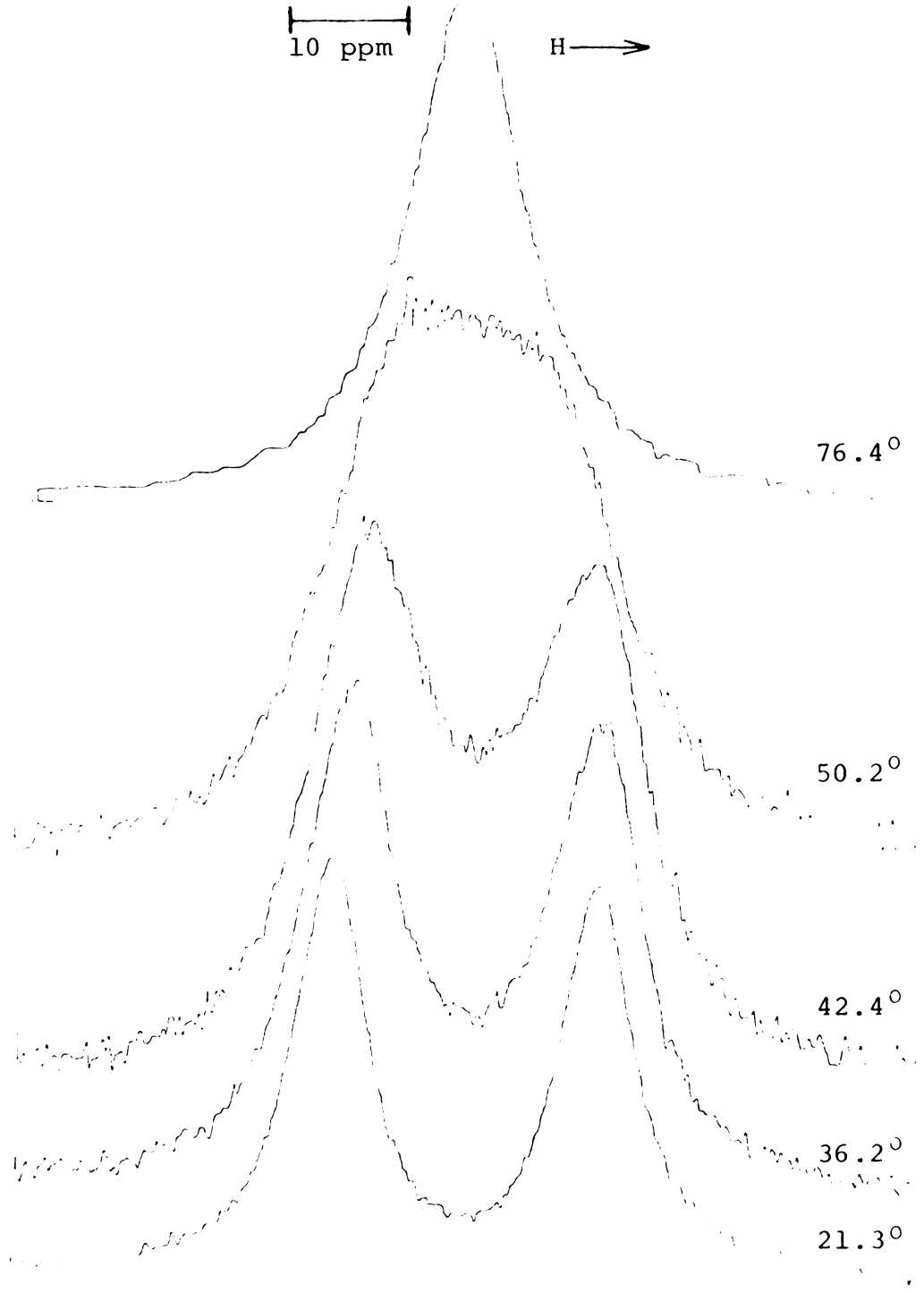

Figure 18. Spectra at various temperatures for a solution of 0.30 M C_{222} and 0.6 M NaBr in EDA (1 ppm = 15.87 Hz).

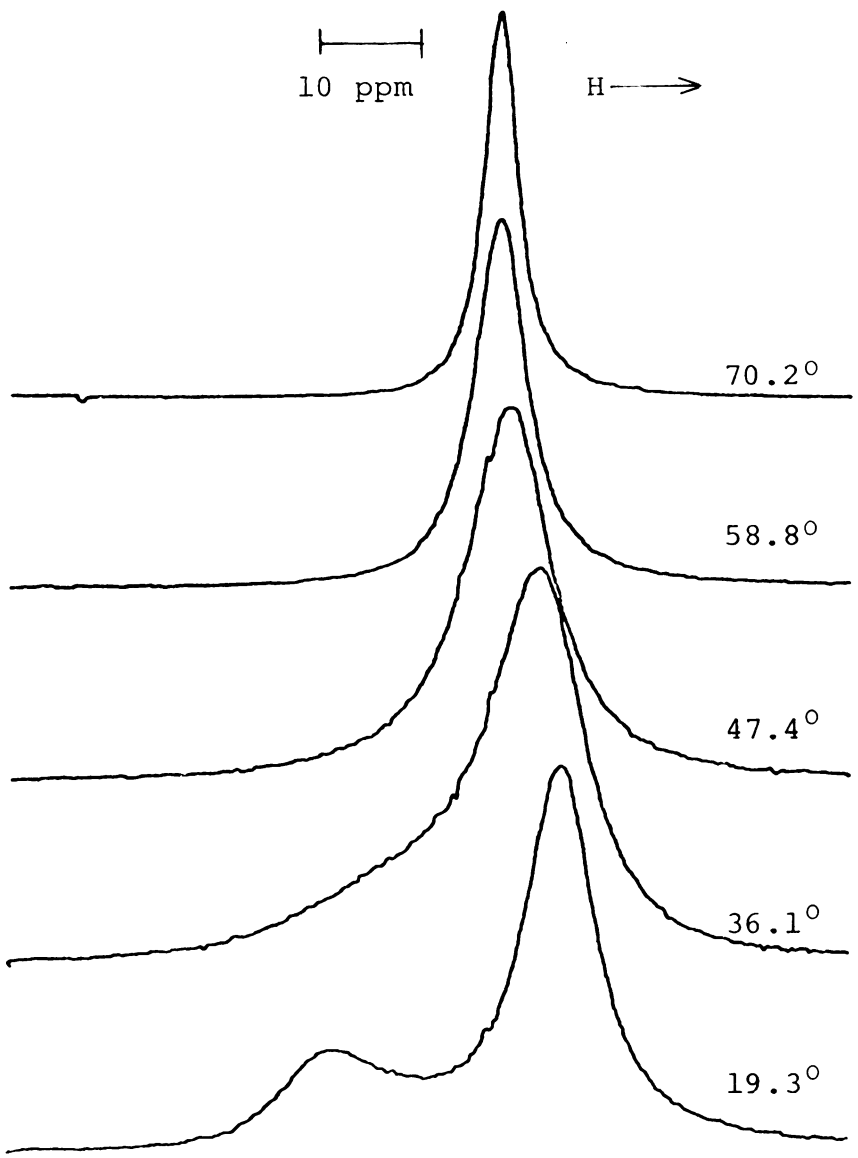

Figure 19. Spectra at various temperatures for a solution of 0.45 M C_{222} and 0.6 M NaBr in EDA (1 ppm = 15.87 Hz).

were analyzed by using Equation 5.3'. The spectra from EDA 2 were also analyzed by using Equation 5.3', but the value of θ_1 was determined by computer adjustment of a modified form of Equation 5.3'. The Δ term was dropped and ω_A, ω_B and θ_1 were allowed to float (along with K, C, τ, θ_o) to obtain the best fit of Equation 5.3' to the experimental data. The three lowest temperature spectra were fitted and the average value of θ_1 was computed. This value (θ_1 = 264°) was then used to analyze all the spectra from solution EDA 2 by using the unmodified form of Equation 5.3'. Some typical fits for these data are shown in Figures 20-25. Variations in τ values with temperature are listed in Tables XIV-XVI.

5.2.2.2. Exchange Times in THF, H_2O and PYR Solutions - A single solution of each solvent was examined. Equation 5.3' was used and no θ_1 corrections were made (θ_1 = 0). For the H_2O solution, the Δ parameter was not used. Some of the fits for H_2O solutions are shown in Figures 26 and 27. Noticeable intensity differences between calculated and observed values at low temperatures in the vicinity of the broad peak (bound cation) occurs with the experimental intensity lower than the calculated intensity. This may be partly caused by the spectrometer delay time. After the pulse, a delay time of 200 to 300 microseconds occurs before collection of the free induction decay. The area under a peak in the frequency domain is proportial to the intensity of the free induction decay at time zero. If a

a

b

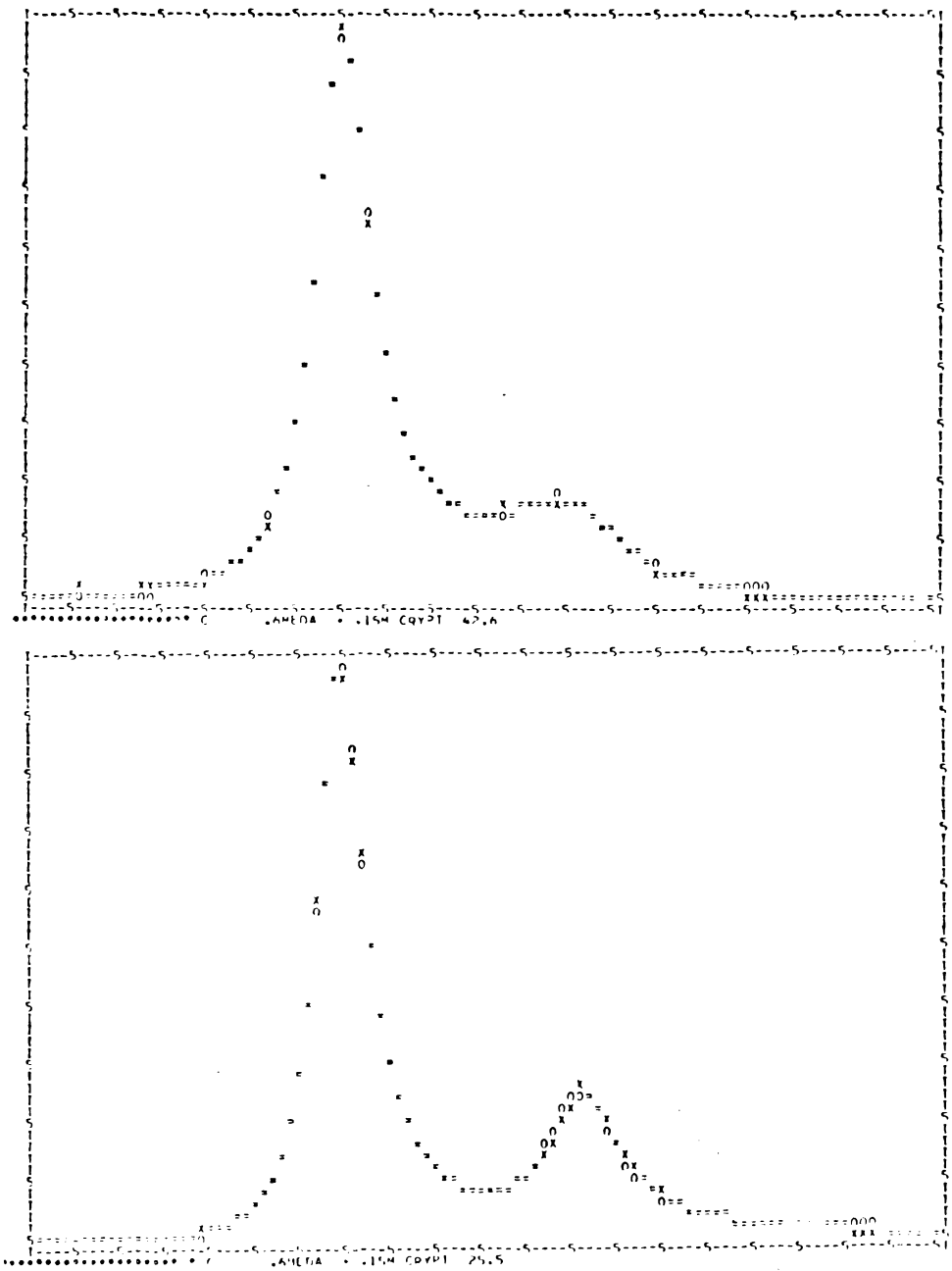

Figure 20. Computer fit of spectra obtained with 0.15 M C_{222} and 0.6 M NaBr in EDA. (a) 42.6°C; (b) 25.5°C.

a

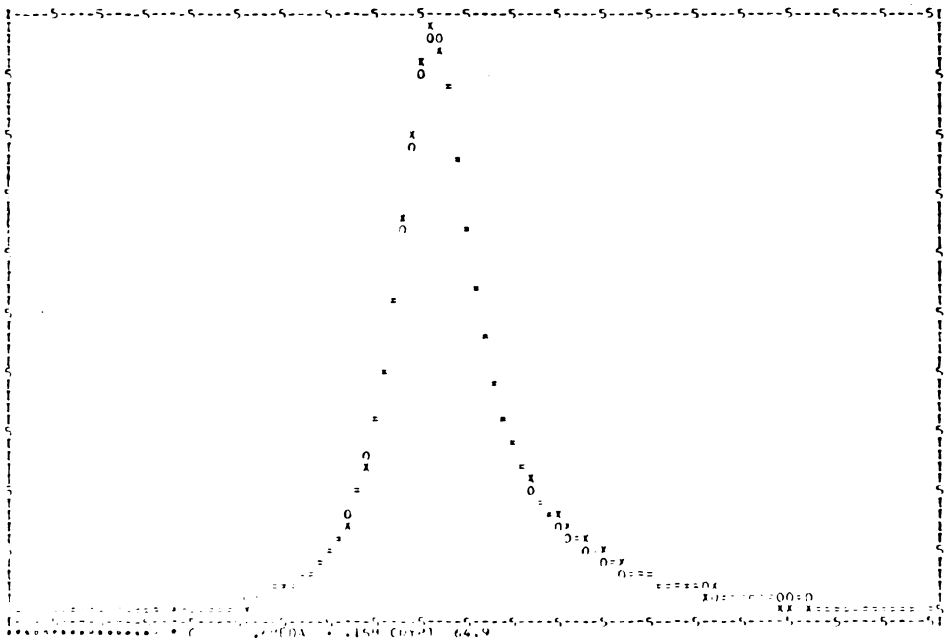

b

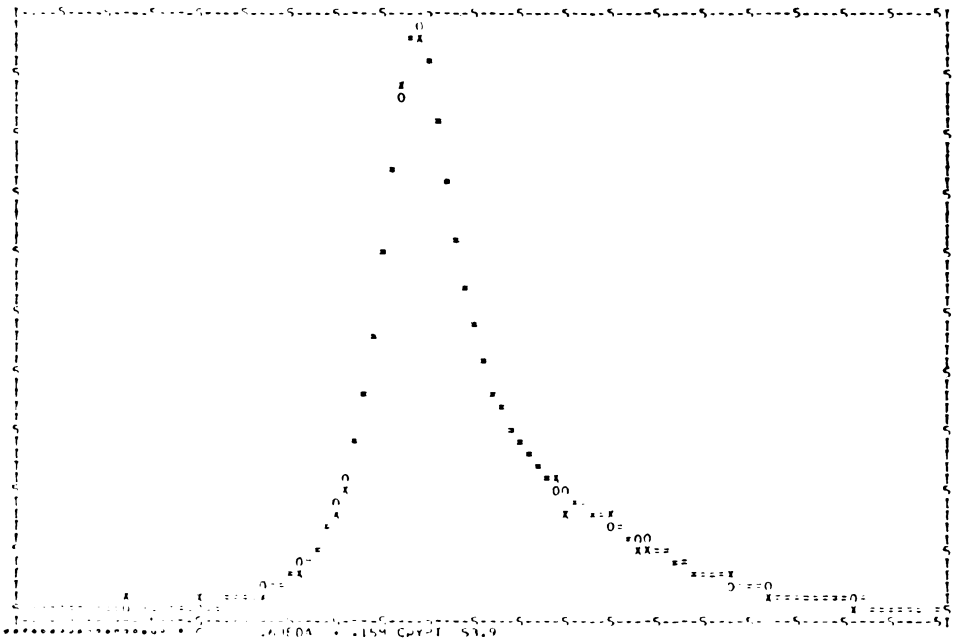

Figure 21. Computer fit of spectra obtained with 0.15 M C_{222} and 0.6 M NaBr in EDA. (a) 64.9^{O}C; (b) 53.9^{O}C.

a

b

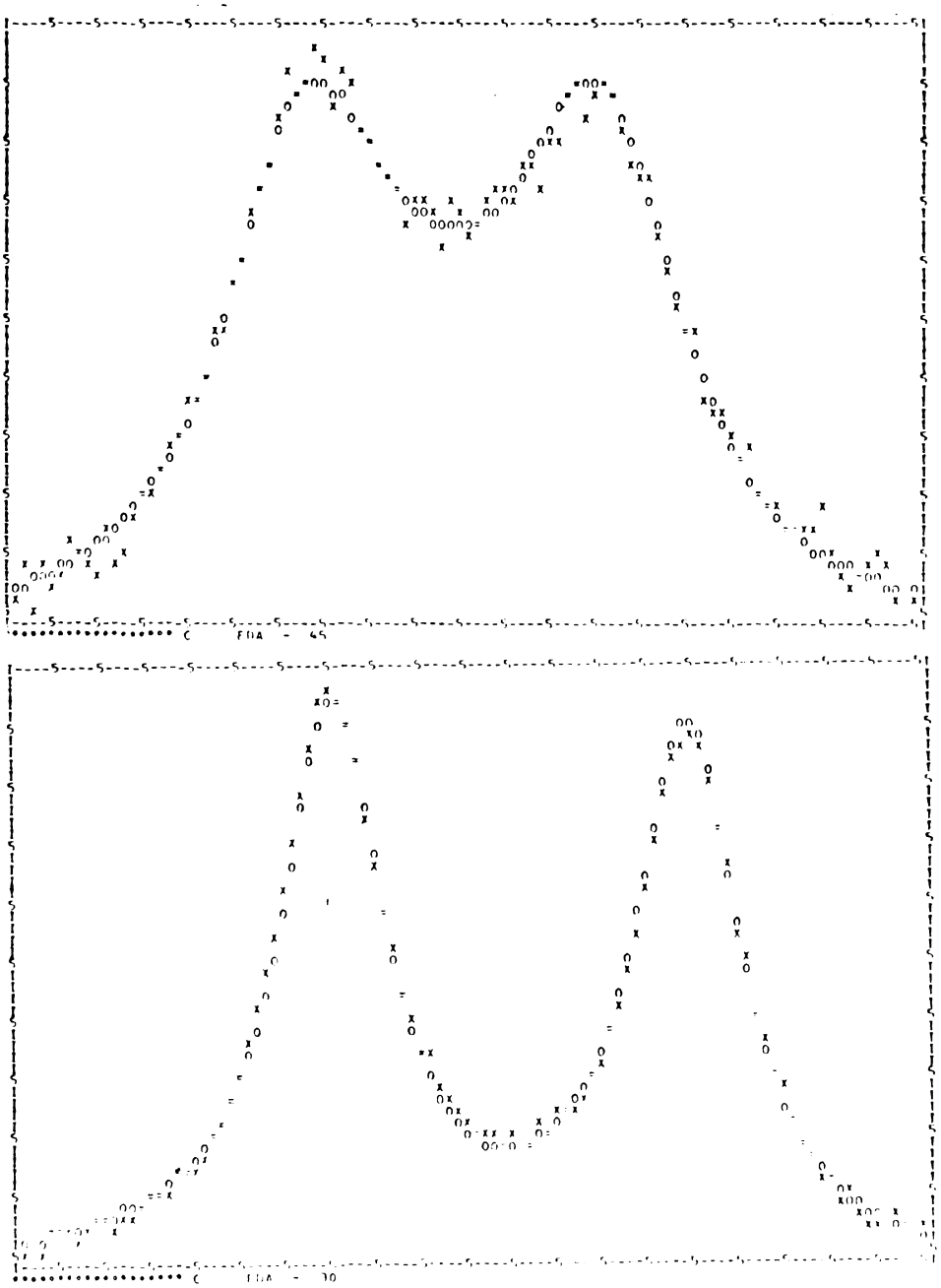

Figure 22. Computer fit of spectra obtained with 0.30 M C_{222} and 0.6 M NaBr in EDA. (a) 45.0°C; (b) 30.4°C.

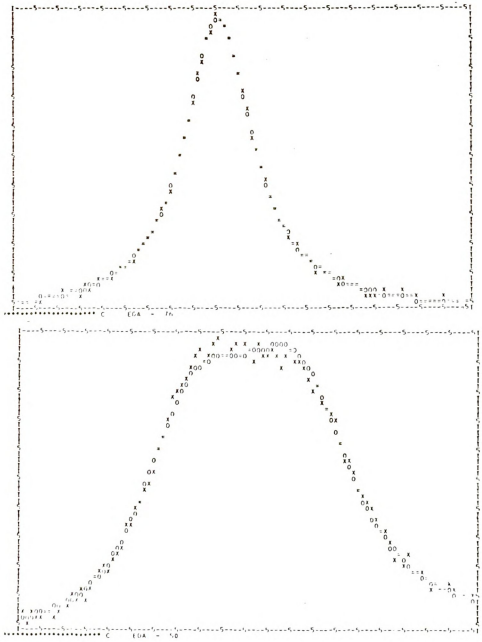

Figure 23. Computer fit of spectra obtained with 0.30 M C_{222} and 0.6 M NaBr in EDA. (a) 76.4°C; (b) 50.2°C.

a

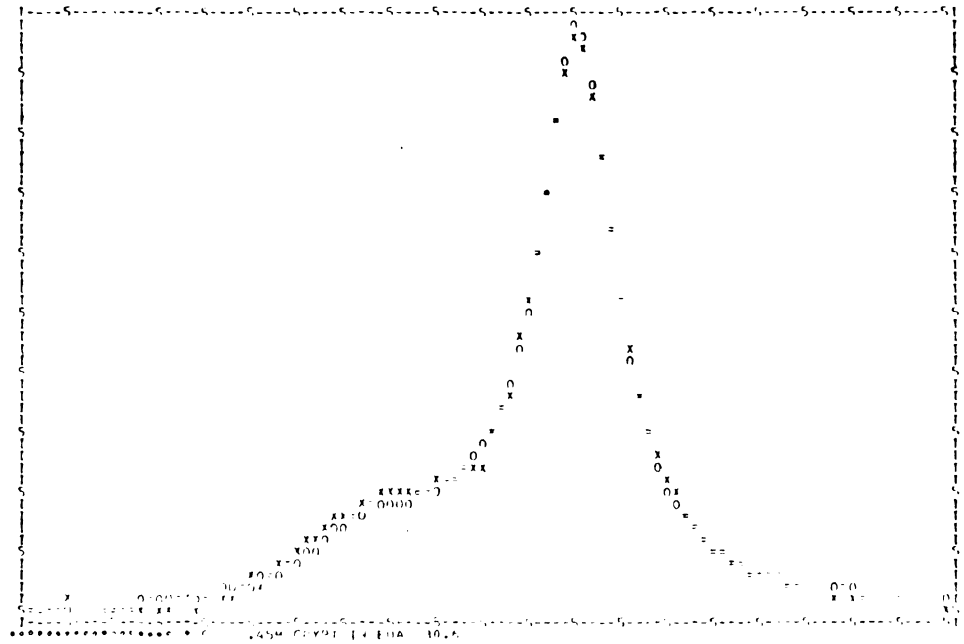

b

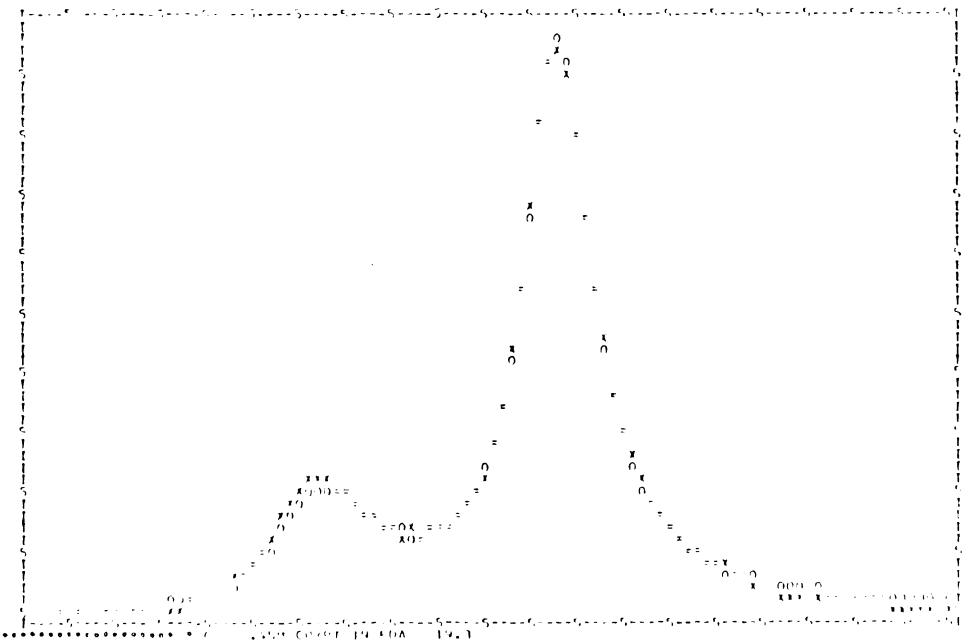

Figure 24. Computer fit of spectra obtained with 0.45 M C_{222} and 0.6 M NaBr in EDA. (a) 30.6°C; (b) 19.3°C.

a

b

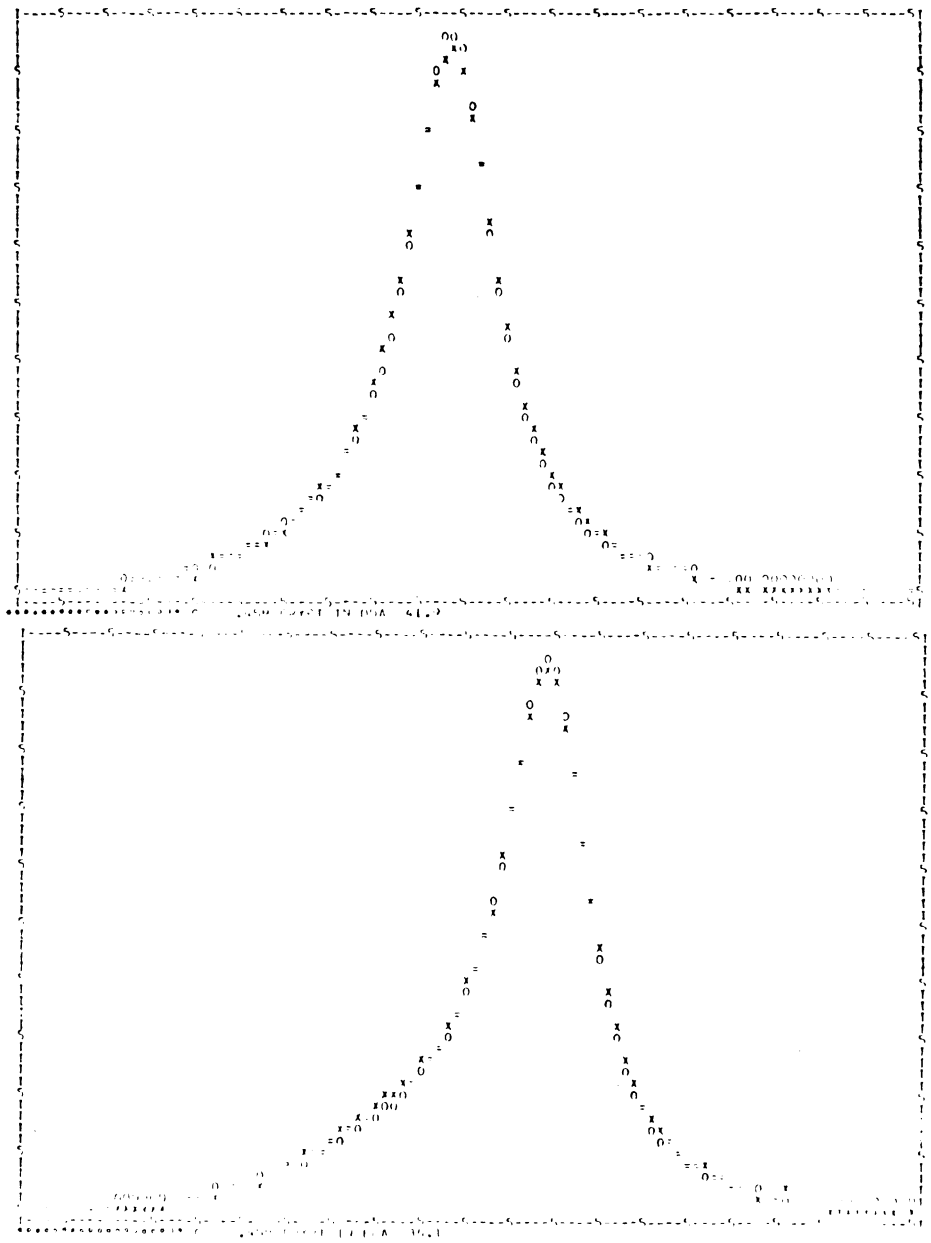

Figure 25. Computer fit of spectra obtained with 0.45 M C_{222} and 0.6 M NaBr in EDA. (a) 41.9°C; (b) 36.1°C.

Table XIV. Temperature dependence of the exchange time in EDA1 and corresponding relaxation rates in the absence of exchange.[a]

T(°C)	τ(msec)	$1/T_{2A}$(sec)	$1/T_{2B}$(sec)
19.9	6.65 (0.16)[b]	272	283
25.5	4.353 (0.08)	237	247
31.3	2.851 (0.03)	211	222
36.8	2.042 (0.02)	190	192
42.6	1.376 (0.009)	170	170
48.3	0.9508 (0.007)	153	151
53.9	0.6633 (0.009)	139	136
59.5	0.4856 (0.01)	127	123
64.9	0.3462 (0.003)	116	112
70.3	0.2500 (0.002)	106	102

a) 0.15 M C_{222} + 0.6 M NaBr.

b) Standard deviation.

Table XV. Temperature dependence of the exchange time in EDA2 and corresponding relaxation rates in the absence of exchange.[a]

T(°C)	τ(msec)	$1/T_{2A}$(sec)	$1/T_{2B}$(sec)
30.4	2.338 (0.03)[b]	256	270
36.2	1.603 (0.02)	189	191
38.0	1.413 (0.01)	182	184
41.4	1.126 (0.008)	171	171
42.4	1.048 (0.008)	168	167
45.0	0.8913 (0.008)	160	159
50.2	0.6154 (0.004)	145	143
53.8	0.4862 (0.004)	136	133
60.8	0.3111 (0.003)	121	117
69.0	0.1918 (0.002)	106	101
76.4	0.1238 (0.001)	93.9	84.0

a) 0.30 M C_{222} + 0.6 M NaBr.

b) Standard deviation.

Table XVI. Temperature dependence of the exchange time in EDA3 and corresponding relaxation rates in the absence of exchange.[a]

T(°C)	τ(msec)	$1/T_{2A}$(sec)	$1/T_{2B}$(sec)
19.3	2.154 (0.04)[b]	271.5	288.3
24.4	1.448 (0.02)	243.8	255.0
30.6	0.956 (0.02)	215.1	221.0
36.1	0.600 (0.02)	193.3	195.8
41.9	0.486 (0.02)	173.4	173.4
47.4	0.3586 (0.005)	157.0	155.3
53.3	0.2295 (0.002)	141.6	138.7
58.8	0.1626 (0.0007)	129.1	125.4
64.4	0.1162 (0.0007)	117.9	113.7
70.2	0.08232 (0.0005)	107.6	103.2

a) 0.45 M C_{222} + 0.6 M NaBr.

b) Standard deviation.

a

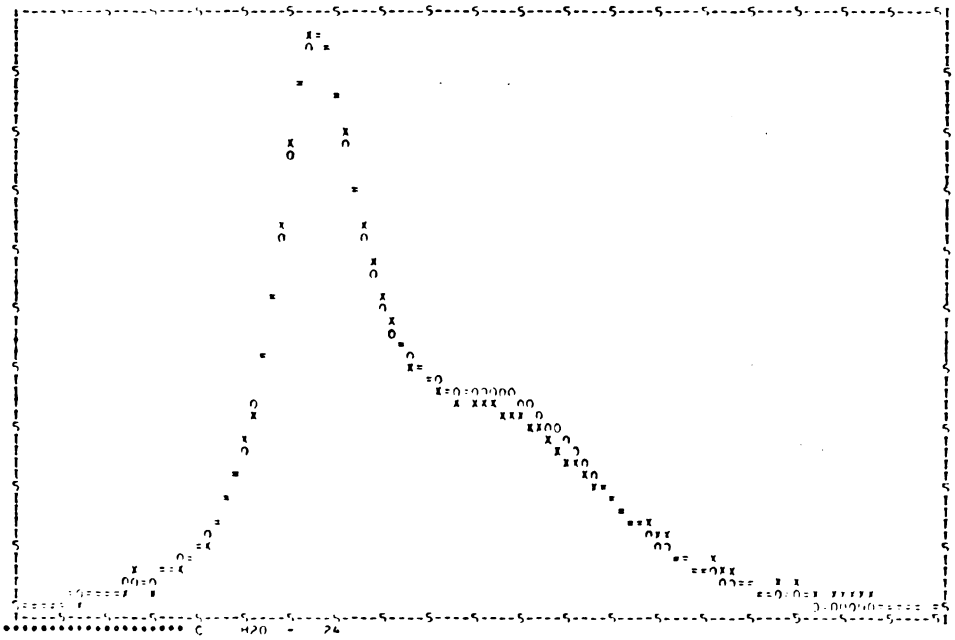

b

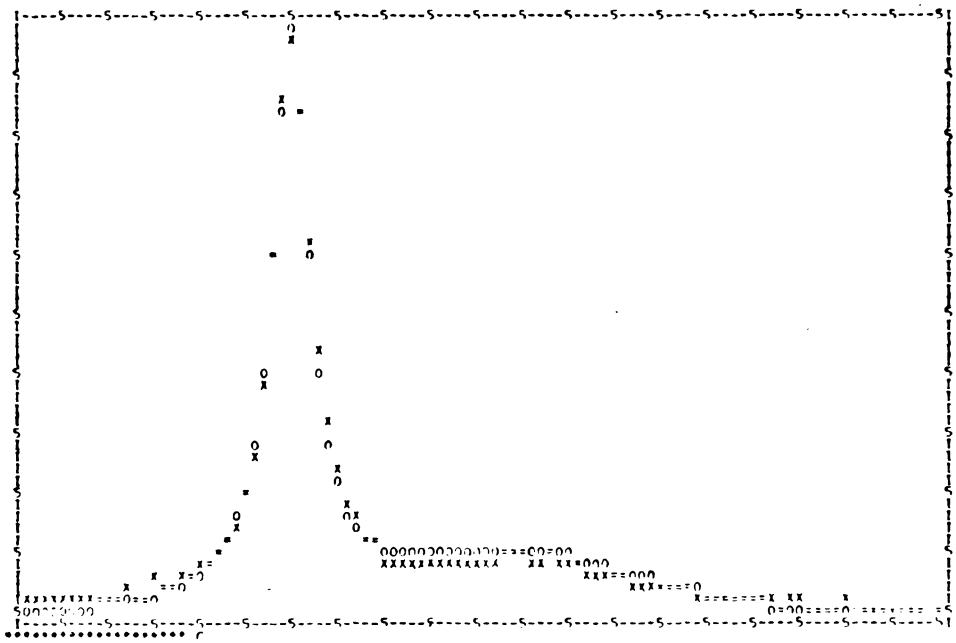

Figure 26. Computer fit of spectra obtained with 0.2 M C_{222} and 0.4 M NaI in H_2O. (a) 23.6^{o}C; (b) 3.3^{o}C.

a

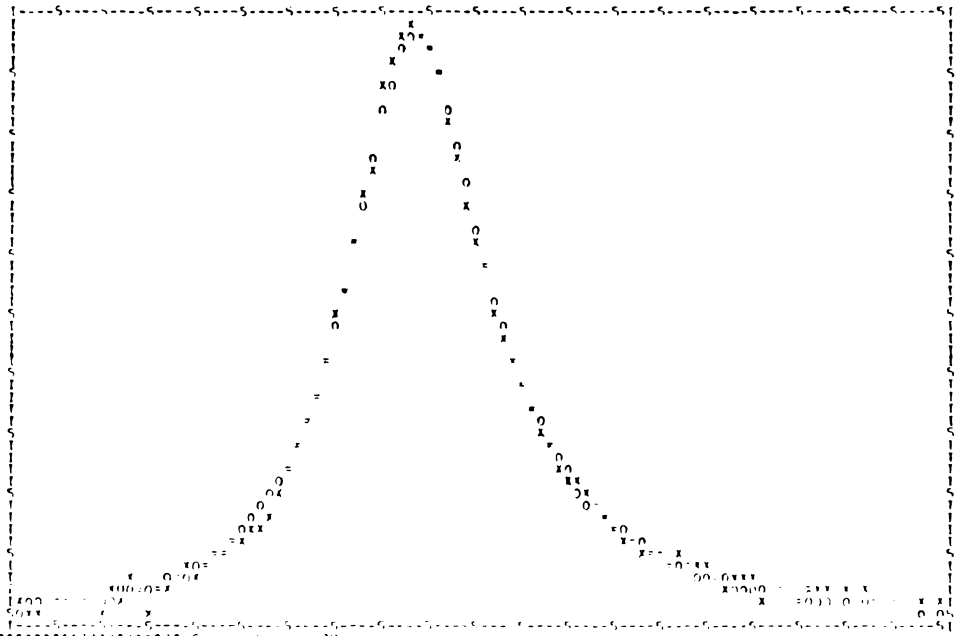

b

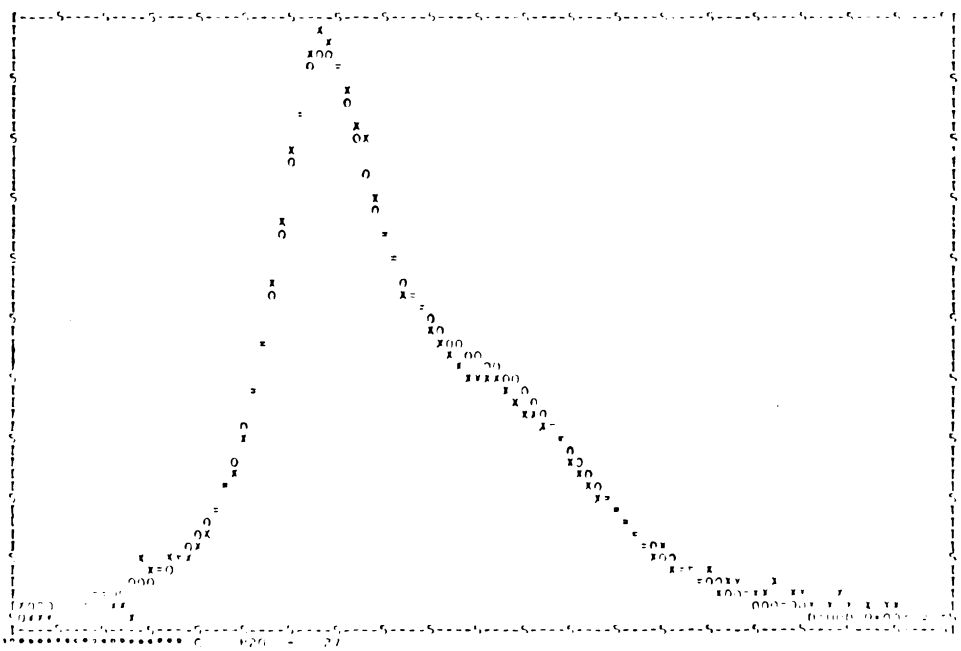

Figure 27. Computer fit of spectra obtained with 0.2 M C_{222} and 0.4 M NaI in H_2O. (a) 39.3°C; (b) 26.9°C.

delay occurs and one relaxation time is much shorter than the other, as in this case, some of the intensity of the faster relaxing site will be lost. As a consequence, the observed intensity of the broad peak will be lower than that of the calculated. Spectra from the PYR solution were analyzed with Equation 5.3'. In the slow exchange limit, the Λ parameter was dropped and ω_A and ω_B along with the usual parameters were allowed to be adjusted to obtain the best fit of 5.3' to the experimental data. Some fits for spectra from PYR solution are shown in Figures 28 and 29. Spectra from the THF solution were also fit with an unmodified form of 5.3'. A few of the fits for THF are shown in Figures 30 and 31. Variations of τ with temperature for H_2O, PYR and THF solution are listed in Tables XVII and XIX.

5.3 Results and Discussion

5.3.1. Some Sources of Systematic Error

Many sources of systematic error occur when the Fourier transform NMR technique is used. These can cause distortion of the observed lineshapes. Some sources are pulse feed-through, the first-order phase correction and narrow-band audio filtering. The effects that they produce can sometimes be eliminated instrumentally and/or the calculated lineshape can be modified to include these effects. For example, the calculated NMR lineshapes included the first-order phase correction as described previously.

a

b

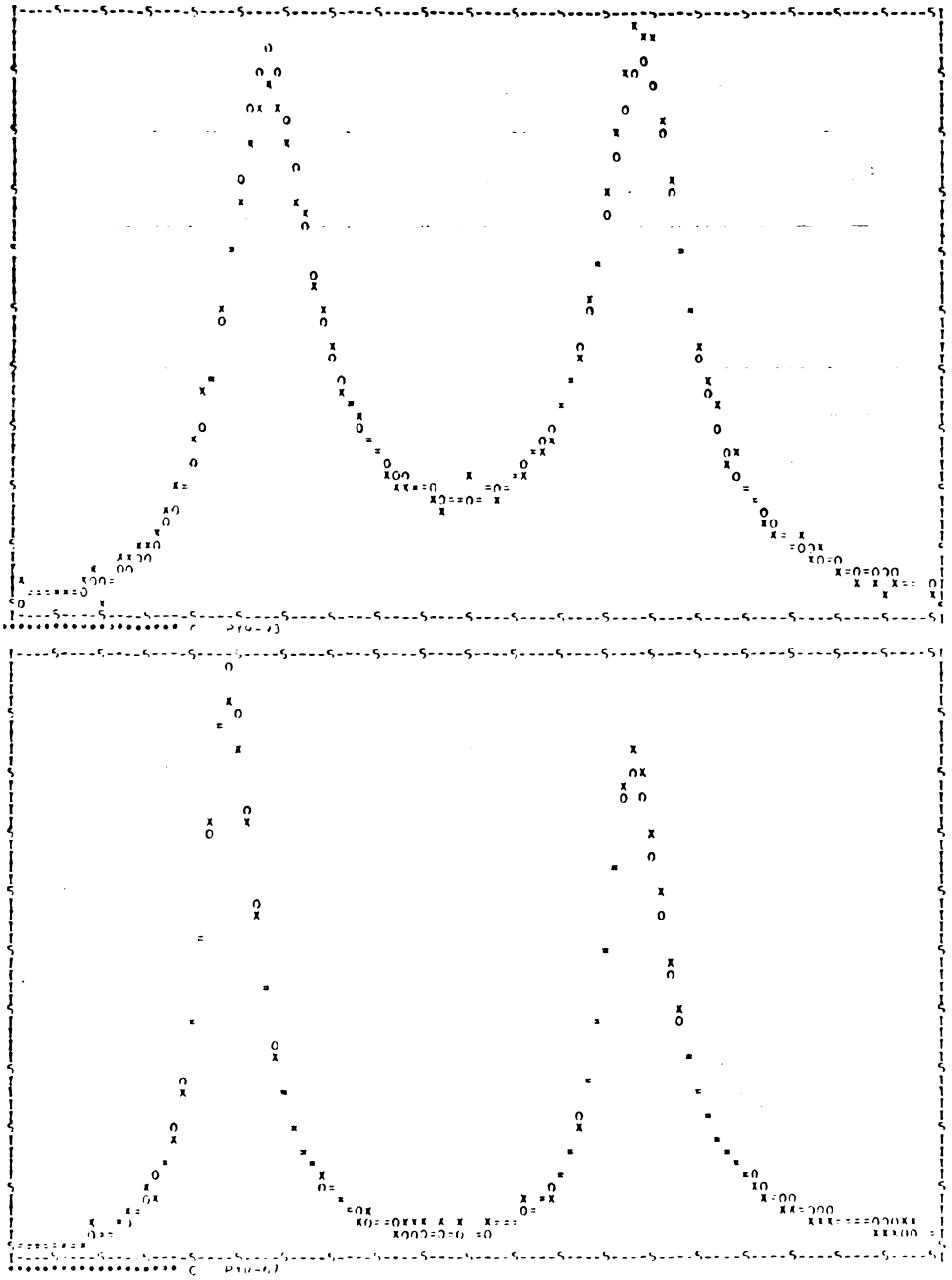

Figure 28. Computer fit of spectra obtained with 0.2 M C_{222} and 0.4 M $Na\phi_4B$ in PYR. (a) 93.2°C; (b) 66.7°C.

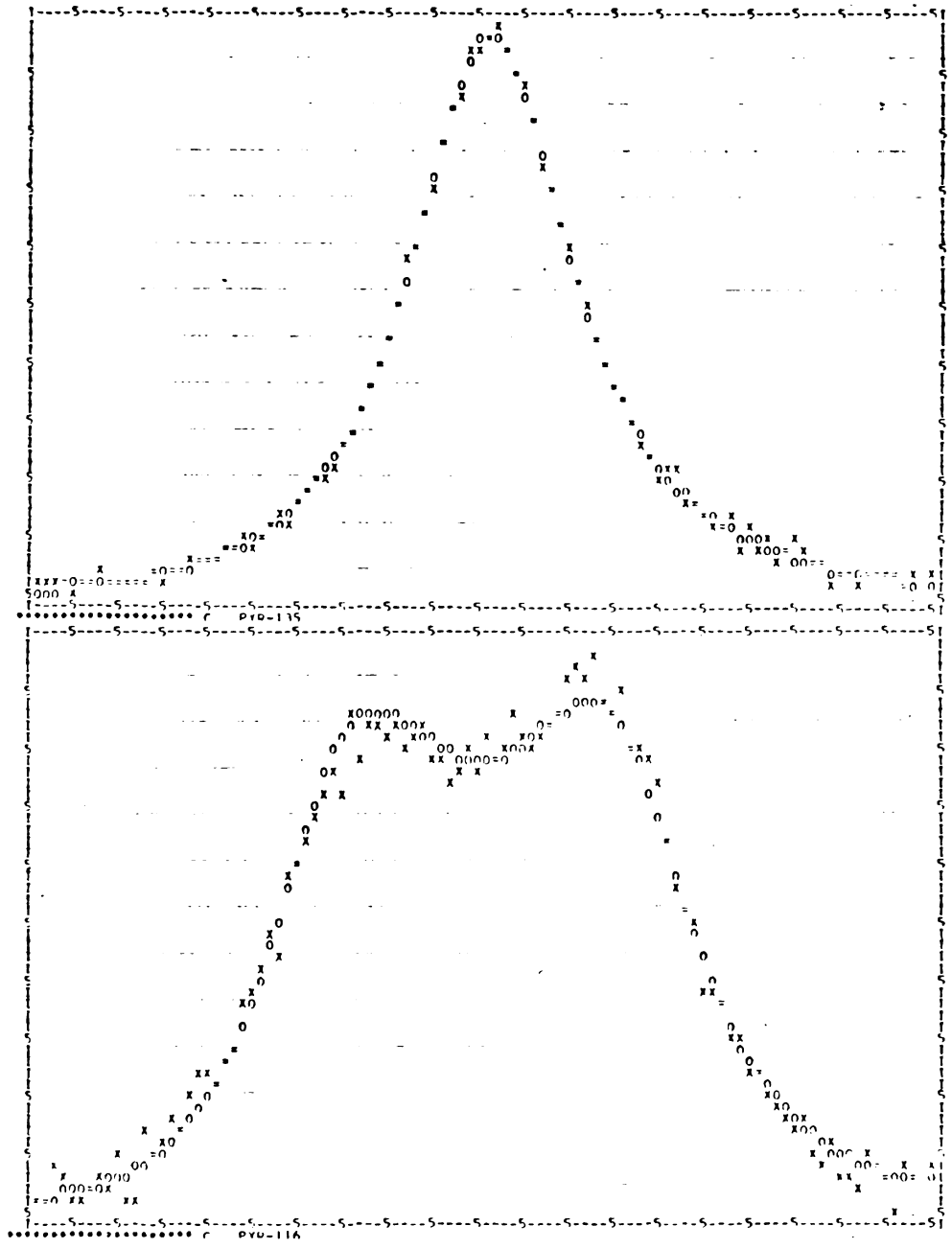

Figure 29. Computer fit of spectra obtained with 0.2 M C_{222} and 0.4 M $Na\phi_4B$ in PYR. (a) 135.4°C; (b) 116.4°C.

a

b

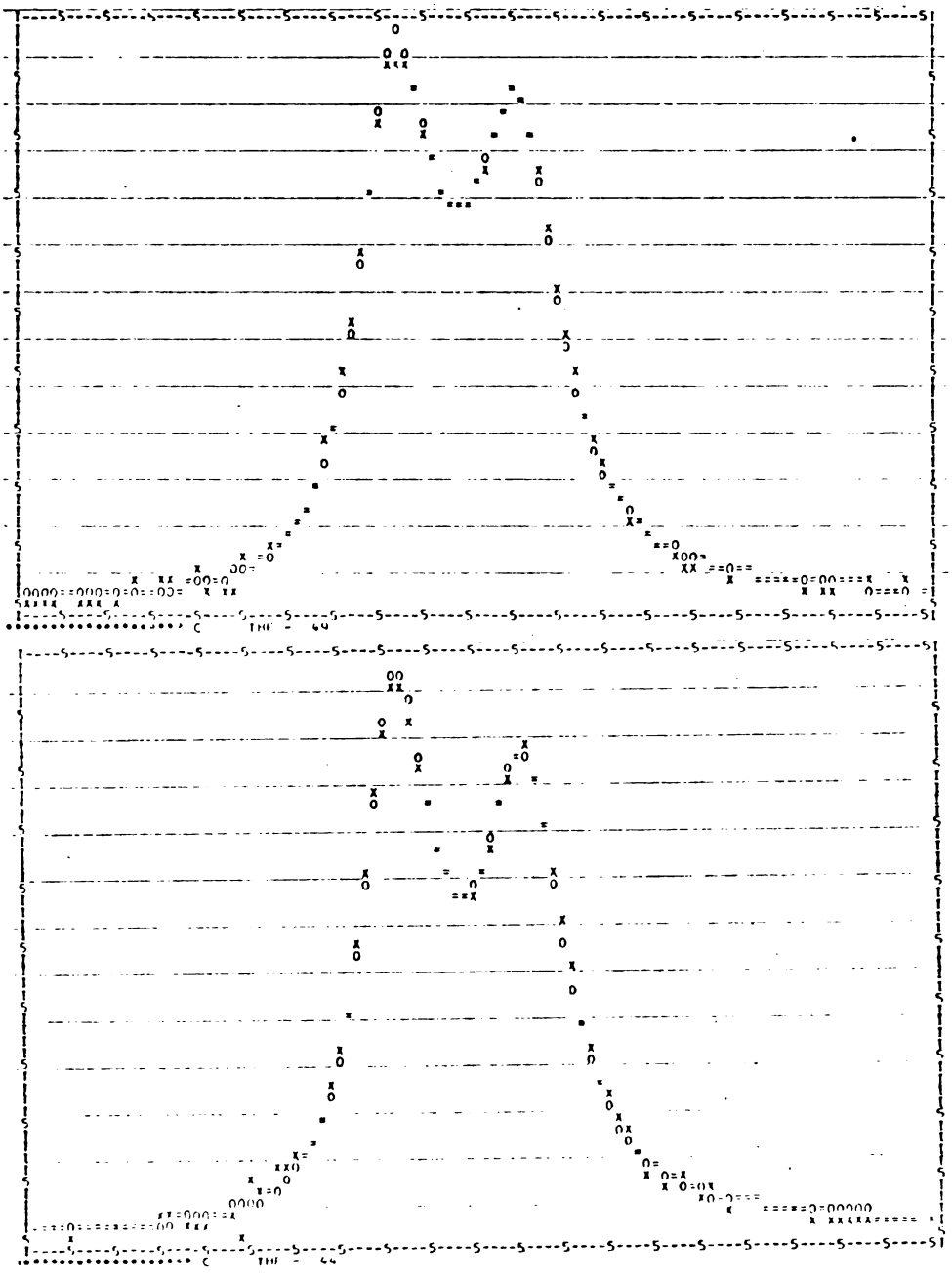

Figure 30. Computer fit of spectra obtained with 0.2 M C_{222} and 0.4 M $Na\phi_4B$ in THF. (a) 49.4°C; (b) 44.1°C.

a

b

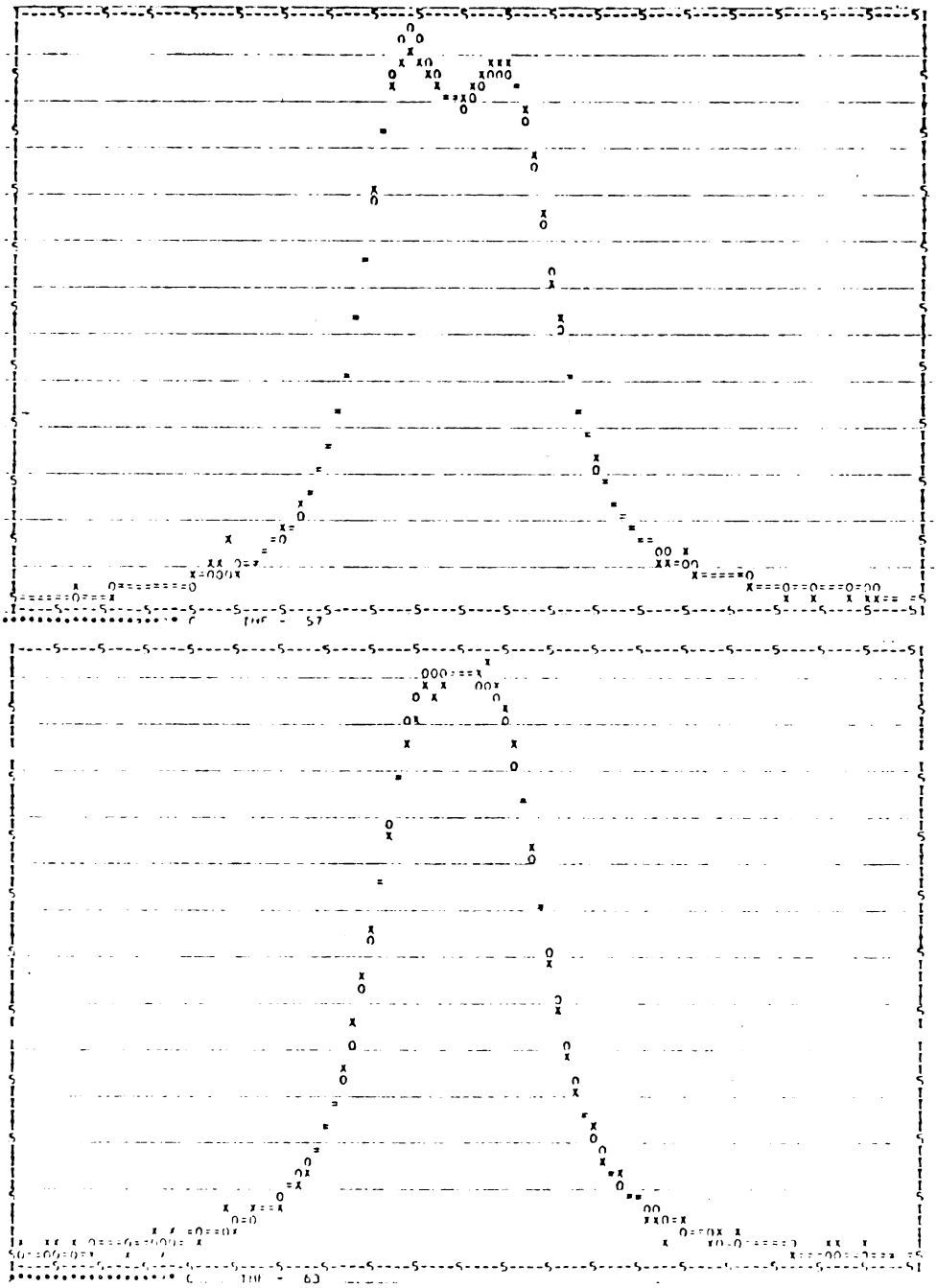

Figure 31. Computer fit of spectra obtained with 0.2 M C_{222} and 0.4 M $Na\phi_4B$ in THF. (a) 56.8°C; (b) 62.8°C.

Table XVII. Temperature dependence of the exchange time in H_2O and corresponding values for relaxation rates in the absence of exchange.[a]

T(°C)	τ(msec)	$1/T_{2A}$(sec)	$1/T_{2B}$(sec)
3.3	34.5 (3.1)[b]	61.0	503
12.0	11.34 (0.4)	49.4	389
22.2	4.335 (0.07)	42.3	294
23.6	3.830 (0.05)	41.5	284
26.9	2.877 (0.04)	39.8	261
29.2	2.178 (0.02)	38.7	247
30.6	2.030 (0.02)	38.0	238
33.8	1.616 (0.02)	36.8	221
37.0	1.120 (0.02)	35.8	205
39.3	0.892 (0.01)	35.4	195
45.9	0.5122 (0.009)	32.3	168
52.3	0.3333 (0.008)	31.3	147

a) 0.2 M C_{222} + 0.4 NaI.

b) Standard deviation.

Table XVIII. Temperature dependence of the exchange time in PYR and corresponding relaxation rates in the absence of exchange.[a]

T(°C)	τ(msec)	$1/T_{2A}$(sec)	$1/T_{2B}$(sec)
55.2	32.0 (4.3)[b]	83.8	115
66.7	21.9 (2.1)	78.8	102
73.3	15.2 (1.4)	76.3	98.0
81.4	9.82 (0.5)	74.8	88.4
93.2	5.31 (0.2)	73.3	80.4
98.7	3.82 (0.1)	73.3	77.8
102.0	3.157 (0.09)	73.3	77.4
105.4	2.815 (0.06)	73.8	77.4
109.6	2.333 (0.06)	73.8	76.9
116.4	1.609 (0.02)	74.1	76.5
125.8	1.013 (0.011)	74.8	75.4
129.4	0.8607 (0.008)	75.8	75.4
135.4	0.6611 (0.006)	76.8	74.9
142.1	0.5051 (0.006)	77.8	

a) 0.2 M C_{222} + 0.4 M $Na\phi_4B$

b) Standard Deviation.

Table XIX. Temperature dependence of the exchange time in THF and corresponding relaxation rates in the absence of exchange.[a]

T(°C)	τ(msec)	$1/T_{2A}$(sec)	$1/T_{2B}$(sec)
35.5	24.2 (1.2)[b]	108	146
39.4	20.2 (0.8)	106	139
44.1	15.0 (0.4)	105	132
45.8	12.7 (0.3)	104	129
49.4	10.2 (0.2)	103	124
52.2	8.43 (0.1)	102	120
56.8	6.089 (0.09)	100	114
59.1	5.334 (0.08)	99.3	111
62.8	4.063 (0.05)	98.1	107
65.0	3.510 (0.03)	97.5	105
68.2	2.876 (0.03)	96.5	102
71.3	2.363 (0.03)	95.6	98.7
74.6	1.872 (0.02)	94.6	95.7

a) 0.2 M C_{222} + 0.4 M $Na\phi_4B$.

b) Standard deviation.

It is not at all obvious by inspection of the spectra that a first-order phase correction is needed. This is because a single-line spectrum can be phased to appear as an absorption mode signal by using only a zero-order phase correction. Even in the case of a doublet, the spectrum can be visually phased to an apparent absorption mode signal without using a first-order phase correction (an example of this is shown by the spectra in Figure 17, in which the total change in phase from one end of the spectrum to the other is 44.5°). By contrast ^{13}C NMR spectra usually exhibit many narrow lines which span the entire frequency range sampled. In this case visual evaluation of the first-order phase correction is easily made from a single spectrum.

The first-order phase correction will have its maximum effect on the lineshape for an exchanging system at the slow exchange limit (low temperatures), where the spectral intensities are spread out over a broad frequency range. Figures 32a and 32b, which contain the same experimental data, show the effect of θ' upon the fit. The lineshape calculated in Figure 32a does not include a first-order phase correction term whereas that calculated in Figure 32b includes the proper first-order phase correction. The fit in Figure 32b is slightly better than in 32a.

Failure to make such a correction usually only causes small differences between the calculated and observed lineshapes. However the effect is magnified for large chemical shift differences such as we observed with EDA solu-

a

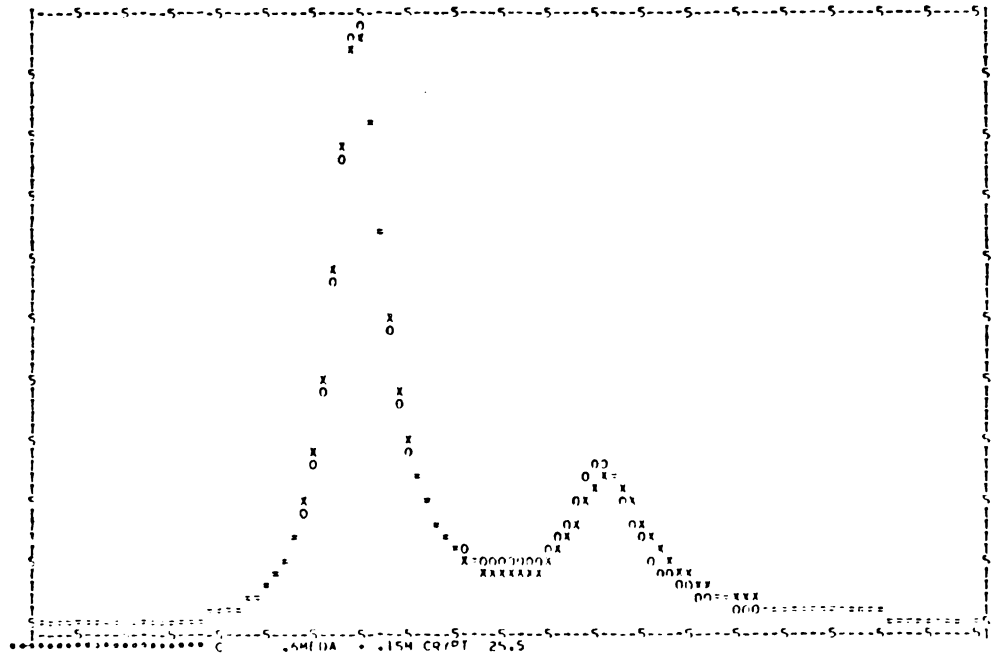

b

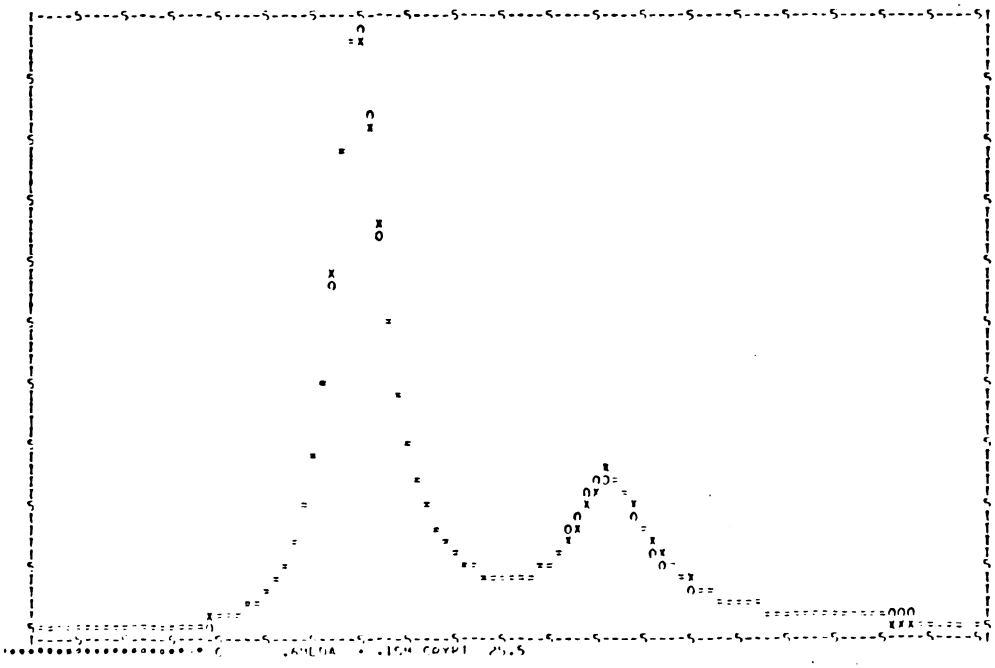

Figure 32. Computer analysis of the ^{23}Na lineshape for a solution containing 0.15 M C_{222} and 0.6 M NaBr in EDA at 25.5°C. (a) No first-order phase correction; (b) first-order phase corrected.

tions. In addition as shown in Figure 33, straight line Arrhenius plots result in either case, but give different activation energies. The experimental data are the same for both sets of calculations shown in Figure 33, but the τ values were evaluated with and without first-order phase correction. This shows that failure to make the proper first-order phase correction might not be readily apparent but it can have a pronounced effect on the results. In this case (EDA 1), neglect of θ' correction gives an 8% error in the calculated activation energy.

Another source of error can come from the 4-Pole Butterworth active audio filters which are frequently used in Fourier-transform NMR spectroscopy. All the experiments discussed were performed with a sweep-width of 5000 Hz. To obtain an optimum signal-to-noise ratio, a narrow band filter (0 - 5000 Hz) was used. A perfect filter would be one which passes any frequency between 0 and 5000 Hz and has an infinitely sharp cutoff at 5000 Hz. However, no such filter exists. The attenuation characteristics of the filter employed in these experiments is shown in Figure 34. An input sine wave which is passed through the filter at 1 volt (peak to peak) and 5000 Hz frequency is attenuated by 40%. The attenuation at 3000 Hz is only 3.1%. The intensity function shown in Figure 34 can be matched to within better than 1% with an equation of the form

$$I = ax^2 + bx + c,$$

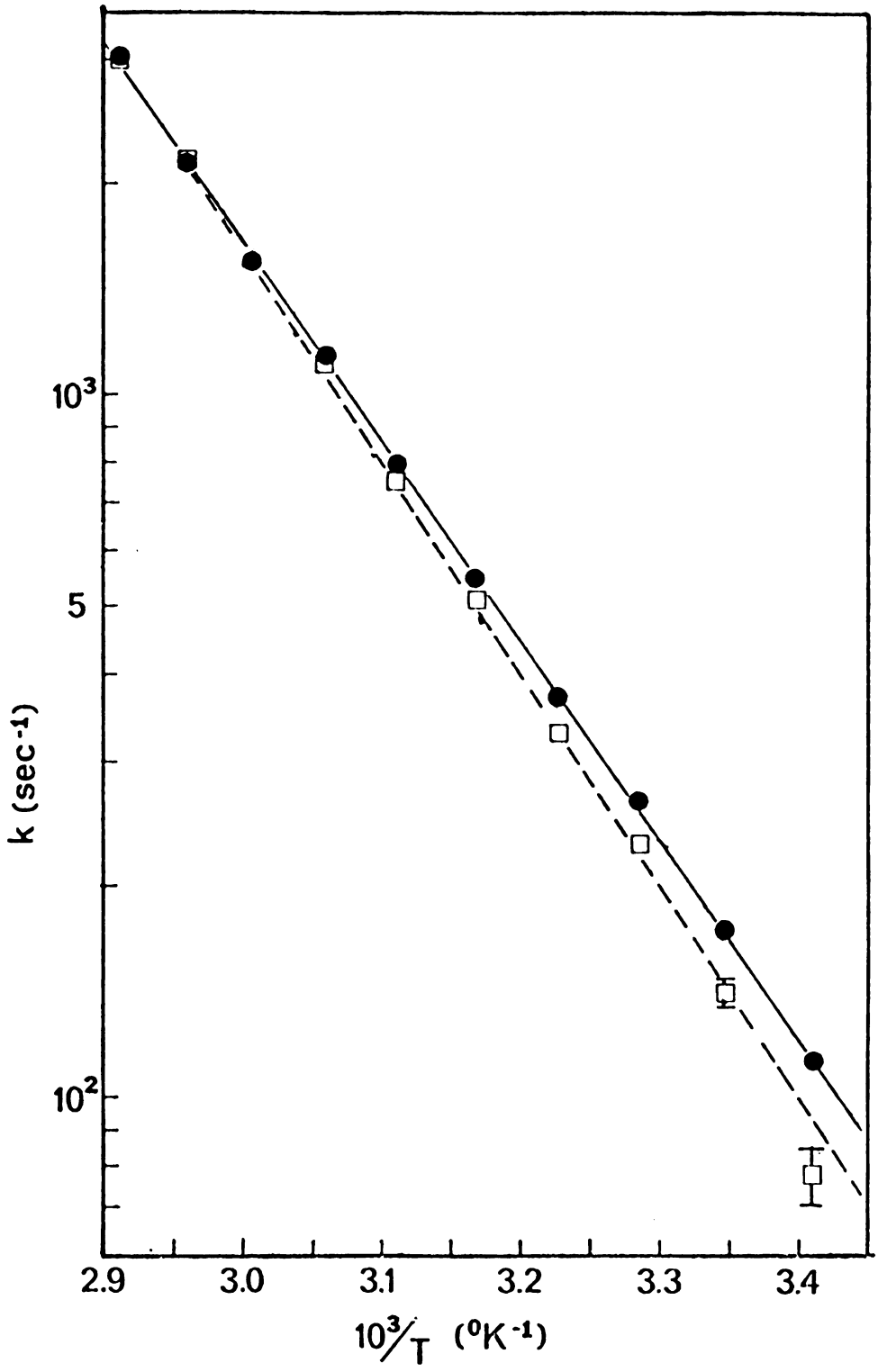

Figure 33. Arrhenius plot of k (rate of release of Na^+ from C_{222}) for EDAl solution. (□) No first-order phase correction; (●) first-order phase corrected.

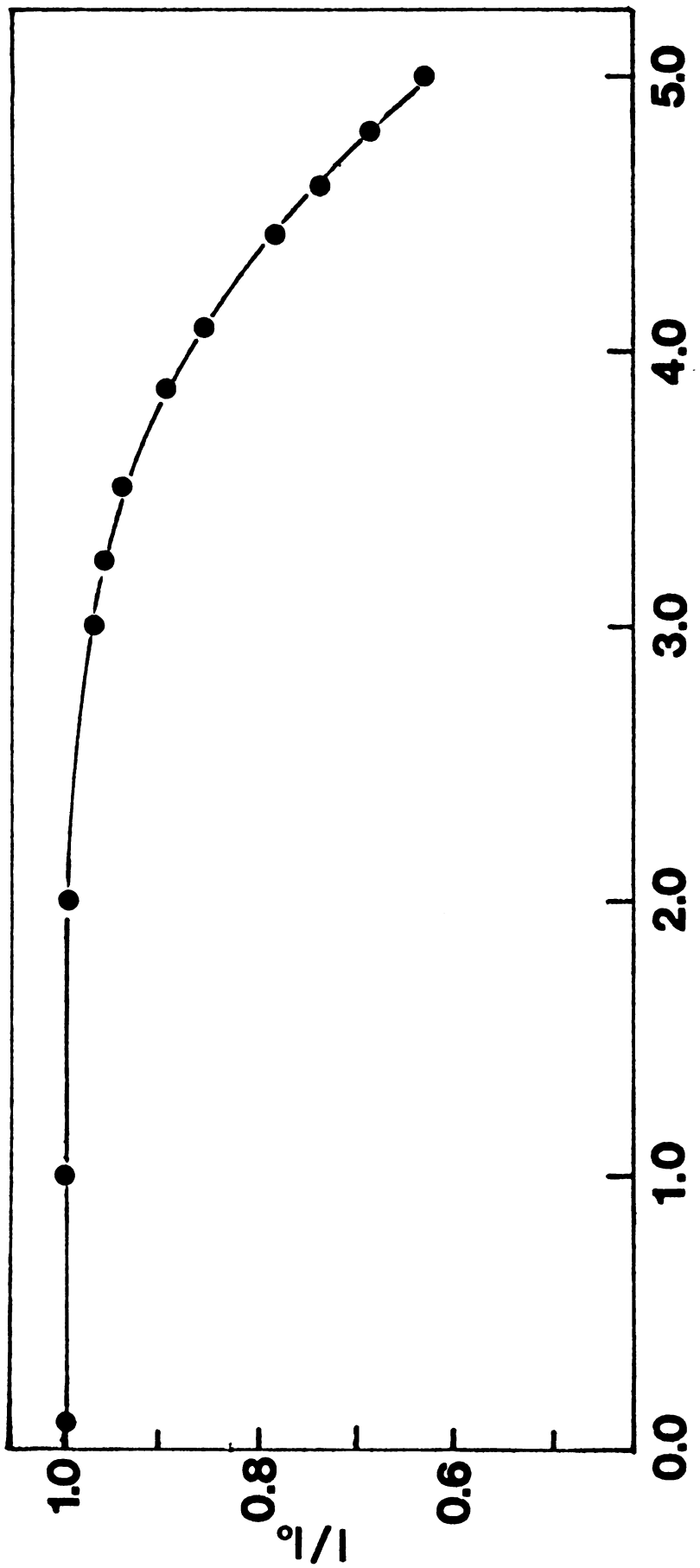

Figure 34. Plot of attenuated intensity I/I_o vs frequency for a 5000 Hz 4-Pole Butterworth active filter.

where x represents frequency and I is the intensity. A least-squares fit of the above equation to the data in Figure 35 was performed to evaluate the coefficients, a, b and c. This calculated intensity function was then inserted into Equation 5.3' as an amplitude adjustment. The corrected intensity form of Equation 5.3' was fit to the EDA 3 data (these data were used since, of all the spectra, they had the most spectral intensity at the highest frequency and this is where most attenuation would occur). A comparison of τ values calculated from the best fit of 5.3' with and without this intensity correction to the observed data from EDA 3 solution is given in Table XX. From these results it is clear that no intensity corrections are needed for this work.

Another source of error comes from the digital sampling which is characteristic of a Fourier transform spectrum. Even if an ideal spectrometer with no baseline distortion from pulse-feedthrough were used, baseline artifacts could occur because of the digital sampling. If we are interested in a spectrum with frequencies as high as δ Hz, we must sample the free induction decay at a rate which is at least 2δ in order to properly represent the spectrum in digital form (this is known from information theory). If we sample at a rate 2δ, and frequency of $\delta + \varepsilon$ (where ε is positive) is examined, then there will be less than 2 points per cycle representing the frequency $\delta + \varepsilon$ and the frequency $\delta - \varepsilon$ also has the same value at each of the sampled points. Thus the frequency $\delta + \varepsilon$ is indistinguishable from the frequency $\delta - \varepsilon$, and any

Table XX. Comparison of exchange times with and without intensity correction for EDA3.

Temp(°C)	τ(msec)	τ_{corr}(msec)
19.3	2.154 (0.04)[a]	2.151 (0.04)
24.4	1.448 (0.02)	1.447 (0.02)
30.6	0.956 (0.02)	0.956 (0.02)
36.1	0.600 (0.02)	0.601 (0.02)
41.9	0.486 (0.02)	0.486 (0.02)
47.4	0.3586 (0.005)	0.3584 (0.005)
53.3	0.2295 (0.02)	0.2293 (0.002)
58.8	0.1626 (0.0008)	0.1625 (0.0008)
64.4	0.1162 (0.0007)	0.1161 (0.0007)
70.2	0.0823 (0.0005)	0.0823 (0.0005)

a) Standard deviation.

information of the former is aliased to the lower frequency $\delta - \varepsilon$.

Taking a simple case, if a spectrum is obtained which has a single peak which is broad (say a factor of 20 times smaller than the sweep width) then baseline distortion will occur and might be observable with a good signal-to-noise ratio. Any intensity on the wings outside the sweep width is folded back into the spectrum. The dispersion mode spectrum is much more distorted than the absorption mode spectrum because of higher intensity in the wings. This folding back of the wings causes a baseline distortion. If a phase correction is performed, the larger distortion folded into the nearly pure dispersion mode spectrum is mixed into the phase corrected absorption mode spectrum. Foldover from the wings of the dispersion line becomes worse as the width of the line is increased compared to the width of the spectrum. Normally, the linewidth of a peak is smaller than two percent of the total width of the spectrum and the signal-to-noise ratio is smaller than 100, so that the spectral distortion is negligible. In conclusion, even a perfect spectrometer can give Fourier transformed spectra which are baseline distorted because of digital sampling which leads to only a finite range of distinguishable frequencies.

5.3.2. Mechanism of Exchange

Two possible mechanisms of exchange were considered. The first (I) is given by Equation 5.12 and assumes exchange

proceeds through an association-dissociation process.

$$(C_{222}) + (Na^+) \underset{k_{-1}}{\overset{k_1}{\rightleftarrows}} (Na^+C_{222}) \qquad 5.12$$

The second mechanism (II), given by Equation 5.13, is bimolecular and also represents the overall exchange process.

$$*(Na^+) + (Na^+C_{222}) \overset{k_2}{\rightleftarrows} *(Na^+C_{222}) + (Na^+) \qquad 5.13$$

Results of Lehn et al.[39] combined with those of Ceraso and Dye[40] indicated a preference for mechanism I, but mechanism II was not shown to be inconsistent with the data. The complexation of crown polyethers with sodium ions proceeds via mechanism I. To determine whether mechanism I or II is consistent with the data at all temperatures, we examined the concentration dependence of τ. The data from EDA 1, 2 and 3 were used since P_A varies as 0.25, 0.5 and 0.75 respectively.

The relationship of τ to a mechanism is made through the definition of τ_i

$$1/\tau_i = \frac{\text{rate of removal of nuclei from sites of type i}}{\text{number of nuclei in sites of type i}}. \qquad 5.14$$

From Equations 5.9, 5.10 and 5.12-5.14 we obtain the following equation for τ.

$$\text{Mechanism I} \qquad \tau = P_A/k_{-1} \qquad 5.15$$

Mechanism II $\tau = 1/2k_2(Na^+)_{total}$ 5.16

Mechanism I predicts a dependence of τ upon the relative population of site A while mechanism II predicts a dependence of τ upon the total concentration of sodium ion. Table XXI gives the calculated activation energies for each solution from the best fit of an Arrhenius expression to the data. To test for consistency with either mechanism I or II an exchange time, τ_{calc}, was calculated from the average value of the activation energies and relaxation times of all three solutions. Then τ_{calc} values were calculated for equal populations, $P_A = P_B = 0.5$, at each temperature for which the experimental exchange time, τ_{obs}, had been evaluated. The ratio of τ_{obs}/τ_{calc} is plotted against temperature for each solution in Figure 35. It is clear that the data at all temperatures are consistent with mechanism I, since the values are proportional to P_A. Measurements with solution EDA 2 were performed before the importance of an instrumentally determined first-order phase correction had been realized and a computer estimate of θ' was used (previously described) to calculate lineshapes. This might be the cause of the systematic deviations shown for this solution.

Activation energy plots, log k_{-1} *vs* 1/T, are shown in Figures 33, 36 and 37 for EDA 1, 2 and 3 respectively. Activation energy plots for H_2O, PYR and THF are shown in Figure 38. Activation energies, rate constants (k_{-1}) and values of $\Delta H_o^{\neq}$, $\Delta S_o^{\neq}$ and $\Delta G_o^{\neq}$ for the release of Na^+ from the

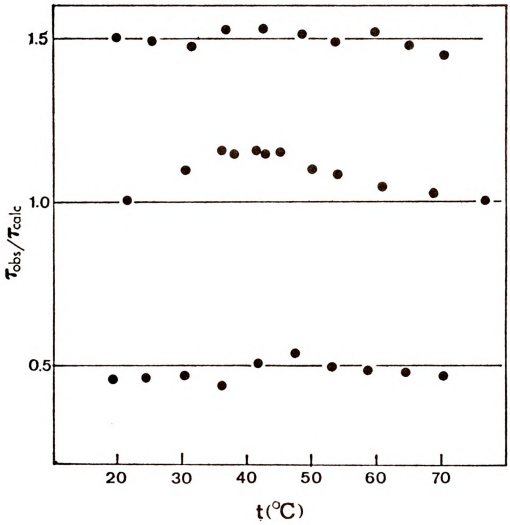

Figure 35. Plot of the ratios τ_{obs}/τ_{calc} vs temperature (°C) for EDA1, EDA2 and EDA3 solutions.

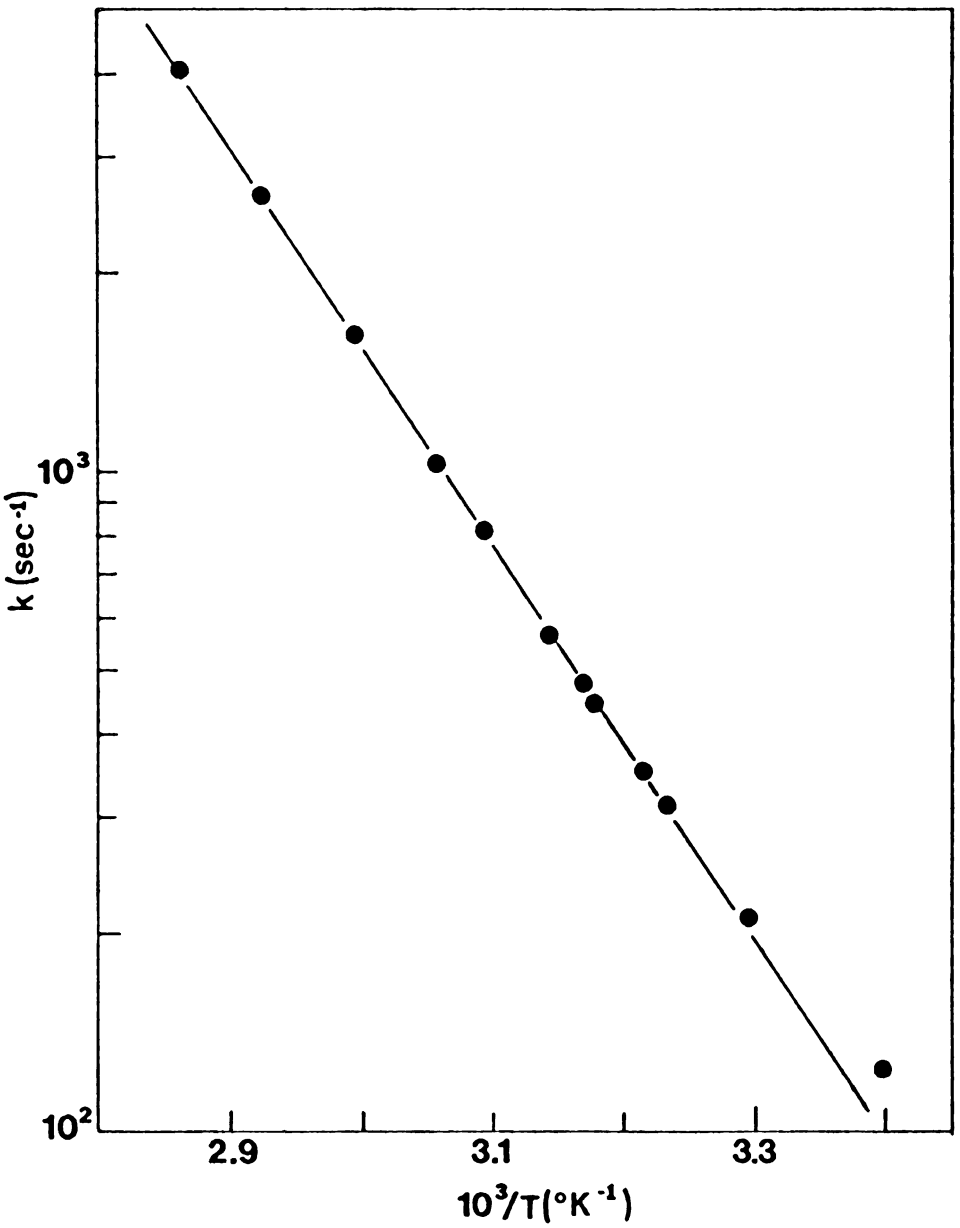

Figure 36. Arrhenius plot of k (rate of release of Na^+ from C_{222}) for EDA2 solution.

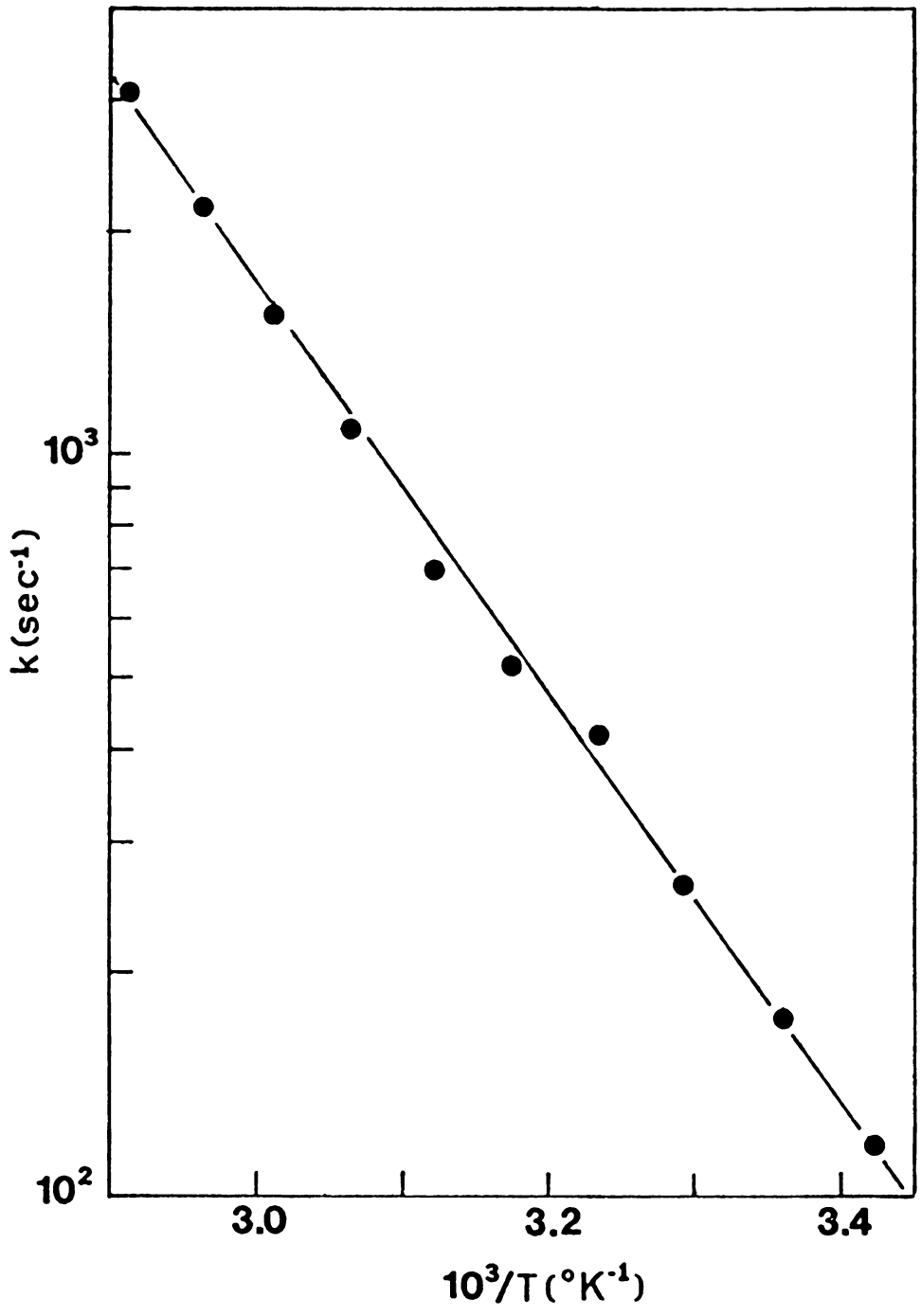

Figure 37. Arrhenius plot of k (rate of release of Na^+ from C_{222}) for EDA3 solution.

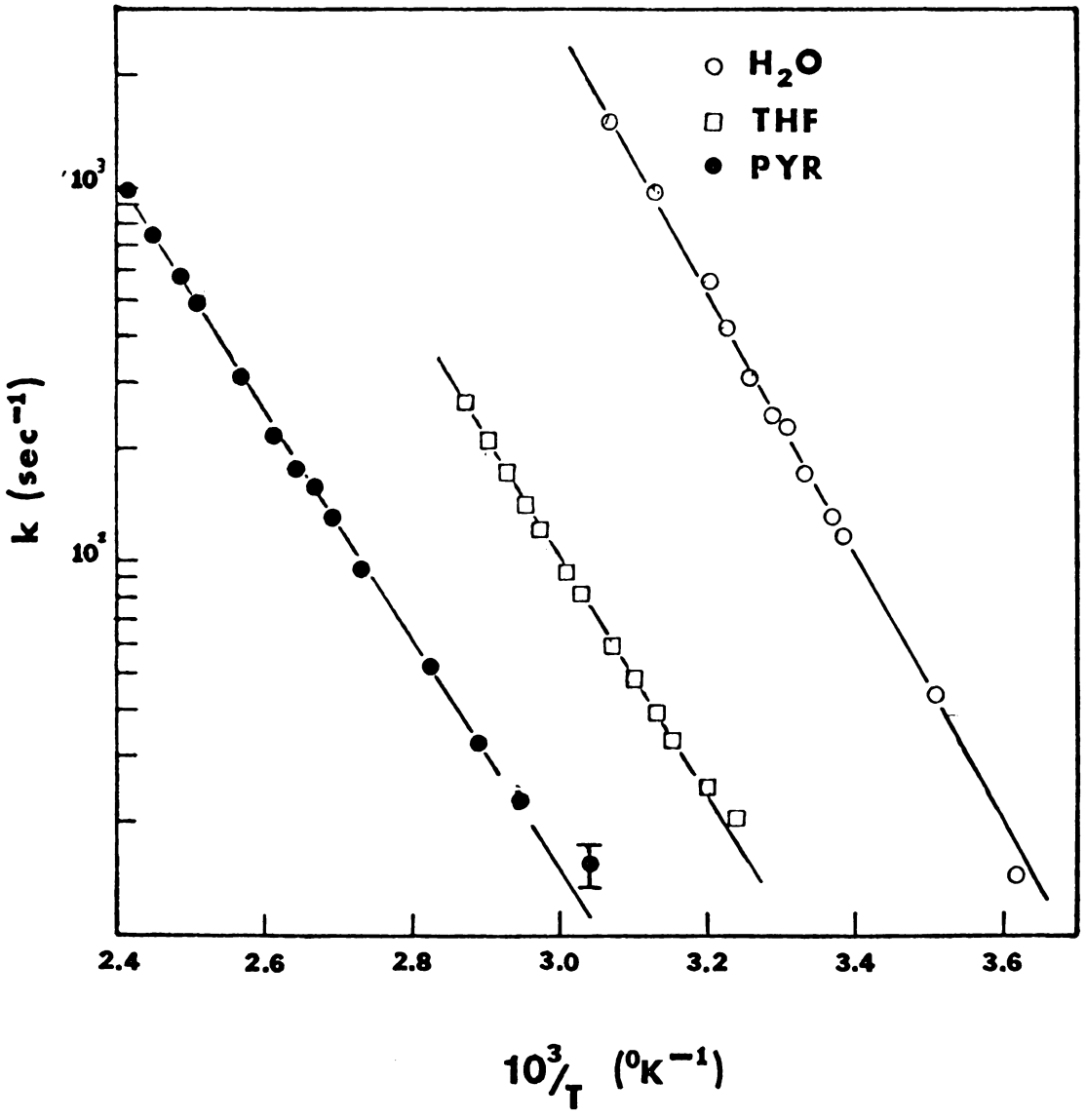

Figure 38. Arrhenius plots of k (rate of release of Na^+ from C_{222}) for H_2O, THF and PYR solutions.

cryptate complex are given in Table XXI. Rate constants were calculated from τ values by assuming that the pathway of sodium ion exchange for H_2O, PYR and THF solutions also proceeds via mechanism I. A complete error analysis, including the cross correlation terms, which account for the coupling of the parameters was performed in all cases. The free energy of activation is directly determined from k_{-1} and has the smallest standard deviation.

As expected, the average value of the activation energy for EDA solutions (listed in Table XXI) is in good agreement with the value of 12.2±1.1 kcal obtained by Ceraso and Dye[40] by using continuous wave ^{23}Na NMR techniques. For the H_2O solution a forward rate of association k_1 is calculated from k_{-1} and K_a to be 1.2 x $10^6 M^{-1}sec^{-1}$. A value of k_{-1} = 27 sec^{-1} was reported for sodium ion exchange in D_2O solution at 3±4°C and is in fair agreement with our calculated value of k_{-1} = 16 sec^{-1}, at 3°C for sodium ion exchange in H_2O solution.

Activation energies vary by nearly 4 kilocalories, indicating the definite presence of a solvent dependence. A variation in activation energy with solvent for Li-cryptate decomplexation has been reported by Cahen et al.[135] They observed a rough correlation between activation energy and donicity of the solvent as expressed by the Gutmann donor number (D.N.). As solvent donor number increases the activation energy for release of Li^+ from the cryptate complex increases. In our case, no correlation is indicated (the

Table XXI. Exchange rates and thermodynamic parameters of sodium cryptate exchange in various solvents.

Solvent	E_a kcal mole^{-1}	k-1 sec^{-1} (298°K)	$\Delta H_o^{\neq}$ kcal mole^{-1}	$\Delta S_o^{\neq}$ cal K^{-1} mole^{-1}	$\Delta G^{o\neq}$ kcal mole^{-1} (298°K)
PYR	14.2 (0.2)[a]	1.14 (0.09)	13.6 (0.2)	-12.6 (0.6)	17.374 (0.004)
THF	14.4 (0.2)	8.03 (0.27)	13.8 (0.2)	- 8.1 (0.6)	16.22 (0.02)
H_2O	16.7 (0.2)	147.4 (2.6)	16.1 (0.2)	+ 5.3 (0.8)	14.49 (0.01)
EDA1	12.96 (0.08)	169.4 (1.8)	12.37 (0.08)	- 6.9 (0.3)	14.43 (0.01)
EDA2	13.0 (0.3)	150.5 (6.9)	12.4 (0.3)	- 7.0 (1.0)	14.48 (0.03)
EDA3	12.7 (0.2)	175.2 (5.8)	12.1 (0.2)	- 7.8 (0.6)	14.39 (0.02)
EDA-AV	12.9 (0.2)	165.0 (4.9)	12.3 (0.2)	- 7.6 (0.6)	14.44 (0.02)

a) Standard deviation.

donor numbers for THF, H_2O, PYR and EDA are 20.0, 33.0, 33.1 and 55.0 respectively). In both the lithium case and our case, the exchange rate in PYR solution is very much slower than the corresponding rates in H_2O solution. By contrast, Shchori *et al.*[136-138] found that the activation energy for release of a Na^+ ion from certain crown ethers was independent of solvent (to within ±1 kcal). They suggest that the energy barrier to exchange may be determined by the energy barrier for a conformational twist of a crown molecule. However, their data are restricted to three solvents with very similar donicities and more solvents are needed to test their hypothesis.

The positive entropy of activation of H_2O is significant. It indicates that solvent participates in the transition state. Values for entropies of transfer ΔS_{tr} of univalent electrolytes from water to other solvents show that the standard partial molar entropy of the cation in water is higher than in other solvents[143] (after corrections have been made for differences in dielectric constants). This is due to extensive structure-breaking of bulk water when an ionic solution is formed. The positive value for $\Delta S_o^{\neq}$ in H_2O is therefore a strong indication that the solvent participates in the transition state.

VI. ALKALI METAL NMR STUDIES OF SODIUM, RUBIDIUM AND CESIUM ANIONS

6.1 Introduction

It had been evident for some time that solutions of the alkali metals in amines and ethers contain species of stoichiometry M^- (see Chapter II). The shift of the optical absorption band with metal, solvent and temperature[29,30] suggests strongly that the species is a centro-symmetric anion. However, other models cannot be ruled out on the basis of optical evidence alone. Figure 39 shows three other contenders for the M^- structure. Indeed, one or more of such structures might be responsible for the diamagnetic species in metal-ammonia solutions which, to date, show no specific evidence for the existence of centro-symmetric anions.

6.2 Magnetic Shielding Constants of Alkali Metal Ions

Optical pumping,[103,104] atomic beam[102] and NMR[99-101] techniques have established the shielding constants of the aqueous cations $^{23}Na^+$, $^{87}Rb^+$ and $^{133}Cs^+$ relative to the gaseous atom with an accuracy of at least 2%. Reliable calculations[105] of the shielding constants of $Na^+(g)$ and $Na^-(g)$ relative to the free atom have been made by using Lamb's complete expression for atomic diamagnetic shielding[144] (first term in Equation 3.2) and analytic Hartree-Fock wavefunctions.[145] The changes in shielding constants are

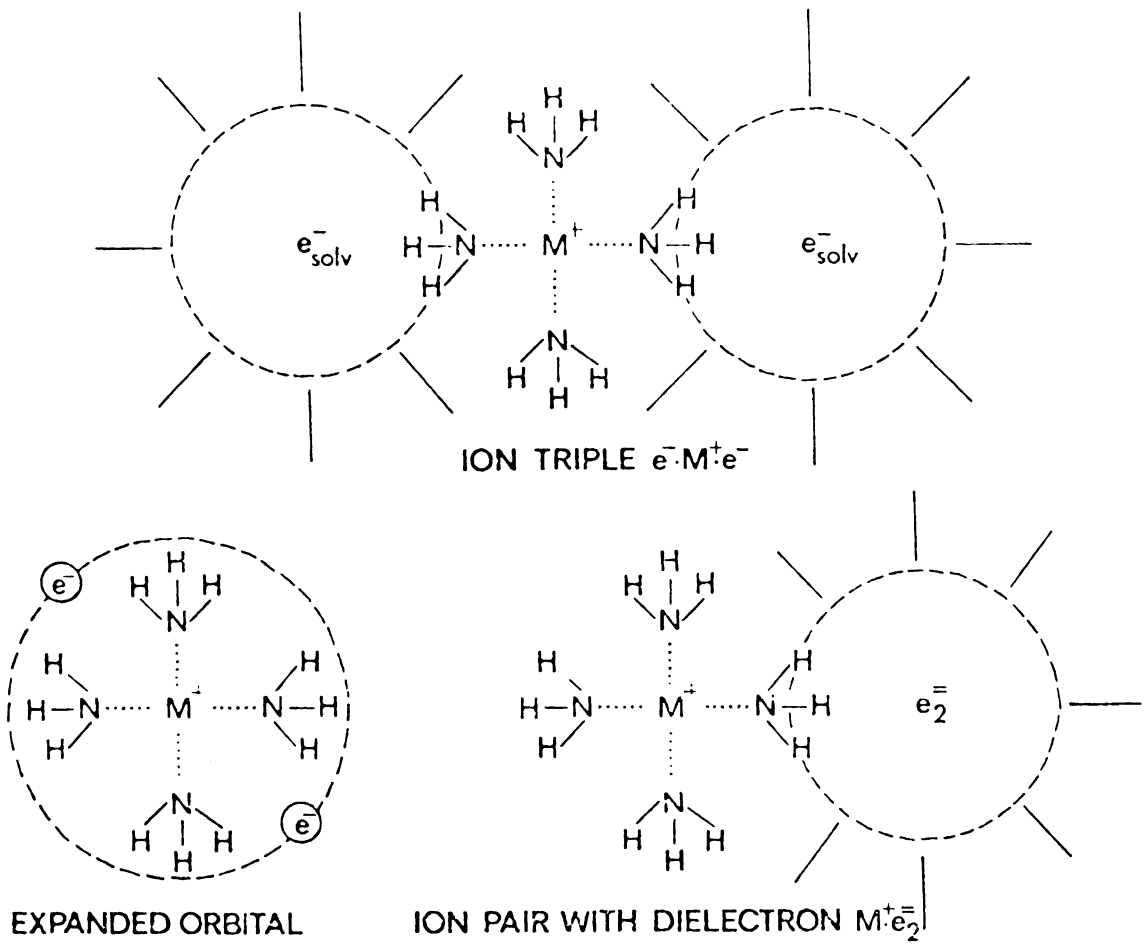

Figure 39. Three possible models for a species of stoichiometry M^- (other than an alkali anion). All of these models permit solvent interaction with the outer p electrons of the cation. Ammonia is used to represent any amine or ether solvent.

relatively small, amounting to only 7.7 ppm (diamagnetic) for the addition of two 3s electrons to gaseous Na^+ to form $Na^-(g)$. Corresponding shifts for $Rb^-(g)$ and $Cs^-(g)$ are also expected to be small. Diamagnetic contributions from solvation are generally only a few ppm[109,110] and the major effect of the solvent, both from theoretical expectations and experimental results[98] is a substantial paramagnetic shift (45 to 75 ppm for Na^+) upon solvation. The magnitude of this shift correlates well with the donicity of the solvent,[111,112,146,147] that is, the ability of the solvent to donate electron density to the cation. It is via the interaction of this solvent electron density with the outer p orbitals of the alkali metal cation which gives the observed paramagnetic effect.

6.3 Results

The key feature which permits us to study the NMR spectra of alkali metal anions is the complexation of the cation by macrocyclic polyethers of the crown[32] and cryptand classes.[34] There are two reasons for the importance of this complexation. First, the pronounced enhancement of metal solubility[30,31,33,36] permits the use of metal concentrations which are high enough to study by alkali metal NMR techniques. Second, the complexed cation is released slowly enough by the complexing agent so that, at low enough temperatures, the exchange of M^+C_{222} with solvated cations is slow on the NMR time scale as shown by Chapter V. This makes it possible

to observe separate resonances for M^+C_{222} and M^-.

Figure 40 shows a typical spectrum of $Na^+C_{222} \cdot Na^-$ in ethylamine. On the basis of the positions and linewidths of NMR spectra of salt solutions which contain the cryptated cation, NaC^+, the broad peak in Figure 40 is attributed to this species. The narrow peak at high fields is then assigned to the sodium anion. Although detectable amounts of free Na^+ cannot be present (because of reaction with Na^- to precipitate sodium metal) its normal position in this solvent is also indicated on the figure. As expected from the solution stoichiometry the areas under the two peaks are equal within the error of their determination. The existence of two peaks rather than a single averaged peak, which would result from rapid exchange between NaC^+ and Na^-, is expected on the basis of the results from the previous chapter.

The ^{23}Na NMR spectrum of $Na^+C_{222} \cdot Na^-$ has been studied as a function of temperature in three solvents, tetrahydrofuran (THF), ethylamine (EA) and methylamine (MA). The ^{87}Rb NMR spectrum of $Rb^+C_{222} \cdot Rb^-$ in EA and THF and the ^{133}Cs NMR spectrum of $^{133}Cs^+C_{222} \cdot Cs^-$ in THF have also been studied. The results are summarized in Table XXII.

6.4 Discussion

The spectra for $Na^+C_{222} \cdot Na^-$ in THF, EA and MA are compared in Figure 41. The most striking feature is the absence of a solvent-induced paramagnetic shift for Na^- and

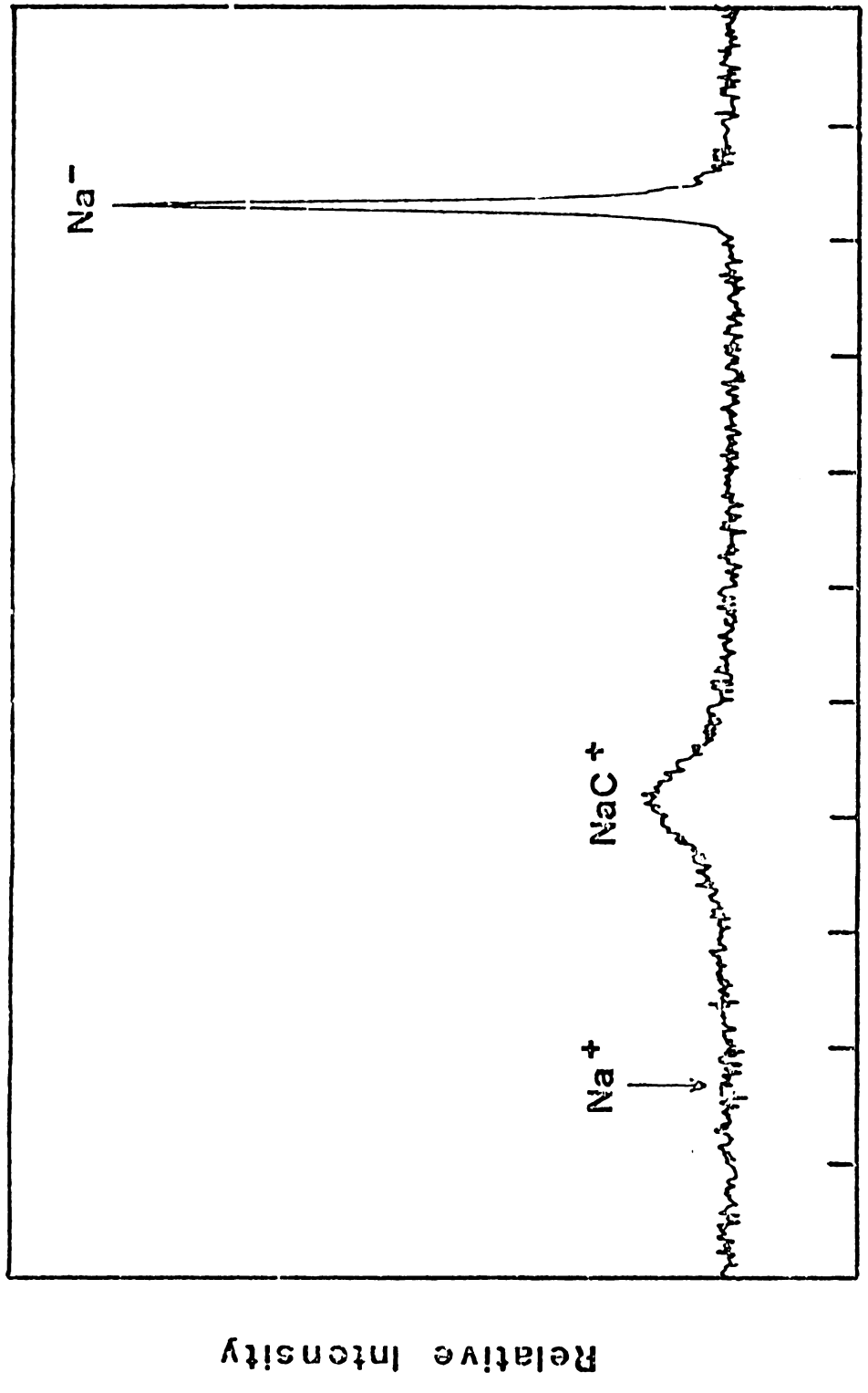

Figure 40. ^{23}Na NMR spectrum of a solution of $Na^+C_{222} \cdot Na^-$ in EA (≃0.2 M) at 1.4°C. Reference is saturated aqueous NaCl; positive shifts are diamagnetic.

Table XXII. Selected list of shielding constants and linewidths.

Ion	Concentration (M)	Temp (°C)	Solvent	$\sigma(M_{solv}$ vs $M_g)$ [a] (ppm)	$\Delta\nu_{1/2}$ [b] (Hz)	Ref. [c] σ	Ref. [c] $\Delta\nu_{1/2}$
Na^+	∞dil.	25	H_2O	-60.5±1	5.16	102	124
Rb^+	∞dil.	25	H_2O	-211.6±1.2	----	102	
Cs^+	∞dil.	25	H_2O	-344.3±5.8	0.02	102	124
F^-	∞dil.	25	H_2O	-168±2 [d]	----	110, 149	
Br^-	∞dil.	25	H_2O	-194(calc) [d]	----	96	
Na^+	Sat. NaCl	25	H_2O	-61.2	8.0	108	
Na^+	0.3 NaI	-15	MA	-72.2	9.0		
Na^+	0.25 NaI	25	EA	-74.4	17.9		
Na^+	0.2 $Na\phi_4B$	25	THF	-52.9	23.0		
Na^+C [e]	0.15 Na^+C, Na^-	-15	MA	-49.8	30.8		
Na^+C	0.15 Na^+C, Na^-	-17 to +1	EA	-50.8	120-170		
Na^+C	0.15 Na^+C, Na^-	-4	THF	-50.4	51		
Na^-	Gas	---	---	+2.6 (calc)	----	105	
Na^-	0.15 Na^+C, Na^-	-15	MA	+1.4	11		

Table XXII. (cont'd)

Ion	Concentration (M)	Temp (°C)	Solvent	$\sigma(M_{solv}$ vs $M_g)$[a] (ppm)	$\Delta\nu_{\frac{1}{2}}$[b] (Hz)	Ref.[c] σ	Ref.[c] $\Delta\nu_{\frac{1}{2}}$
Na^-	0.15 Na^+C, Na^-	-17 to +1	EA	+1.6	6-9		
Na^-	0.15 Na^+C, Na^-	-4	THF	+2.3	<3		
Rb^+	0.1 RbI	25	H_2O	-212.7	158	108	
Rb^+	0.4 RbI	25	CH_3OH	-199.6	300		
Rb^+C	0.4 Rb^+C, I^-	25	H_2O	-262	1300		
Rb^+C	0.4 Rb^+C, I^-	25	CH_3OH	∿-300	4000		
Rb^-	0.1 Rb^+C, Rb^-	-40	EA	-26.2	220		
Rb^-	0.1 Rb^+C, Rb^-	-46	THF	-14.4	15		
Cs^+	0.1 CsI	25	H_2O	-348.4	<3	148	
Cs^+	0.08 CsI	25	CH_3OH	-315.3	<3		
Cs^+C	0.08 Cs^+C, I^-	25	CH_3OH	-476.7	30		
Cs^-	0.1 Cs^+C, Cs^-	-71	THF	-52.3	10		

Table XXII. (cont'd)

---

a) Shielding constant, σ, defined by $\omega = \gamma(1-\sigma)\ H_o$, where H_o is the static magnetic field and γ is the gyromagnetic ratio for the neutral gaseous atom.

b) $\Delta\nu^{\frac{1}{2}}$ = full width at half height.

c) Where no reference is cited, data refer to the present work.

d) Reference state is the gaseous anion.

e) C refers to 2,2,2 cryptand.

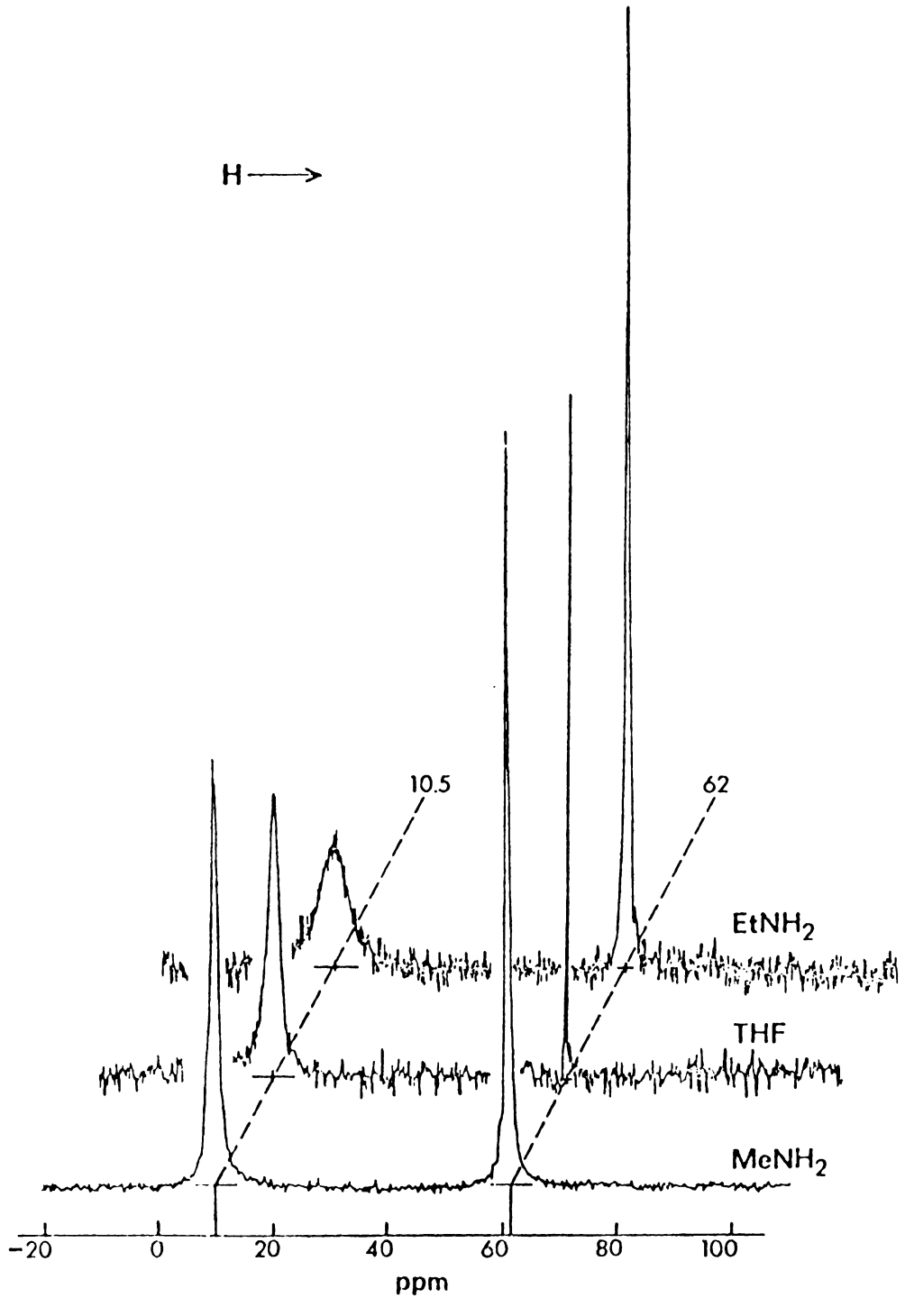

Figure 41. ^{23}Na NMR spectra of $Na^+C_{222} \cdot Na^-$ solutions (≈0.1 M) in three solvents. All chemical shifts are referenced to aqueous Na^+ at infinite dilution.

the narrowness of this line. The complexed cation, Na^+C_{222} has a chemical shift which is also nearly independent of solvent and is at the same position as for ordinary salts of Na^+C_{222} in these solvents. By contrast the solvated cation, Na^+, is strongly solvent-dependent (Table XXII).

The chemical shift of Na^- is not only independent of solvent, but is also nearly the same as that of Na^- in the gas phase. This is completely different from that of any ion with filled outer p orbitals (including halide anions) as indicated in Table XXII. As discussed in Chapter IV, a paramagnetic shift of an ion is caused by the overlap (KY model) of outer s and p orbitals of the solvent molecules with the outer p orbital of the ion. Inner orbitals are not considered, since they are tightly bound and do not extend appreciably between nearest neighbors. The absence of a chemical shift for Na^- shows that the 2p orbitals are well shielded from the solvent by the presence of the filled 3s orbital. This would not be the case for any model shown in Figure 39. We conclude therefore that the most reasonable model for Na^- is that of a centro-symmetric anion with two electrons in the outer s orbital. It is not obvious why the shift is as small as it is, since interaction with the solvent to cause mixing of s and p character could yield a paramagnetic shift. Perhaps the large size of the anion causes the chemical shift to be small.

The extreme narrowness of the line for Na^- also attests to the high spherical symmetry of this species. Quadrupolar broadening of ^{23}Na NMR lines is common (see Table XXII) and results from an electric field gradient at the nucleus. Even such presumably symmetric cations as $Na^+(aq)$ are quadrupole broadened to 5 Hz (full width at half-height). By contrast, the true linewidth of Na^- in THF is less than 3 Hz compared with 23 Hz for Na^+ in THF. Since the lines may also be broadened by the presence of e^-_{solv} via a paramagnetic interaction, it is difficult to obtain the true quadrupole-broadened linewidth. The relative concentration of e^-_{solv} tends to vary from one sample to another depending upon the solvent used and the method of preparation. Therefore, we find that the linewidths are not completely reproducible. Since exchange of sodium between Na^- and either Na^+C or Na^+ would also broaden the line we cannot completely rule this out. However, it seems unlikely since the linewidth of Na^- does not decrease markedly as the temperature is lowered.

Just as for Na^-, Rb^- and Cs^- give narrow lines which are diamagnetically shifted from the corresponding cations by a large amount. The NMR absorptions of Rb^+C and Cs^+C were not observed in the M^+C, M^- samples, probably because of line-broadening. The signal-to-noise ratio was satisfactory for observation of the narrow Rb^- and Cs^- lines but not for the broad lines expected for Rb^+C and Cs^+C. Studies with salts indicate that the linewidth of Rb^+C is far too broad to have

been observed in the metal solution case. The situation for the case of Cs^+C is not as clear. If the linewidth were in excess of 200 Hz the signal would have been lost in the noise. In methanol at 25°C the linewidth of Cs^+C (iodide salt) is 30 Hz. It might be expected to be much broader in THF at -71°C. The aqueous Rb^+ and Cs^+ ions are paramagnetically shifted 212 and 344 ppm from the respective gaseous atoms. Values for the gaseous anions are not known but are presumably shifted diamagnetically a few ppm from the atoms. The resonance positions of Rb^- in EA and THF are shifted 26 and 14 ppm paramagnetically from the atom and Cs^- in THF is shifted 52 ppm. Although the shielding constants are not as close to the gaseous anions as for the case of sodium, they are very close compared with the range of chemical shifts for the corresponding solvated cations.[110,148] The linewidth of Rb^- in THF, 15 Hz, is much narrower than that of the Rb^+ ion in any solvent. However, this is not the case for Rb^- in EA or Cs^- in THF which have linewidths comparable to those of the solvated cations. It is likely that the lines of Rb^- and Cs^- are either paramagnetically broadened by e^-_{solv} or are broadened by exchange.

In conclusion, the NMR studies described in this chapter and the recent isolation of a crystalline salt of the sodium anion[36,37] are the most convincing evidence that genuine alkali anions exist in solution as well as in the crystalline state.

APPENDICES

APPENDIX A

MODIFICATION OF RELAX 2

The data output portion of RELAX 2, a program written by David Wright[128] of Michigan State University for computer controlled timing and data acquisition for two-pulse experiments was slightly modified in order to dump data from the Nicolet 1083 computer. The modifications are

Core Location	Instruction
1310	2001607
1311	2001607
1312	2110577
1313	2404606
1314	2332600
1315	0005144
1316	0000001
1317	2000206
1320	0001346
1321	3110606
1322	3001326
1323	0001327
1324	2000206
1325	0001346
1326	0005051
1327	2124606

1330	2000206
1331	0001346
1332	3110606
1333	3001326
1334	0001340
1335	2000206
1336	0001346
1337	3001563
1340	2001607
1341	2134606
1342	0006454
1343	0162000
1344	0000155
1345	0001314
1346	2404040
1347	0000000
1350	0000037
1351	0001646
1352	2165350
1353	2001404
1354	2001413
1355	2125560

APPENDIX B

PROGRAM CONVERT

Program CONVERT converts data from octal to decimal in a form compatible with KINFIT.

```
      PRØGRAM CØNVERT(INPUT=65,ØUTPUT=65,PUNCH=65)
      DIMENSIØN IX(2), IY(2),X(2),Y(2)
      DATA(MASK=7777777777773777777B)
    5 READ 100,A,B
      IF (EØF(5LINPUT))999,10
  100 FØRMAT (2E10.2)
   10 READ 105,(IX(I),IY(I),I=1,2)
      IF (EØF (5LINPUT))5,8
  105 FØRMAT (2Ø10)
    8 PRINT 110,(IX(I),IY(I),I=1,2)
  110 FØRMAT (1X,2Ø10)
      DØ 15 K=1,2
      IF(IY(K).GE.2000000B)IY(K)=IY(K)+MASK
      X(K)=IX(K)
   15 Y(K)=IY(K)
      PRINT 115,(X(K),A,Y(K),B,K=1,2)
  115 FØRMAT (2(20X,F10.0,F10.8,F10.0,F10.0))
      PUNCH 116,(X(K),A,Y(K),B,K=1,2)
  116 FØRMAT (2)F10.0,F10.8,F10.0,F10.0))
      GØ TØ 10
  999 CØNTINUE
      END
```

APPENDIX C

SOLUTION TO MODIFIED BLOCH EQUATIONS

The Bloch equations which describe the motion of the X and Y components of magnetization in the rotating frame, when modified to include chemical exchange, are given by

$$dG_A/dt + \alpha_A G_A = -i\gamma H_1 M_{OA} + \tau_B^{-1} G_B - \tau_A^{-1} G_A \qquad C1$$

$$dG_B/dt + \alpha_B G_B = -i\gamma H_1 M_{OB} + \tau_A^{-1} G_A - \tau_B^{-1} G_B \qquad C2$$

The solution to these equations for slow passage conditions is obtained by setting $dG_A/dt = dG_B/dt = 0$ and solving C1 and C2 for the total complex moment $G = G_A + G_B$. Solving for G_A in C1 gives

$$G_A = - \frac{i\gamma H_1 M_{OA} + G_B/\tau_B}{(\alpha_A + \frac{1}{\tau_A})} \qquad C3$$

Substitute C3 into C2 and solve for G_B

$$\alpha_B G_B = -i\gamma H_1 M_{OB} + \frac{-i\gamma H_1 M_{OA} + G_B/\tau_B}{(\alpha_A + \frac{1}{\tau_A})\tau_A} - \tau_B^{-1} G_B \qquad C4$$

$$G_B = \frac{(-i\gamma H_1 M_{OB} - \frac{i\gamma H_1 M_{OA}}{\alpha_A \tau_A + 1})\tau_B (\alpha_A \tau_A + 1)}{[(\alpha_B \tau_B + 1)(\alpha_A \tau_A + 1) - 1]} \qquad C5$$

and from inspection

$$G_A = \frac{(-i\gamma H_1 M_{OA} - \frac{i\gamma H_1 M_{OB}}{\alpha_B \tau_B + 1})\tau_A(\alpha_B\tau_B + 1)}{[(\alpha_A\tau_A + 1)(\alpha_B\tau_B + 1) - 1]} \qquad C6$$

$$G = G_A + G_B = u + iv \qquad C7$$

$$G = \{(-i\gamma H_1 M_{OA} - \frac{i\gamma H_1 M_{OB}}{\alpha_B\tau_B+1})\tau_A(\alpha_B\tau_B + 1)$$

$$+ (-i\gamma H_1 M_{OB} - \frac{i\gamma H_1 M_{OA}}{\alpha_A\tau_A+1})\tau_B(\alpha_A\tau_A + 1)\}/$$

$$\{(\alpha_A\tau_A + 1)(\alpha_B\tau_B + 1) - 1\} \qquad C8$$

using $P_A = \frac{\tau_A}{\tau_A+\tau_B}$, $P_B = \frac{\tau_B}{\tau_A+\tau_B}$

and for low values of the radio frequency field $P_A M_O = M_{OA}$, $P_B M_O = M_{OB}$

$$G = -i\gamma H_1 M_O\{(P_A + \frac{P_B}{\alpha_B\tau_B+1})\tau_A(\alpha_B\tau_B + 1)$$

$$+ (P_B + \frac{P_A}{\alpha_A\tau_A+1})\tau_B(\alpha_A\tau_A + 1)\}/$$

$$\{(\alpha_A\tau_A + 1)(\alpha_B\tau_B + 1)-1\} \qquad C9$$

$$\text{or } G = -i\gamma H_1 M_O\{(P_A\alpha_B\tau_B + P_A + P_B)\tau_A + (P_B\alpha_A\tau_A + P_B + P_A)\tau_B\}/$$

$$\{(\alpha_A\tau_A + 1)(\alpha_B\tau_B + 1) - 1)\} \qquad \text{C10}$$

Since $P_A + P_B = 1$

$$G = -i\gamma H_1 M_O\{(P_A\alpha_B\tau_B\tau_A + \tau_A + P_B\alpha_A\tau_A\tau_B + \tau_B)\}/$$

$$\{(\alpha_A\tau_A + 1)(\alpha_B\tau_B + 1) - 1\} \qquad \text{C11}$$

or

$$G = -i\gamma H_1 M_O\{(\tau_A + \tau_B) + \tau_A\tau_B(\alpha_A P_B + \alpha_B P_A)\}/$$

$$\{(\alpha_A\tau_A + 1)(\alpha_B\tau_B + 1) - 1\} \qquad \text{C12}$$

as first obtained by Gutowsky, McCall, and Schlicter.[139]

To obtain the absorption and dispersion mode shape functions, one must separate the real and imaginary parts of Equation C12.

Define $\tau = \dfrac{\tau_A\tau_B}{\tau_A+\tau_B}$

$$\text{Let } Y = \frac{G}{-i\gamma H_1 M_O} = \frac{\tau_A+\tau_B+\tau_A\tau_B(\alpha_A P_B+\alpha_B P_A)}{\alpha_A\alpha_B\tau_A\tau_B+1+\alpha_B\tau_B+\alpha_A\tau_A-1} \qquad \text{C13}$$

dividing numerator and denominator of C13 by $(\tau_A + \tau_B)$

$$Y = \frac{\dfrac{\tau_A}{\tau_A+\tau_B} + \dfrac{\tau_B}{\tau_A+\tau_B} + \dfrac{\tau_A\tau_B}{\tau_A+\tau_B}(\alpha_A P_B+\alpha_B P_A)}{\dfrac{\tau_A\tau_B}{\tau_A+\tau_B}\alpha_A\alpha_B + \dfrac{\tau_B}{\tau_A+\tau_B}\alpha_B + \dfrac{\tau_A}{\tau_A+\tau_B}\alpha_A} \qquad \text{C14}$$

note $P_A + P_B = 1 = \frac{\tau_A}{\tau_A+\tau_B} + \frac{\tau_B}{\tau_A+\tau_B}$

Thus

$$Y = \frac{1 + \tau(\alpha_A P_B + \alpha_B P_A)}{\tau\alpha_A\alpha_B + P_B\alpha_B + P_A\alpha_A} \qquad C15$$

Let $k_A = \frac{1}{T_{2A}}$, $k_B = \frac{1}{T_{2B}}$

then $\alpha_A = k_A - i(\omega_A - \omega)$, $\alpha_A P_A = k_A P_A - iP_A(\omega_A - \omega)$

$\alpha_B = k_B - i(\omega_B - \omega)$, $\alpha_B P_B = k_B P_B - iP_B(\omega_B - \omega)$

Let $k_A P_A = \kappa_A$, $k_B P_B = \kappa_B$

and $\Omega_A = P_A(\omega_A - \omega)$, $\Omega_B = P_B(\omega_B - \omega)$

Then $\alpha_A\alpha_B = \frac{\alpha_A\alpha_B P_A P_B}{P_A P_B} = \frac{(\kappa_A - i\Omega_A)(\kappa_B - i\Omega_B)}{P_A P_B}$

and C15 becomes

$$Y = \frac{1+\tau\{(k_A P_B + k_B P_A) - i[P_B(\omega_A - \omega) + P_A(\omega_B - \omega)]\}}{\tau[\frac{(\kappa_A - i\Omega_A)(\kappa_B - i\Omega_B)}{P_A P_B}] + (\kappa_A + \kappa_B) - i[\Omega_A + \Omega_B]} \qquad C16$$

$$Y = \frac{1+\tau\{(k_A P_B + k_B P_A) - i[P_B(\omega_A - \omega) + P_A(\omega_B - \omega)]\}}{\tau[\frac{(\kappa_A\kappa_B - \Omega_A\Omega_B - i(\Omega_A\kappa_B + \Omega_B\kappa_A)}{P_A P_B}] + \kappa_A + \kappa_B - i[\Omega_A + \Omega_B]} \qquad C17$$

or

$$Y = \frac{1+\tau\{(k_A P_B + k_B P_A) - i[P_B(\omega_A-\omega) + P_A(\omega_B-\omega)]\}}{\kappa_A+\kappa_B+\tau\frac{(\kappa_A\kappa_B-\Omega_A\Omega_B)}{P_AP_B} - i[(\Omega_A+\Omega_B)+\tau\frac{(\Omega_A\kappa_B+\Omega_B\kappa_A)}{P_AP_B}]} \qquad C18$$

Define: $$S = \kappa_A + \kappa_B + \tau\frac{(\kappa_A\kappa_B-\Omega_A\Omega_B)}{P_AP_B} \qquad C19$$

$$T = \Omega_A + \Omega_B + \tau\left(\frac{\Omega_A\kappa_B+\Omega_B\kappa_A}{P_AP_B}\right) \qquad C20$$

$$U = 1 + \tau(k_A P_B + k_B P_A) \qquad C21$$

$$V = \tau[P_B(\omega_A-\omega) + P_A(\omega_B-\omega)] \qquad C22$$

Substituting C19-C22 into C18 gives

$$Y = \frac{U-iV}{S-iT} = \frac{(U-iV)(S+iT)}{S^2+T^2} \qquad C23$$

$$Y = \frac{(SU+TV) + i(UT-SV)}{S^2+T^2} \qquad C24$$

and

$$G = -i\gamma H_1 M_o Y = +\gamma H_1 M_o \frac{[-i(SU+TV) + (UT-SV)]}{S^2+T^2} \qquad C25$$

Define $I = + \frac{(SU+TV)}{S^2+T^2}$, absorption mode shape function

$$R = \frac{(UT-SV)}{S^2+T^2}, \text{ dispersion mode shape function}$$

and $G = u + iv = \gamma H_1 M_O [R-iI]$ C26

where

$$S = \frac{P_A}{T_{2A}} + \frac{P_B}{T_{2B}} + \frac{\tau}{P_A P_B}\left[\frac{P_A P_B}{T_{2A}T_{2B}} - P_A P_B(\omega_A-\omega)(\omega_B-\omega)\right] \quad C27$$

$$S = \frac{P_A}{T_{2A}} + \frac{P_B}{T_{2B}} + \frac{\tau}{T_{2A}T_{2B}} - \tau(\omega_A-\omega)(\omega_B-\omega) \quad C28$$

$$U = 1 + \tau\left(\frac{P_B}{T_{2A}} + \frac{P_A}{T_{2B}}\right) \quad C29$$

$$T = P_A(\omega_A-\omega) + P_B(\omega_B-\omega) + \frac{\tau}{P_A P_B}\left[\frac{P_B P_A}{T_{2B}}(\omega_A-\omega) + \frac{P_A P_B}{T_{2A}}(\omega_B-\omega)\right] \quad C30$$

$$T = P_A\omega_A - P_A\omega + P_B\omega_B - P_B\omega + \tau\left(\frac{\omega_A-\omega}{T_{2B}} + \frac{\omega_B-\omega}{T_{2A}}\right) \quad C31$$

$$T = P_A\omega_A + P_B\omega_B - \omega + \left(\frac{\omega_A-\omega}{T_{2B}} + \frac{\omega_B-\omega}{T_{2A}}\right)\tau \quad C32$$

and

$$V = \tau[P_B(\omega_A-\omega) + P_A(\omega_B-\omega)] \quad C33$$

$$V = \tau[P_B\omega_A + P_A\omega_B - \omega] \qquad C34$$

In summary, the complex moment, $G(\omega)$, is given as

$$G(\omega) = u + iv = \gamma H_1 M_O[R - iI] \qquad C35$$

$$R = \frac{(UT-SV)}{S^2+T^2}, \text{ dispersion mode} \qquad C36$$

$$I = \frac{(SU+TV)}{S^2+T^2}, \text{ absorption mode} \qquad C37$$

where

$$S = \frac{P_A}{T_{2A}} + \frac{P_B}{T_{2B}} + \frac{\tau}{T_{2A}T_{2B}} - \tau(\omega_A-\omega)(\omega_B-\omega) \qquad C38$$

$$U = 1 + \tau\left(\frac{P_B}{T_{2A}} + \frac{P_A}{T_{2B}}\right) \qquad C39$$

$$T = P_A\omega_A + P_B\omega_B - \omega + \tau\left(\frac{\omega_A-\omega}{T_{2B}} + \frac{\omega_B-\omega}{T_{2A}}\right) \qquad C40$$

$$V = \tau[P_B\omega_A + P_A\omega_B - \omega] \qquad C41$$

BIBLIOGRAPHY

BIBLIOGRAPHY

1. W. Weyl, Ann. Phys., 197, 601 (1863).

2. C. A. Kraus, J. Franklin Inst., 212, 537 (1931).

3. R. A. Ogg, Jr., J. Chem. Phys., 14, 295 and 1141 (1946).

4. W. Bingel, Ann. Physik., 12, 57 (1953).

5. M. F. Deigen, Trudy Inst. Fiz. Akad. Nauk., Ukr., S.S.R., 5, 119 (1954); Zh. Eksp. Theor. Fiz., 26, 300 (1954).

6. E. Becker, R. H. Lindquist and B. J. Alder, J. Chem. Phys. 25, 971 (1956).

7. E. Arnold and A. Patterson, Jr., J. Chem. Phys., 41, 3089 and 3098 (1964); Metal-Ammonia Solutions, Colloque Weyl I, p. 160, G. Lepoutre and M. J. Sienko, eds. W. A. Benjamin; New York (1964).

8. M. Gold, W. L. Jolly and K. S. Pitzer, J. Am. Chem. Soc. 84, 2264 (1962).

9. Metal-Ammonia Solutions, Colloque Weyl I, p. 144, G. Lepoutre and M. J. Sienko, eds. W. A. Benjamin; New York (1964).

10. S. Golden, C. Guttman and T. R. Tuttle, Jr., J. Am. Chem. Soc., 87, 135 (1965); J. Chem. Phys., 44, 3791 (1966).

11. C. A. Kraus, J. Am. Chem. Soc., 43, 749 (1921).

12. R. R. Dewald and J. H. Roberts, J. Phys. Chem., 72, 4224 (1968).

13. E. Huster, Ann. Physik, 33, 477 (1938).

14. S. Freed and N. Sugarman, J. Chem. Phys., 11, 354 (1943).

15. C. A. Hutchison and R. C. Pastor, Rev. Mod. Phys., 25, 285 (1953); J. Chem. Phys., 21, 7959 (1953).

16. R. C. Douthit and J. L. Dye, J. Am. Chem. Soc., 82, 4472 (1960).

17. M. Gold and W. L. Jolly, Inorg. Chem., 1, 818 (1962).

18. D. F. Burow and J. J. Lagowski, Advances in Chemistry Series No. 50, 125 (1965).

19. C. A. Hutchison, Jr. and D. E. O'Reilly, J. Chem. Phys., 34, 1279 (1961).

20. V. L. Pollak, J. Chem. Phys. 34, 864 (1961).

21. D. E. O'Reilly, J. Chem. Phys., 35, 1856 (1961).

22. S. R. Gunn and L. J. Green, J. Chem. Phys., 36, 363 (1962); J. Am. Chem. Soc., 85, 358 (1963).

23. S. R. Gunn, J. Chem. Phys., 47, 1174 (1967).

24. J. L. Dye, Metal-Ammonia Solutions, Colloque Weyl II, p. 1. J. J. Lagowski and M. J. Sienko, eds. Butterworths; London (1970).

25. K. D. Vos, J. L. Dye, J. Chem. Phys., 38, 2033 (1963).

26. L. R. Dalton, J. D. Rynbrandt, E. M. Hansen, J. L. Dye; J. Chem. Phys., 44, 3969 (1966).

27. K. Bar-Eli, T. R. Tuttle, Jr., J. Chem. Phys., 40, 2508 (1964).

28. R. Catterall, I. Hurley, M. C. R. Symons, J. Chem. Soc., 1972, 139.

29. S. Matalon, S. Golden, M. Ottolenghi, J. Phys. Chem., 73, 3098 (1969).

30. M. T. Lok, F. J. Tehan, J. L. Dye, J. Phys. Chem., 76, 2975 (1972).

31. J. L. Dye, M. G. DeBacker, V. A. Nicely, J. Am. Chem. Soc. 92, 5226 (1970).

32. C. J. Pedersen, J. Amer. Chem. Soc., 89, 7017 (1967).

33. J. L. Dye, M. T. Lok, F. J. Tehan, R. B. Coolen, N. Papadakis, J. M. Ceraso, M. DeBacker, Ber.Bunsen-Gesellsch. Phys. Chem., 75, 659 (1971).

34. B. Dietrich, J. M. Lehn and J. P. Sauvage, Tetrahedron Lett. 1969, 2885, 2889.

35. J. M. Ceraso and J. L. Dye, J. Chem. Phys., 61, 1585 (1974).

36. J. L. Dye, J. M. Ceraso, M. T. Lok, B. L. Barnett and F. J. Tehan, J. Amer. Chem. Soc., 96, 608 (1974).

37. F. J. Tehan, B. L. Barnett and J. L. Dye, J. Amer. Chem. Soc., 96, 7203 (1974).

38. J. L. Dye, C. W. Andrews and J. M. Ceraso, Submitted to J. Phys. Chem.

39. J. M. Lehn, J. P. Sauvage and B. Dietrich, J. Amer. Chem. Soc., 92, 2916 (1970).

40. J. M. Ceraso and J. L. Dye, J. Amer. Chem. Soc., 95, 4432 (1973).

41. G. Lepoutre and M. J. Sienko (Editors), Metal-Ammonia Solutions, Colloque Weyl. W. A. Benjamin, Inc. (1964).

42. J. J. Lagowski and M. J. Sienko (Editors), Metal-Ammonia Solutions, Colloque Weyl II. Int. Union Pure and Appl. Chem., Butterworth and Company, London (1970).

43. J. Jortner and N. R. Kestner (Editors), Electrons in Fluids. Springer-Verlag, Berlin (1973).

44. The Nature of Metal-Ammonia Solutions, To Be Published, J. Phys. Chem., 79 (1975).

45. J. L. Dye, R. F. Sankuer and G. E. Smith, J. Am. Chem. Soc., 82, 4797 (1960).

46. H. M. McConnell and C. H. Holm, J. Chem. Phys., 26, 1517 (1957).

47. J. Acrivos and K. S. Pitzer, J. Phys. Chem., 66, 1693 (1962).

48. D. E. O'Reilly, J. Chem. Phys., 41, 3729 (1964).

49. W. A. Seddon, J. W. Fletcher, J. Jevcak and F. C. Sopchyshyn, Can. J. Chem., 51, 3653 (1973).

50. J. W. Fletcher and W. A. Seddon, Submitted to J. Phys. Chem.

51. A. DeMortier, M. DeBacker and G. Lepoutre, J. Chim Phys., 380 (1972).

52. M. T. Lok, Ph.D. Thesis, Michigan State University (1973).

53. F. J. Tehan, PhD. Thesis, Michigan State University (1973).

54. J. Kaplan and C. Kittel, J. Chem. Phys., 21, 1429 (1953).

55. R. Catterall and M. C. R. Symons, J. Chem. Soc., 13 (1966).

56. R. A. Ogg, Phys. Rev., 69, 669 (1946); J. Amer. Chem. Soc., 68, 155 (1946).

57. T. L. Hill, J. Chem. Phys., 16, 394 (1948).

58. R. H. Land, J. Chem. Phys., 46, 4496 (1967).

59. D. E. O'Reilly, ibid., 55, 474 (1971).

60. K. Fueki, ibid., 50, 5381 (1969).

61. K. Fueki and S. Noda, Metal-Ammonia Solutions, Colloque Weyl II, J. J. Lagowski and M. J. Sienko (Editors), p. 19. Butterworths, London (1970).

62. K. Fueki, D. F. Feng and L. Kevan, J. Amer. Chem. Soc., 95, 1398 (1973).

63. J. W. Fletcher, W. A. Seddon, J. Jevcok and F. C. Sopchyshyn, Chem. Phys. Lett., 18, 592 (1973).

64. J. W. Fletcher, W. A. Seddon, J. Jevcok and F. C. Sopchyshyn, Can. J. Chem., 51, 2975 (1973).

65. F. Y. Jou and L. M. Dorfman, J. Chem. Phys., 58, 4715 (1973).

66. R. Bockrath and L. M. Dorfman, J. Phys. Chem., 77, 1002 (1973).

67. L. M. Dorfman, F. Y. Jou and R. Wageman, Ber. Bunsenges Phys. Chem., 75, 681 (1971).

68. J. L. Dye, M. G. DeBacker and L. M. Dorfman, J. Chem. Phys., 52, 6251 (1970).

69. I. Hurley, T. R. Tuttle, Jr. and S. Golden, J. Chem. Phys., 48, 2918 (1968).

70. J. L. Dye, Electrons in Fluids, Colloque Weyl III, p. 77. J. Jortner and N. R. Kestner (Editors), Springer-Verlag, Berlin (1973).

71. R. R. Dewald and J. L. Dye, J. Phys. Chem., 68, 128 (1964).

72. D. S. Berns, E. C. Evers and P. W. Frank, Jr., J. Am. Chem. Soc., 79, 5118 (1957).

73. R. R. Dewald and K. W. Browall, J. Phys. Chem., 74, 129 (1970).

74. K. Bar-Eli and T. R. Tuttle, Jr., Bull. Am. Phys. Soc., 8, 352 (1963).

75. L. R. Dalton, M. S. Thesis, Michigan State University (1966).

76. J. Eloranta and H. Linschitz, J. Chem. Phys., 38, 2214 (1963).

77. M. Ottolenghi, K. Bar-Eli and H. Linschitz, J. Chem. Phys., 43, 206 (1965).

78. A. Gaathon and M. Ottolenghi, Israel J. Chem., 75, 286 (1971).

79. D. Huppert and K. Bar-Eli, J. Phys. Chem., 74, 3285 (1970).

80. S. H. Glarum and J. H. Marshall, J. Chem. Phys., 52, 6251 (1970).

81. J. G. Kloosterboer, L. J. Giling, R. P. H. Rettschnick and J. D. W. Van Voorst, Chem. Phys. Lett., 8, 457, 462 (1971).

82. J. W. Fletcher and W. A. Seddon, Proceedings of Colloque Weyl IV, J. Phys. Chem., To Be Published.

83. For references to experimental evidence see S. Golden, C. Guttman and T. R. Tuttle, Jr., J. Chem. Phys., 44, 3791 (1966).

84. M. Smith and M. C. R. Symons, Trans. Faraday Soc., 54, 338, 346 (1958).

85. G. Stein and A. Treinen, Trans. Faraday Soc., 55, 1086, 1091 (1959).

86. I. Burak and A. Treinen, Trans. Faraday Soc., 59, 1490 (1963).

87. J. L. Dye, M. G. DeBacker, J. A. Eyre and L. M. Dorfman, J. Phys. Chem., 76, 839 (1972).

88. M. G. DeBacker, Ph.D. Thesis, Michigan State University (1970).

89. M. G. DeBacker, J. L. Dye, J. Phys. Chem., 75, 3092 (1971).

90. T. R. Tuttle, Jr., Chem. Phys. Lett., 20, 371 (1973).

91. R. V. Pound, Phys. Rev., 79, 685 (1950).

92. H. S. Gutowsky and B. R. McGarvey, J. Chem. Phys., 21, 1423 (1953).

93. N. F. Ramsey, Phys. Rev., 6, 699 (1950).

94. K. Yosidu and T. Moriya, J. Phys. Soc. Japan, 11, 33 (1956).

95. J. Kondo and J. Yamashita, J. Phys. Chem. Solids, 10, 245 (1959).

96. D. Ikenberry and T. P. Das, Phys. Rev., 138, A822 (1965).

97. D. Ikenberry and T. P. Das, J. Chem. Phys., 43, 2199 (1965).

98. C. Deverell, Progr. Nucl. Magn. Reson. Spectrosc., 4, 278 (1969).

99. O. Lutz, Physics Letters, 25A, 440 (1967).

100. O. Lutz, A. Naturforschung, 23a, 1202 (1968).

101. O. Lutz and A. Schwenk, Physics Letters, 24A, 122 (1967).

102. A. Beckmann, K. D. Boklen and D. Elke, Z. physik, 270, 173 (1974).

103. C. W. White, W. M. Hughes, G. S. Hayne and H. G. Robinson, Phys. Rev., 174, 23 (1968).

104. G. S. Hayne, C. W. White, W. M. Hughes and H. G. Robinson, Bull. Am. Phys. Soc., 13, 20 (1968).

105. G. Malli and S. Fraga, Theoret. Chim. Acta, 5, 275 (1966).

106. D. W. Hofmeister and W. H. Flygare, J. Chem. Phys., 44, 3584 (1966).

107. F. J. Adrian, Phys. Rev., 136, A980 (1964).

108. C. Deverell and R. E. Richards, Molecular Physics, 10, 551 (1966).

109. A. Saika and C. P. Slichter, J. Chem. Phys., 22, 26 (1954).

90. T. R. Tuttle, Jr., Chem. Phys. Lett., 20, 371 (1973).

91. R. V. Pound, Phys. Rev., 79, 685 (1950).

92. H. S. Gutowsky and B. R. McGarvey, J. Chem. Phys., 21, 1423 (1953).

93. N. F. Ramsey, Phys. Rev., 6, 699 (1950).

94. K. Yosidu and T. Moriya, J. Phys. Soc. Japan, 11, 33 (1956).

95. J. Kondo and J. Yamashita, J. Phys. Chem. Solids, 10, 245 (1959).

96. D. Ikenberry and T. P. Das, Phys. Rev., 138, A822 (1965).

97. D. Ikenberry and T. P. Das, J. Chem. Phys., 43, 2199 (1965).

98. C. Deverell, Progr. Nucl. Magn. Reson. Spectrosc., 4, 278 (1969).

99. O. Lutz, Physics Letters, 25A, 440 (1967).

100. O. Lutz, A. Naturforschung, 23a, 1202 (1968).

101. O. Lutz and A. Schwenk, Physics Letters, 24A, 122 (1967).

102. A. Beckmann, K. D. Boklen and D. Elke, Z. physik, 270, 173 (1974).

103. C. W. White, W. M. Hughes, G. S. Hayne and H. G. Robinson, Phys. Rev., 174, 23 (1968).

104. G. S. Hayne, C. W. White, W. M. Hughes and H. G. Robinson, Bull. Am. Phys. Soc., 13, 20 (1968).

105. G. Malli and S. Fraga, Theoret. Chim. Acta, 5, 275 (1966).

106. D. W. Hofmeister and W. H. Flygare, J. Chem. Phys., 44, 3584 (1966).

107. F. J. Adrian, Phys. Rev., 136, A980 (1964).

108. C. Deverell and R. E. Richards, Molecular Physics, 10, 551 (1966).

109. A. Saika and C. P. Slichter, J. Chem. Phys., 22, 26 (1954).

110. C. Deverell, Mol. Phys., 16, 491 (1969).

111. R. H. Erlich and A. I. Popov, J. Am. Chem. Soc., 93, 5620 (1971).

112. M. Herlem and A. I. Popov, J. Am. Chem. Soc., 94, 1431 (1972).

113. V. Gutmann and E. Wychera, Inorg. Nucl. Chem. Lett., 2, 257 (1966).

114. Y. M. Cahen, J. L. Dye and A. I. Popov, J. Phys. Chem., 79, 1289 (1975).

115. A. Abragam, "The Principles of Nuclear Magnetism," Oxford UP, London (1961).

116. R. M. Sternheimer, Phys. Rev., 84, 244 (1951); 86, 316 (1952); 95, 736 (1954).

117. F. W. Langhoff and R. P. Hurst, Phys. Rev., 139A, 1415 (1965).

118. J. P. Kintzinger, J. M. Lehn, J. Amer. Chem. Soc., 96, 3313 (1974).

119. R. E. Richards and B. A. Yorke, Mol. Physics, 6, 289 (1963).

120. R. A. Craig and R. E. Richards, Trans. Faraday Soc., 59, 1972 (1963).

121. C. Deverell, D. J. Frost and R. E. Richards, Mol. Physics, 9, 565 (1965).

122. C. Hall, G. L. Haller, and R. E. Richards, Mol. Physics, 16, 377 (1969).

123. C. Hall, R. E. Richards, G. N. Schulz and R. R. Shang, Mol. Physics, 16, 528 (1969).

124. H. G. Hertz, Ber. Bunsenges. Physik. Chem., 78, 531 (1973).

125. R. R. Dewald, Ph.D. Thesis, Michigan State University (1963).

126. Micovic, O. S., I, 264.

127. D. D. Traficante and J. A. Simms, J. Mag. Res., 15, 484 (1974).

128. D. A. Wright, Ph. D. Thesis, Michigan State University (1974).

129. V. A. Nicely and J. L. Dye, J. Chem. Educ., 48 (1971).

130. P. D. Moras and R. Weiss, Acta Cryst., B29, 396, 400 (1973).

131. P. D. Moras, B. Metz and R. Weiss, Acta Cryst., B29, 383, 388 (1973).

132. J. M. Lehn, Struc. Bonding (Berlin), 16, 1 (1973).

133. R. M. Izatt, D. J. Eatough and J. J. Christensen, Struct. Bonding (Berlin), 16, 161 (1973).

134. J. J. Christensen, D. J. Eatough and R. M. Izatt, Chemical Reviews, 74, 351 (1974).

135. Y. M. Cahen, J. L. Dye and A. I. Popov, J. Phys. Chem., 79, 1292 (1975).

136. E. Shchori, J. Jagur-Grodzinski, Z. Luz and M. Shporer, J. Amer. Chem. Soc., 93, 7133 (1971).

137. E. Shchori, J. Jagur-Grodzinski and M. Shporer, J. Amer. Chem. Soc., 95, 3842 (1973).

138. M. Shporer and Z. Luz, J. Amer. Chem. Soc., 97, 665 (1975).

139. H. S. Gutowsky, D. W. McCall and C. P. Slichter, J. Chem. Phys., 21, 279 (1953).

140. H. M. McConnell, J. Chem. Phys., 28, 430 (1958).

141. R. K. Gupta, T. P. Pitner and R. Wasylishen, J. Mag. Res., 13, 383-385 (1974).

142. D. E. Woessner, J. Chem. Phys., 35, 41 (1961).

143. B. G. Cox, G. R. Hedwig, A. J. Parker and D. W. Watts, Aust J. Chem, 27, 477 (1974).

144. W. Lamb, Phys. Rev., 60, 817 (1941).

145. E. Clementi, Tables of Atomic Functions, International Business Machines Corporation, (1965).

146. R. H. Erlich, E. Roach and A. I. Popov, J. Amer. Chem. Soc., 92, 4989 (1970).

147. M. S. Greenberg, R. L. Bodner A. I. Popov, J. Phys. Chem, 77, 2449 (1973).

148. J. D. Haliday, R. E. Richards and R. R. Sharp, Proc. Roy. Soc. Lond., A313, 45 (1969).

149. M. R. Baker, C. H. Anderson and N. F. Ramsey, Phys. Rev., A133, 1533 (1964).